CHALMERS
UNIVERSITY OF TECHNOLOGY

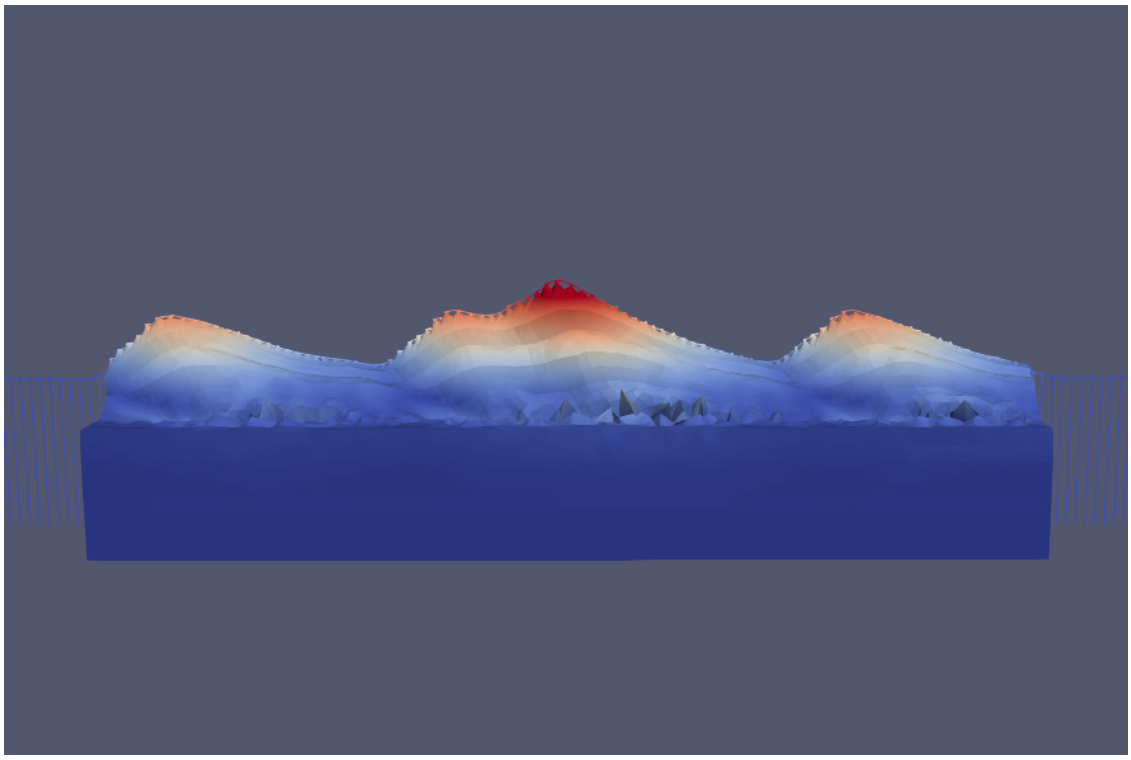

Dynamic soil response to high speed rail

Master's thesis in the Master's Programme Structural engineering and building technology

Simon Jobäck
Hanan Sabri

DEPARTMENT OF ARCHITECTURE AND CIVIL ENGINEERING
DEVISION OF GEOLOGY AND GEOTECHNICS

CHALMERS UNIVERSITY OF TECHNOLOGY
Master's thesis ACEX30
Gothenburg, Sweden 2025

MASTER'S THESIS ACEX30

Dynamic soil response to high speed rail

Master's Thesis in the Master's Programme Structural engineering and Building technology

Simon Jobäck
Hanan Sabri

CHALMERS
UNIVERSITY OF TECHNOLOGY

Department of Architecture and Civil Engineering
Division of Geology and Geotechnics
CHALMERS UNIVERSITY OF TECHNOLOGY
Gothenburg, Sweden 2025

Dynamic soil response to high speed rail

Master's Thesis in the Master's Programme Structural engineering and Building technology

Simon Jobäck
Hanan Sabri

Supervisor: Tara Wood, Head of Sustainability and Innovation at Ramboll
Supervisor: Dawn Yun-Cheng Wong, Division of Geology and Geotechnics
Examiner: Jelke Dijkstra, Division of Geology and Geotechnics

Master's Thesis 2025
Department of Architecture and Civil Engineering
Division of Geology and Geotechnics
Chalmers University of Technology
SE-412 96 Gothenburg
Sweden
Telephone +46 31 772 1000

Cover: A figure representing dynamic displacement in a 3D model.

Department of Architecture and Civil Engineering
Gothenburg, Sweden, 2025

Dynamic soil response to high speed rail

Master's thesis in the Master's Program Structural engineering and Building technology

Simon Jobäck

Hanan Sabri

Department of Architecture and Civil Engineering
Division of Geology and Geotechnics
Chalmers University of Technology

ABSTRACT

Dynamic effects create many difficulties in the construction of railways in the soft soil of western Sweden. Soft soil has a low critical speed and amplifies dynamic forces. Sweden's planned expansion of the rail network and the desire to increase the speed of trains are in need of an easy and efficient method to estimate dynamic responses. This study uses the ROSE and STEM numerical models to obtain the dynamic displacements under these conditions. Both models are open-source, and fully model the train-track interaction to provide an accurate distribution of the forces. Analyses are performed for natural transition zones and at higher velocities that amplify dynamic effects. The results indicate that the dynamic amplification is much higher for a sudden transition than for more gradual cases and that higher speeds increase dynamic displacement. Soil improvements are also analyzed and resulted in a very small area ratio for the lime cement columns to meet the requirements. To implement these complex conditions, the uncoupled method used in ROSE is too simplified. The determination of soil spring stiffness used for ROSE is inadequate when there are multiple soil layers. For future use of the models, a different method is recommended. However, STEM is capable of modeling more complex models and dynamic effects.

Dynamisk jord respons från höghastighetståg

Examensarbete inom masterprogrammet Konstruktionsteknik och byggnadsteknologi

Simon Jobäck

Hanan Sabri

Institutionen för arkitektur och samhällsbyggnadsteknik
Avdelningen för Geologi och Geoteknik
Chalmers Tekniska Högskola

SAMMANFATTNING

Dynamiska effekter skapar många komplikationer med järnvägskonstruktioner i de lösa jordarna i västra Sverige. Lös jord har en låg kritisk hastighet och amplifierar dynamiska krafter. Sveriges expansionsplan av järnvägsnätet och önskan till att öka hastigheten behöver en enkel och effektiv metod för att beräkna dynamisk respons. Denna studie använder analysmetoderna ROSE och STEM för att beräkna den dynamiska förskjutningen under dessa förhållanden. Båda modelerna har en öppen källkod som modellerar interaktionen mellan tåg och räls för att ge en noggrann fördelning av krafter. Analyser utförs för naturliga övergångszoner och högre hastigheter som amplifierar dynamiska effekter. Resultatet indikerar på att den dynamiska amplifikationen är mycket högre för en plötslig övergång än en gradvis övergång, samt att högre hastigheter ökar dynamisk förskjutning. Jordförstärkning analyseras även och resulterade i stora avstånd mellan kalkcementpelare som klarar kraven. För att implementera dessa komplexa förhållanden är den frikopplade metoden som används i ROSE för simplifierad. Framtagandet av jordens fjäderstyvhet som används i ROSE är otillräcklig. För den framtida användningen av modelen rekommenderas en annan metod. Däremot kan STEM modellera mer komplexa system och dynamiska effekter.

Contents

List of Figures

List of Tables

Preface

This thesis would not have been possible without the help of all the wonderful people who have supported us in the process. We would like to give special thanks to our supervisor Dawn Yun-Cheng Wong for all the great help and guidance. Without her we would not have been able to run the models. We would also like to thank our examiner Jelke Dijkstra for his expertise, direction and critiques.

Further thanks goes out to our industry supervisor Tara Wood at Ramboll for her support alongside the other colleges at Ramboll for their welcoming attitude and aid during the project.

1 Introduction

Sweden is experiencing a major expansion of its high-speed rail network, both geographically and in train speeds. An increase of train speeds creates greater dynamic responses of the soil. Railway induced ground vibrations can give rise to stability issues, material degradation and derailment (Hall et al., 2023). With the expansion of high-speed rail, the dynamic soil response of railways becomes a more critical factor. An appropriate analysis method is needed to accurately assess the impact due to dynamic soil-structure interaction. This thesis investigates the numerical codes ROSE and STEM to determine their utility in soil dynamic railway analysis.

1.1 Background

Ground vibrations from railways are generated when a moving cart wheel of is in contact with the rail (Esveld, 2001). Repeated dynamic loading cause degradation of the track and increase the need for maintenance. The contact creates two different forces, a quasi-static force and a dynamic force. Quasi-static forces are dependent on the weight of the train and primarily influence an area up to one-quarter of the wavelength from the source (Ouakka et al., 2022). The vibrations are then generated by the track deflections due to the quasi-static forces. Dynamic forces are dependent on speed, where higher velocities increase the amplitude of train-induced vibrations generated in the soil. These forces are dependent on differential rail displacement that can be influenced by transition zones, soil support conditions and irregularities. There are also dynamic effects dependent on wave propagation in the soil relating to the critical speed (Krylov, 2000.The quasi-static and dynamic forces create stress patterns in the soil (J. P. Wolf, 1985, Hall et al., 2023). The stress pattern forms in the soil under the wheels and when the train moves it generates vibrations from the dynamic loads.

To estimate the dynamic soil response, numerical methods are most common due to the complexities of the systems. Two such methods are ROSE and STEM (Noordam and Zuada Coelho, 2024),(Coelho et al., 2023). The numerical models are open-source and Python-based. ROSE creates a train-track interaction model that can output the dynamic response and track degradation. The model uses the Winkler method, for soil spring stiffness and damping. STEM instead uses three dimensional finite element modeling to compute the dynamic response of more complex systems and geometries.

1.2 Case study

To analyze Swedish conditions, a case study is conducted on the Högsjö bypass. Before investigating the Högsjö case, a validation study is conducted on Malmbanan due to available experimental data. The Högsjö bypass is 2.2-kilometer-long and part of a larger project to increase capacity of “västra stambanan”, which is the main railway track through central Sweden. The main complication of the area are long stretches of peat (Trafikverket, 2024). This can cause problems due to low soil stiffness with large quasi-static deformations. Further, the transition zone between the low stiffness peat and stiffer surrounding soil could cause vibrations from differential stresses (Zuada Coelho and Hicks, 2016).

1.3 Aim

The aim of this thesis is to study two numerical models and compare their applicability. The thesis investigates the differences of using a model with and without wave propagation. This is done using Swedish train and soil parameters. In addition, the project aims to investigate soil improvement, transition zones, velocities and their impact on soil dynamics in the two models.

1.4 Delimitations

The thesis investigates the short-term dynamic response of railways in two case studies. Long-term dynamic effects such as settlement and degradation of the track are therefore outside the scope of the study. This is because a linear elastic soil model is adopted in this study and the accumulated pore water pressure is not considered. The strain dependence of stiffness and damping in soil is also not considered in the thesis.

1.5 Societal, ethical and ecological aspects

The thesis focuses on the mechanical response of the built-up infrastructure, but vibrations also have a human impact that needs to be considered. Vibrations are known to have effects on humans and animals, where specific vibrations of different amplitudes and frequencies can have a negative effect and cause disturbance and health problems. In addition, the maintenance of railways can become very costly due to degradation caused by ground vibrations. Maintenance is not only costly, but can cause a disturbance in traffic and the surrounding area.

2 Theory

The dynamic response of the soil to the railway traffic is dependent on several factors including the vehicle, track, and soil (Esveld, 2001). Vibrations arise from the interaction between the systems. The chapter describes the scientific understanding of railway vibrations along with the different methods used to model these systems.

2.1 System modeling methods

Ground vibrations caused by railway traffic have several different modeling methods (Kouroussis et al., 2014). Most methods use some type of numerical calculation either through a commercial software or code built for the situation. A code built to model the interaction between different subsystems is needed to couple the parts. The three most commonly used subsystems are soil, track and vehicle model. Different method has these systems interact in various ways or in some be separated and use the output as input to the other subsystems. For information about the soil models used in this chapter, see appendix A.

The vehicle is often modeled as a system of masses, springs and dampers or as a moving load. The use of moving load to simulate the train is a simple method used in reports by Hall et.al (2023), Powrie et.al (2007) and Sheng et.al (2006). These reports have a large focus on the soil and track system, and modeling the vibrations in these subsystems. The models are limited in being unable to observe dynamic effects since a constant moving load has no way of generating a dynamic response. Some reports such as that by Brien and Rizos (2005) uses the moving load model as a proof of concept for the soil model they utilize. Lu et.al (2006) and Yang et. al (2003) makes the moving load have dynamic effect by having a variance in the load over time. Lu introduces a random variation based on probabilities that can be found in real trains. Yang instead has a periodic variance introduced by a frequency.

To more accurately model dynamic loading and vehicle-track interaction, several methods have been developed which include a vehicle model (Kouroussis et al., 2014). The most simplified vehicle model consists of a bogie connected to a wheel with a spring and a damper used in reports by Galvín et.al (2010) and Connolly et.al (2013). This model works well for modeling the impact in the soil, but does not account for the differences between the wheels of a cart or for the combined effects of multiple carts. To account for different loads in individual wheels, a vehicle model with a full bogie is needed. This is done in another report by Galvín et. al (2010) and by Nielsen & Igeland (1995). The mass-spring vehicle model can be further increased in complexity by modeling the cart with both bogies and all wheels, all connected by springs and dampers. This is done in a paper by Lamprea-Pineda et. al (2022) which simulate the whole vehicle.

The mass-spring model does not consider inertia or any form of rotation. Because of this, Sheng et. al (2003) and Kouroussis & Verlinden (2013) created a multi body system for the spring-based vehicle models. For these models, the shape of each part alongside their relative displacement has an impact on the modeling. Dynamic effects therefore become more pronounced and can be more accurately modeled.

The vehicle model can be coupled or uncoupled with the rest of the model. Connolly et.al (2013) models the system so that the soil and vehicle are completely separated

while both have the rail integrated. This means that most of the dynamic effects can be accounted for while the impact of soil vibration on the vehicle is discounted. Gavin et.al (Galvín, François, et al., 2010, Galvín, Romero, and Domínguez, 2010) instead couples the whole system together through a program where each part is a simpler model. Sheng et.al (2003) along with Kouroussis & Verlinden (2013) use separate models for each part while keeping the complexity high for each. The models were coupled through the input of the generated loads.

The track system models the connection between the vehicle and the track(Kouroussis et al., 2014). The contact between wheel and rail is most commonly modeled as a Hertzian spring (Kouroussis et al., 2014, Connolly et al., 2013,Galvín, François, et al., 2010, Nielsen and Igeland, 1995). This is a good approximation since these two elements are in contact without anything to couple them. The rail is most commonly modeled as a beam element. If shear is not considered the Euler model is often used as in Sheng et.al (2003) and Lu et. al (2006). This adequately describes the behavior for the full structure if the soil model used is non-shear-strain dependent. To account for the shear force in the rail, Timoshenko beams can be used as in Nielsen & Igeland (1995) or Connolly et. al. (2013). Alternatively, the Hughes-Liu beam method can be used, which is done by Wang & Markine (2018).

For the coupling of the rail to the soil, the sleepers and sometimes rail pads are modeled (Kouroussis et al., 2014). When only vertical displacement is considered, spring-mass systems are a computationally efficient way of modeling these parts, which is the method used by Hall (2003) and Sheng et.al (2003). Several more methods such as those used by Wang & Markine (2018), Kouroussis & Verlinden (2013) and Fernándes-Ruiz et.al (2021) incorporate a spring for the railpad but have different models for the sleeper. Kurossis & Verlinden (2013) use a mass spring system for the whole track due to the focus on the soil and vehicle model. The report by Fernándes-Ruiz et.al (2021) uses a similar method but instead of discrete sleepers one continuous element is used. This method gives roughly the same result with only a slight loss of accuracy. Wang & Markine (2018)use a model which extend the finite elements to the sleepers with each sleeper containing multiple elements, this requires more computational power, but the coupling is automatic.

Soil modeling methodology is variable depending on (Kouroussis et al., 2014). A Winkler based soil model requires far less computational power than most other methods. Today, the Winkler model is seldom used as the only soil modeling method for a project, but rather as a complement or in parts of the system to speed up the computation. Nielsen & Igeland (1995) use Winkler springs for the subsoil while modeling the ballast as a viscoelastic foundation. Hall (2003) uses these springs as a comparison with a more complex method. An even less computationally demanding method is described by Thomson et. al (2019). They used analytical wave propagation method which should only be used for simple geometries.

Finite element modeling (FEM) is a more computationally demanding calculation method that has wide use in dynamic soil modeling of rail (Kouroussis et al., 2014). Wang & Zeng (2004) present a two-dimensional simplification of this method. This is done by modeling a cross section of the system with the elements having an assumed infinite length in the direction of the train. This is done since the vibration mechanism is the focus and the added complexity of three-dimensional modeling is unnecessary. Yang

et. al (2009) utilize a similar 2D method for analyzing the dynamic stress of ballast. The model focuses on integrating the vehicle load and rail system along with vertical stress. Using an extra degree of freedom in the track-direction alongside a changing load Yang et. al (2003) approximates 3D effects in a 2D system. This creates a 2.5 dimensional FEM model which saves on computational power while still somewhat accounting for 3D effects. This requires an assumption of a fully uniform soil structure over the length of the rail. The model is based on creating a 2D calculation for each wavenumber (Galvín, François, et al., 2010).

The 2.5D finite element model can be combined with a boundary element model (BEM) to better model wave propagation at large offsets. Since this method works in infinite domains (Kouroussis et al., 2014). Galvín et. al (2010) uses the benefits of both FEM and BEM to combine and couple a 2.5D system. This was done in half-space to model domains too large for the traditional methods. The model can also be more clearly split between BEM and FEM which is done in the study by Sheng et.al (2006). In this report the track elements are finite elements, and the soil is modeled as boundary elements. This is done to increase computational speed as BEM is less computationally demanding than 3D FEM but more accurate than 2D FEM. The boundary element method can also be utilized for fully 3D problems as in Galvín et.al (2010). This method has the drawback of not working in complex geometries.

Fully 3D models can also be incorporated in the finite element model (Kouroussis et al., 2014). Depending on the complexity of the model, the finite element model can have different parameters for each element and in all directions. The system can be fully coupled, and absorbing boundaries can be added for accuracy at boundaries. The main drawback of this method is the large computational power it needs. Hall et. al (2023), Fernándes-Ruiz et.al (2021), Wang & Markine (2018), Kouroussis & Verlinden (2013) along with Powrie et.al (2007), all use 3D finite element method in slightly different ways.

2.2 Vibration mitigation

In order to reduce the negative effects of vibrations, mitigation measures can be employed (Ouakka et al., 2022, Ouakka et al., 2021). These measures can be applied to different parts of the railway system, such as the vehicle, track and transmission path. Generally, ground vibrations are assessed according to each country's standard which determines where mitigation measures are needed (Ouakka et al., 2021). Most standards differentiate between new and existing rail.

There are several mitigation methods applied on the vehicle(Ouakka et al., 2022, Ouakka et al., 2021). One of the causes of excessive vibrations is due to irregularities in the wheel and therefore the roundness of the wheels, resilience and maintenance are of importance. Irregularities found in wheels can be due to the manufacturing processes, but also a result of repeated high frequency loading (Ouakka et al., 2021). Another improvement is to reduce the mass connected to the suspensions, wheels and bogies. This measure can be done by optimizing the shape of the cross section and/or the material for reducing vibrations (Ouakka et al., 2022). This can be difficult since it has clashing optimizations compared to the dynamic design of the vehicle, safety criteria and internal comfort. Therefore, other mitigation measures are often preferred.

The stiffness of the track is a crucial factor for track vibrations (Ouakka et al., 2022).

Low stiffness causes an increase in deformations in the track foundation and if the stiffness is too high, it generates corrugations. The stiffness requirements of the track are based on the type of traffic it will be used for, but als o on the country where the track is located. Therefore, elements such as rail, rail pad, rail fastener sleeper, ballast and overall track irregularities are crucial to the formation and propagation of vibrations (Ouakka et al., 2022, Ouakka et al., 2021). The choice of rail and proper alignment of the rail to minimize irregularities in the track are mitigation measures. Another alternative is an embedded rail system and the use of elastic materials between connections to reduce vibrations. Vehicle mitigation is often considered more difficult compared to that implemented on the track.

Generally, how effective a track mitigation is is characterized by a transmissibility curve. The force transmissibility of a viscously damped single degree of freedom system as a function of frequency and damping ratio Ouakka et al., 2021). The curve is divided into three zones that determine the effect of the mitigation measure, see the figure 2.1. In he first zone in which the transmissibility is close to one, the mitigation measure has no effect. In zone 2 where the transmissibility value is greater than one, the mitigation measure has a negative effect. Lastly, in zone 3 the which has a transmissibility value lower than 1 the mitigation has a positive effect. Based on this curve different track mitigation's are evaluated.

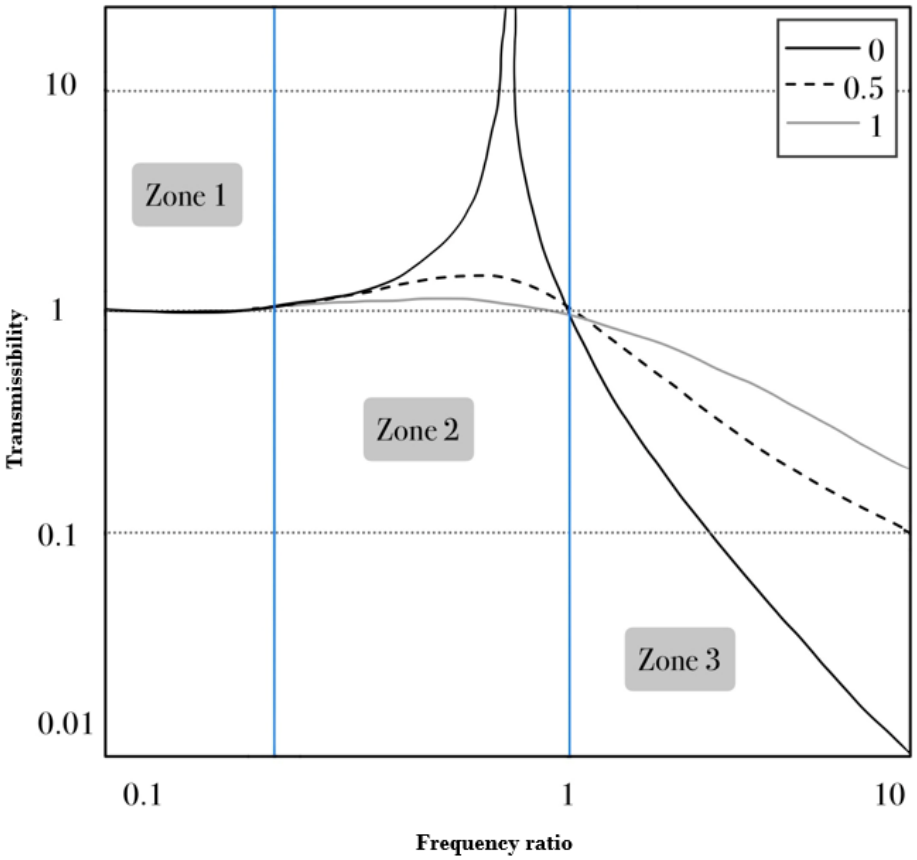

Figure 2.1: Transmissibility curve of different damping ratios. (from Ouakka et al., 2022).

Improving the engineering properties of weak soil is one way to mitigate track vibration problems, by improving the transmission path (Ouakka et al., 2022). By changing the geotechnical properties of the soil, ground vibrations can be mitigated. One common method is ground improvement, which includes lime modification, jet grouting and soil replacement. These methods improve the soil stiffness, bearing capacity and the soils absorption capacity. Since the soil characteristics has a direct relation with wave propagation a reduced soil coherence also reduces vibrations. The embankment is another factor that has an impact on the transmission path (P. J. Wolf and Deeks, 2004). An embankment will keep the track horizontally aligned and minimize surface unevenness, it will also have a significant effect on the vibration transmittance from the track. Vibrations can transmit to a further distance in the soil from the track if the track is not placed on an embankment.

Lime cement columns

Lime cement columns, constructed using dry deep mixing method, is a common ground improvement method used in Sweden (Wong et al., 2024). This method increases stability in soft soils and mitigates deformations in geostructures. The method is to inject the dry binders lime and cement into the ground. These are mixed and formed into lime cement columns using compressed air. The dry deep mixing method can be used to improve both inorganic and organic clays (Hov and Larsson, 2023) and is commonly used under embankments and at the bottom of reinforced deep excavations (Wong et al., 2024). When this method is used for railway infrastructure, the mitigation of vibrations and settlements is more important than the ultimate capacity. Shear strength is often used as the basis for the design of lime cement columns. The improved soil is assumed to have ideal elastoplastic behavior, where both the critical shear stress and the yield stress, determine the elastic part in this case (Moritz and Karlsson, 2014). The specific type and amount of binder are estimated by axial laboratory experiments.

2.3 Cone method

Cone model is a method that can be used to include effects of wave propagation in the emerging stiffness of the surface. The concept of the cone model is that a load is applied to a circular foundation or a disk on the surface of an elastic homogeneous half-space (Khakpour and Hajialilue Bonab, 2018). The force-displacement relation of the disk in the half-space and its dynamic stiffness is determined by prescribing the displacement of the disk and then the corresponding interaction force on the disk is calculated (P. J. Wolf and Deeks, 2004). The half-space under the disk is considered as a truncated semi-infinite bar. The area of the bar varies with depth with the same material properties as the half-space. The load applied to the disk on the surface of the half-space creates stresses in the half-space that increase with depth.

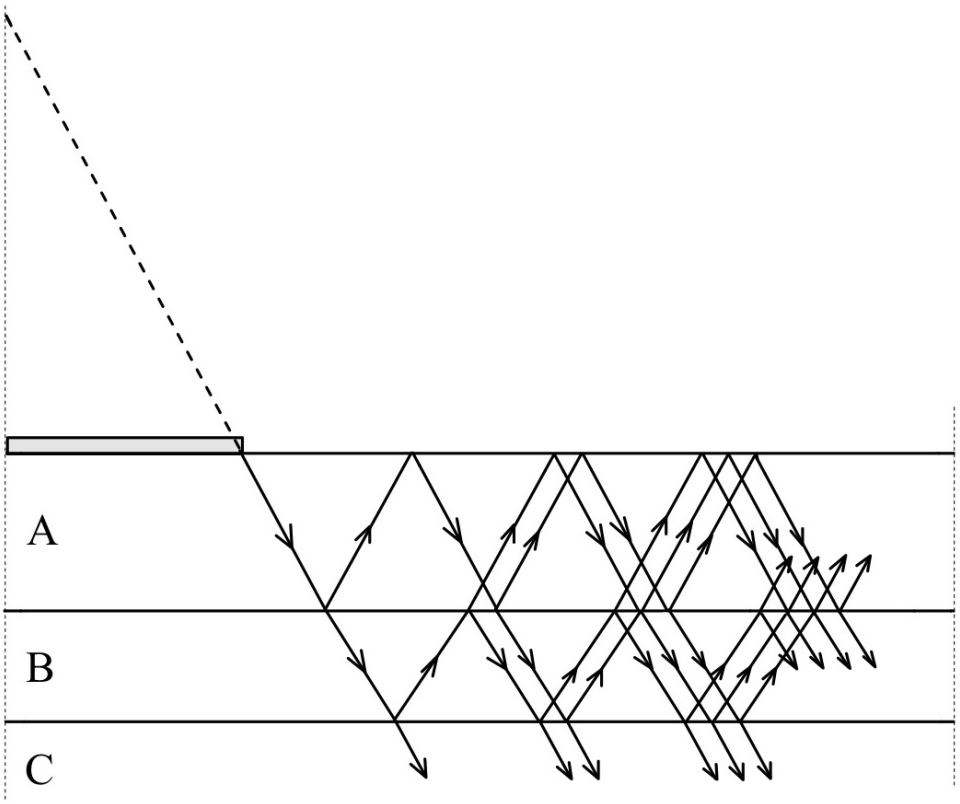

Figure 2.2: Wave propagation through multiple soil layers using cone model. (from P. J. Wolf and Deeks, 2004).

A wave propagates, initially from the disk area and downward through the cone in the half-space (P. J. Wolf and Deeks, 2004). This cone is considered the initial cone, and the cross-sectional area of the cone increases infinity in the same direction in which the wave propagates. If the half-space has layers, the wave encounters material discontinuity. The wave corresponds as an incident wave in the layer interface and creates two waves. One wave is reflected upward and the second is refracted downward through the initial cone. These two waves will again reflect and refract as incident waves when encountering other material discontinuities. A superimposed wave pattern can be formed for a site with different layers up to a certain stage and this is done by tracking each reflected and refracted incident wave continuously. Figure 2.2 represents the cone model with a symmetry line, where A, B and C are soil layers in which the waves propagate.

2.4 Critical speed

Critical speed describes the phenomena where the ground movements from wave propagation and direct ground movements from the train amplify through interaction (Krylov, 2000). This phenomena reaches its culmination at the critical speed where the dynamic amplification factor is at its peak. After this the amplification decrease. Railway analysis for lower speeds can therefore be seen as quasi-static until a certain speed (Norén-

Cosgriff et al., 2018). In the Swedish standard the speed at which dynamic effects and critical speed should be investigated is at 160 km/h and above (Karlsson and Moritz, 2016). The effects of critical speed are larger for softer soil since the wave propagation velocity is lower (Fernández-Ruiz and Pereira, 2024). This results in soil improvements being a good mitigating effect for the amplification caused near critical speed. The amplification starts to occur well below the critical speed with a gradual increase with velocity until the critical speed is reached (Norén-Cosgriff et al., 2018).

2.5 Transition zones

Transition zones are some of the most critical areas for soil dynamics, experiencing substantially large degradation and vibrations than a uniform track (H. Wang and Markine, 2018). For an area of the track to be defined as a transition zone, it needs to have a significant difference in stiffness over a short distance. The most distinctive transition zone is when the track changes from an embankment on soil to that of a built structure, such as a bridge. If no mitigation measures are enacted, the stiffness difference can be several magnitudes larger from one sleeper to the next. Most transition zones are not as definitive. Other examples are changes in the subsoil profile, rail joints and switches (Dahlberg, 2010). These either observe a smaller difference in stiffness or distribute the change over a larger distance.

Settlements in transition zones are differential, with the stiffer parts experiencing a lower degree of relative settlement (H. Wang and Markine, 2018). This difference in settlement causes an acceleration in the wheel increasing the dynamic load in those areas Nasrollahi et al., 2023. The differential settlement also causes further settling mechanisms in the ballast through frictional sliding caused by the new gradient of the embankment. More abrupt changes in settlements can have further problems with loss of wheel-track contact (Puzavac et al., 2012). If this occurs the stress increases due to the lower contact area and a sudden contact force is created when wheel-track contact is resumed. Rapid change in stiffness has a similar but separate effect to the differential settlements. The difference results in changes in the elastic deformation which leads to acceleration and vibrations in the ground.

The increased and redistributed load in the transition zone causes damage to the track due to the lack of train-track interaction and differential settlements (H. Wang and Markine, 2018). When an area of track has started to degrade and experience discontinuities or sudden differential settlement, it expedites the process of degradation. Differential settlements create internal stresses in the track, contributing to degradation. Differences also cause disturbed drainage and penetration of ballast into the subgrade. The negative effects and degradation amplify vibrations in both the train and ground, increasing the discomfort of passengers and possible damage to surrounding structures.

Mitigating measures for transition zones

Reducing the effects of transition zones consists of methods trying to change the stiffness and damping distribution (Sañudo et al., 2016). Changes to stiffness are made to either create a more gradual stiffness distribution, to reduce problems relating to sudden changes in stiffness or to reduce total difference. Increasing the damping of the system impacts the dynamic response, and vibrations of the system reduce the risk of amplification. Mitigation can also be taken to reduce the secondary effects such as degradation.

The main measure taken to reduce the effect of transition zones is increased maintenance, which is costly and could require a track shutdown. In the Netherlands, transition zones require at least 4 times greater maintenance compared to uniform conditions (H. Wang and Markine, 2018).

3 Models

In order to predict the dynamic behavior of the soil, two different numerical methods are used, called ROSE and STEM. ROSE is the simpler of the two methods, utilizing a Winkler spring system to model soil. The 3D model in STEM, instead utilizes meshing to create a space where calculations through different constitutive models can be used. The cart and track model are similar in both, utilizing a mass-spring system to model the constitutive parts.

3.1 ROSE

ROSE is a numerical model based on Euler's beam theory and Winkler's spring method (Noordam and Zuada Coelho, 2024). The model creates a train, track and soil interaction as a system of masses and springs. This is done by modeling the vehicle and track separately, assembling their interaction and generating an uncoupled mesh for the system. Forces are calculated numerically using an equation of mass, acceleration, damping, velocity, stiffness and displacement. By integrating this equation, a list of results is generated in either nodes and/or elements in a time domain.

The vehicle is modeled as a system of masses and springs that includes three parts, the cart, bogie and wheels. In the model the configurations of the three parts are set up according to the specific train model. The connection between the parts is modeled as a system of suspensions where the cart is connected to the bogie by a spring with stiffness and damping. The bogie is connected to the wheels similarly by a spring for each wheel. The cart and the bogie act as masses on the springs and their mass inertia is also included in the model. The vehicle moves along the track by introducing a velocity. See figure 3.1 for a visual presentation of the train-track model.

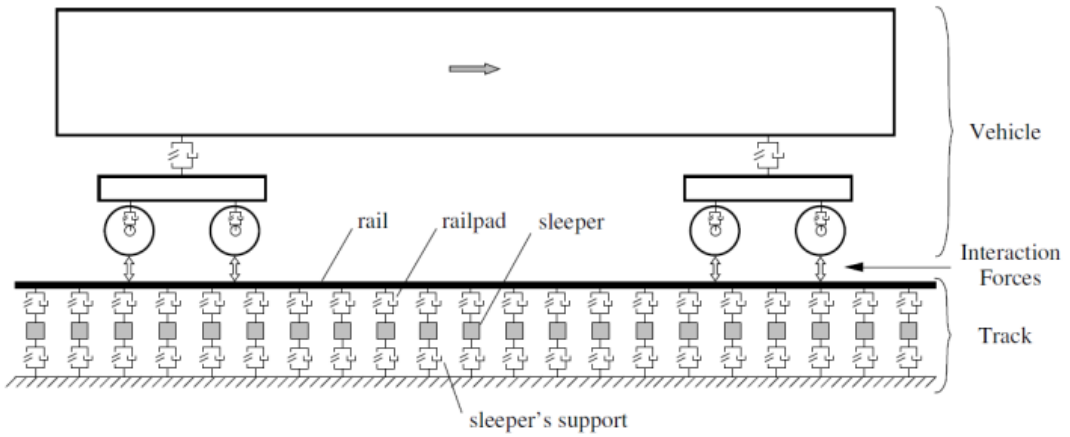

Figure 3.1: Model in ROSE. (from Noordam and Zuada Coelho, 2024).

The track is modeled as an independent mass-spring system which includes the rail, rail pads, sleepers and soil parameters. The rail is modeled as an Euler beam, including its elastic modules, density, poison's ratio, area, and inertia. The Euler beam is set on top of rail pads, where each rail pad is considered as an individual spring with stiffness and damping that is connected to a sleeper. The sleeper which is modeled as a mass and is then connected to another spring which represents the ballast and soil. In figure 3.1 the

ballast and soil are presented as sleeper's support. The geometry of the track is set up as segments where the length of each segment is based on the number of sleepers used, including the spacing between sleepers. The number of sleepers per segment is chosen based on the velocity of the vehicle and the area of interest. The vehicle has to be within the segment during the total duration of the calculation. After assembling the track, a horizontal track geometry is meshed and connected with bottom and side boundaries assigned to the model.

The train-track interaction model assembles the vehicle and track model. The interaction between the wheel and rail is modeled using the Hertzian contact theory. The interaction model also includes Rayleigh damping and radial frequencies. By integrating the assembled model in a time domain, desired results, such as forces and displacements, are obtained. Time integration is set up in two stages, the initial phase and in the calculation phase. This is done to decrease the uncertainty of the initial train-track interaction, where the train is first introduced in the model. The integration is solved through the Newmark time integration method when solving the force equation.

3.2 STEM

STEM is a finite element model which couples the soil, track and vehicle model as a multi body system. The method primarily uses the linear elastic soil method although the model is capable of applying other methods. The linear elastic soil model in STEM uses four parameters, two are used for deformation and two calculate the mass of the soil. The elastic modulus is the main parameter that determines the deformation response of the soil in the vertical direction. Poisson's ratio, together with the elastic modulus, gives the shear modulus through equation 3.1. The density of the soil, along with porosity, are mainly used to calculate the mass of the soil, and therefore the pressure exerted. The method considered as a single phase material.

$$G = \frac{E}{2(1+v)} \tag{3.1}$$

The soil profile is input through the model as different soil layers. These are modeled as 2D objects that are extruded to a specified length. This creates the possibility of modeling different geometries in the directions perpendicular to the rail. For railways this is mainly used for the modeling of inclination for the embankment. Several connected shapes can be placed in the non-track direction, creating a non-uniform layering structure through depth and width. In the direction of the track, different layers can also be created through choice of the starting points for extrusions. The main limitation in this direction is that the extrusion is parallel to the direction of the track. This means that gradual differences along the track such as sloping layers cannot be modeled. The edges of soil layers are modeled with boundary conditions that can be fixed or absorbing in the coordinate axes. Each soil layer is divided into smaller parts by meshing triangular shapes.

The interaction between the rail and soil is modeled using nodes that represent sleepers that exert force on the soil from the superstructure. The superstructure consists of the stationary track and moving cart, both of which are modeled using mass-spring systems. The train is divided into bogie, cart and wheel systems. Each of these has a mass, stiffness and damping. The complete system is shown in figure 3.2. Together, these

parts create a mass-spring system that distributes force down from the cart to the track. The modeling of the superstructure only considers the secondary effects brought to the substructure.

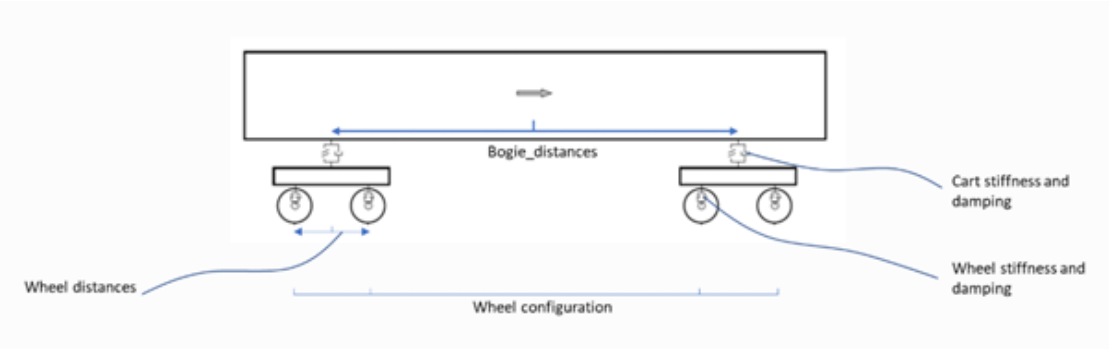

Figure 3.2: Cart model. (from Coelho et al., 2023).

The track is modeled through different methods for each part. The sleepers are modeled as mass-spring systems with dampers. Rail pads are modeled as springs with rotational stiffness and damping. The rail is modeled as a Euler beam with elastic modulus and inertia in different directions. The track uses Hertzian springs to simulate the contact between the wheels and rail. The contact between the soil and track is modeled through sleepers that are springs without stiffness, connected to nodes in the soil and the track. The track can be connected to 1D Winkler springs outside the geometry of the soil. This can be done to replace the 3D modeled soil for increased computational speed. This is required for longer analyses or when multiple carts are added to simulate all parts of the train.

If the regular linear elastic method is chosen for the soil model with constant parameters over time, the Newton Raphson solving method can be used for the calculations with Newmark as the time integration method. In the solving stage, Rayleigh damping and stiffness can also be added. STEM uses Kratosmultypysics (Dadvand et al., 2010) for finite element calculations. The code solves and outputs the nodal displacement, velocity and acceleration as principle unknowns. Irregularities can be added to the rail or wheels to further model dynamic effects.

4 Site description

This thesis studies different railway lines for different types of analysis. Malmbanan is a railway line in northern Sweden that is studied due to having experimental field data on sleeper displacements for two different trains. This makes it a suitable location to test the efficacy and accuracy of the models and calibrate parameters. The second case study is a bypass at Högsjö for Västra Stambanan (Mattsson, 2020). This case is used due to the prevalence of soft peat layers that transitions to stiff outcrop rock that creates natural transition zones. The relatively thin peat layers facilitates certain types of ground improvement of interest to the thesis.

4.1 Malmbanan

Malmbanan is a 500-kilometer long railway line in Sweden that stretches from coast to coast in northern Sweden and Norway (Trafikverket, 2025). The line contains the heaviest traffic in Sweden due to the ore trains that connect the mines of northern Sweden to the coast. These ore trains have an axle load of 30 tons on 750-meter-long trains. In addition to the ore trains, there are passenger trains of the X2000 model. Problems of freezing and thawing are common on the line, experiencing the heavy winters of northern Sweden Nasrollahi et al., 2023). This creates problems with irregularities and differential settlements. Malmbanan is substantially different from most railway lines in Sweden mainly due to the heavy load which creates unique challenges in its construction. The specific area studied is Gransjö located between Boden and Murjek which can be seen in figure 4.1. The area consists of layers of moraine and is a stiffer part of the line with few settlement problems.

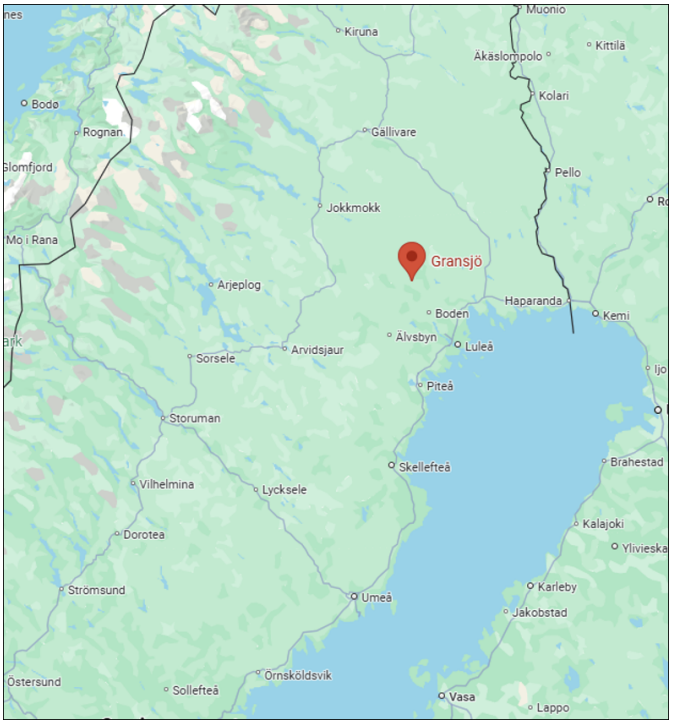

Figure 4.1: The location of Gransjö. (from "Google Maps", 2025)

4.2 Högsjö bypass

The bypass in Högsjö is part of Västra Stambanan between Gnesta and Hallsberg as seen in figure 4.2. The bypass is built to increase the capacity on the line by putting slower trains on this part of the track to let faster trains pass (Trafikverket, 2024). The bypass is 2 200 meters long with several sections that contain unique layering. Some areas are directly on moraine, while others contain layers of peat or mull soil. In some areas there is also outcrop rock.

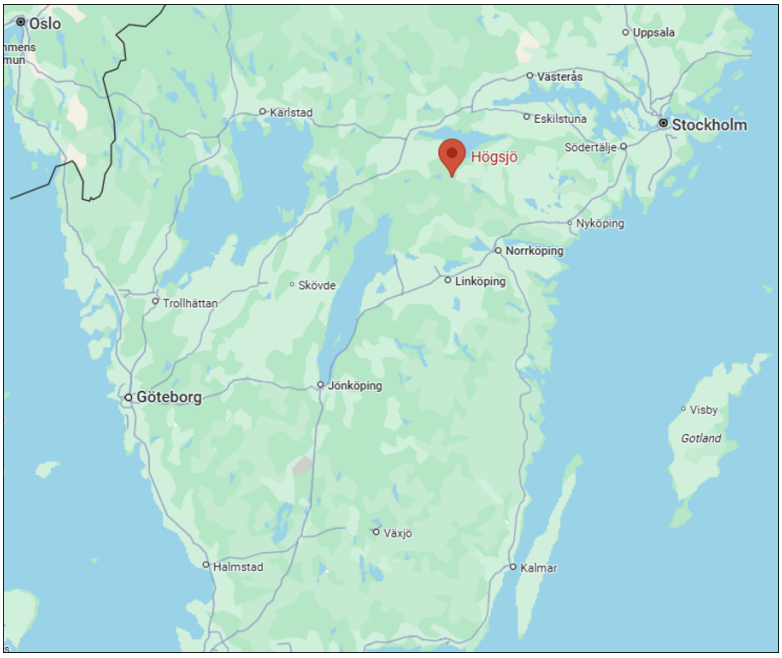

Figure 4.2: The location of Högsjö. (from "Google Maps", 2025)

5 Method

The project consists of two case studies, both of which use two different methods to study dynamic displacement. The cases are Malmbanan which is used to calibrate the models with experimental data and Högsjö which is used to study transition zones, critical speed and soil improvement. For the Malmbanan case two train types are considered, X2000 and iron ore. Malmbanan is used as the control case due to the input parameters being available from previous studies alongside monitoring data of sleeper displacement (Nasrollahi et al., 2023, 2024). Therefore, it is used to calibrate the track stiffness parameters, conduct convergence analysis, and compare between the analysis in ROSE and STEM. The Högsjö case used both models with investigations into the changing dynamics caused by changing parameters of the rail, ballast or complex geometries.

5.1 Malmbanan

Malmbanan is used as a control, based on data from previous studies (Aggestam and Nielsen, 2019; Nasrollahi et al., 2023, 2024. The Nasrollahi 2023 report describes a numerical modeling of Malmbanan which has input data for the rail, train and ballast. This is used as input data for the models in ROSE and STEM. The parameters for the vehicle are shown in table 5.1 and the track in table 5.2. The track is approximated as straight, which means that the case is symmetric and therefore only half of the geometry is modeled. The values in table 5.1 relating to mass, inertia, stiffness and damping are therefore all halved when input to the models. Experimental data from the same site are retrieved from the Nasrollahi 2024 report which is used to compare the numerical results to the real data and fitted parameters. The Malmbanan case is studied with two different trains which have experimental data, an ore train and an X2000 passenger train.

Table 5.1: Parameters for the iron ore train and X2000 used for Malmbanan

Parameter	Iron ore	X2000
Cart mass [kg]	111 000	56 000
Cart inertia [kgm^2]	1 700 000	1 970 000
Cart-bogie stiffness [MN/m]	3.75	0.43
Cart-bogie damping [kNs/m]	10	20
Bogie mass [kg]	800	2 600
Bogie inertia [kgm^2]	730	1 476
Bogie wheel stiffness [MN/m]	30	1.2
Bogie wheel damping [kNs/m]	70	4
Wheel mass [kg]	1 341	1 800
Velocity [km/h]	60	42
Hertzian contact coefficient [N/m]	$9.1 \cdot 10^{-7}$	$9.1 \cdot 10^{-7}$
Hertzian contact power [-]	1	1

Table 5.2: Track parameters for Malmbanan

Rail area $[m^2]$	Rail inertia I_{33} $[mgm^2]$	Rail inertia I_{22} $[mgm^2]$	Torsional inertia $[mgm^2]$
0.00767	30.4	5.1	35.5

Sleeper mass $[kg]$	Rail pad thickness $[m]$	Rail pad stiffness $[MN/m]$	Rail pad damping $[kNs/m]$
150	0.01	110	15

Some parameters required for the models in STEM and ROSE, such as Hertzian coefficients sleeper distances and irregularities, did not have predetermined values. The Hertzian spring coefficient utilized the default values from the code. This gives a suitable approximation for most trains. The sleeper-to-sleeper distance varies within the length of the studied section. Therefore, an iterative analysis is conducted after all other parameters are determined, to find the sleeper distance that corresponds to the experimental data. Irregularities has a separate analysis to test their impact. further, a speed analysis is conducted in ROSE to test how the effect of irregularities changed with velocity.

ROSE

After inputting the respective train parameters and the soil spring stiffness based on seismic tests (Mattsson, 2020), using a semi-analytical cone model (P. J. Wolf and Deeks, 2004) the dynamic analysis is preformed. Soil damping posed no significant changes in the displacement in ROSE. Therefore, an arbitrary value is chosen for the analysis. The analyses in ROSE are conducted together with the analyses in STEM. The soil profile used to calculate the soil spring stiffness for ROSE is the same profile input in STEM. For the determination of soil profile, see section 5.1.3, Determination of soil layers.

To conduct analyses in ROSE a timestep convergence study is conducted to find a suitable timestep. All input parameters remained unchanged except for the timestep that was reduced in each analysis. The average of the absolute deviations of the data points from the mean value of the displacements from all analyses were divided by the maximum displacement value of the analysis with the largest timestep. The quota of the values is given in percentages. See figure 5.1 for the precedential deviation as a function of total number of time steps.

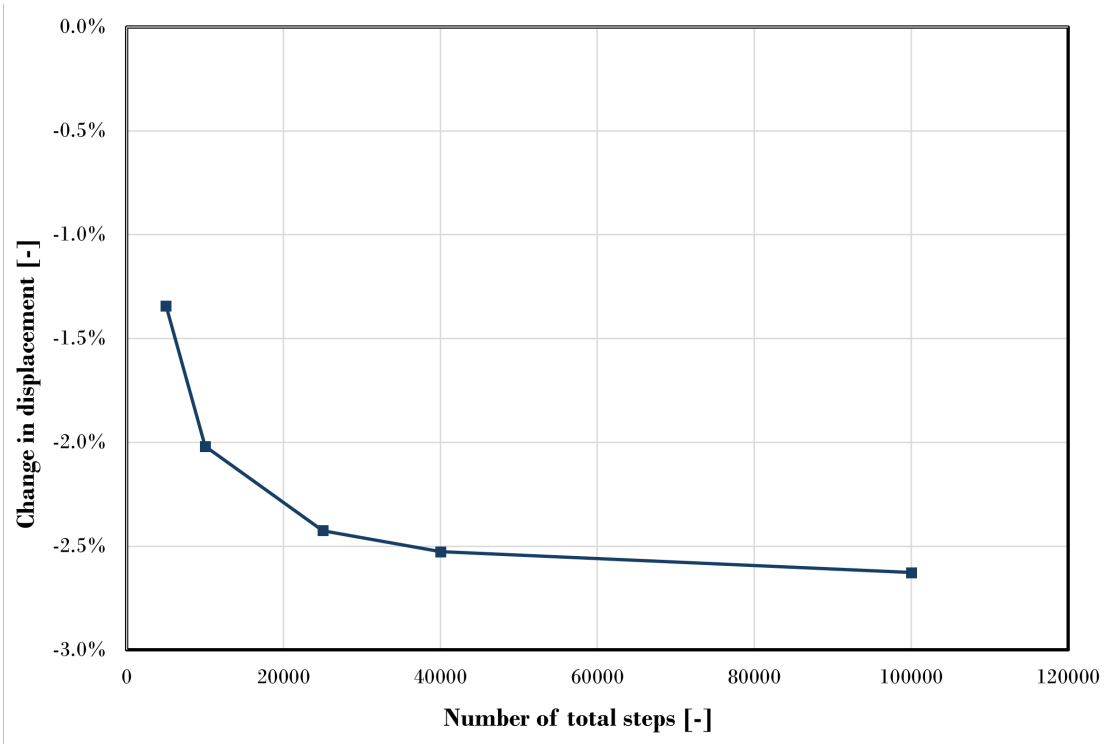

Figure 5.1: Timestep convergence conducted with the iron ore train in ROSE.

According to the timestep convergence analysis conducted within a total calculation of five seconds, it is determined that a total number of forty thousand timesteps is suitable to use. This translates to a timestep of 0.000125 seconds.

STEM parameters

STEM models soil in a 3D environment where the geographical extent, timestep and meshing are limiting parameters that cannot be extracted from field data. In an ideal world all these would be close to infinite but this is countered by a need for computational efficiency. Therefore, these parameters are derived through convergence analyses. Each convergence study is done by using different, more computationally demanding inputs and finding out at which point each parameter is considered adequately. Convergence is measured by the displacement of the rail at a specific point. At each timestep the absolute difference between the displacement of the current and initial parameter is compared. The average of this difference is then calculated, compared and plotted. In an optimal case, this would give an exponentially decaying function. If this is the case, the convergence is taken at the point where the difference is deemed small enough to not have an impact on the results. In other cases, a more specific determination needs to be made.

The parameters a convergence analysis is done for are the geometry of the model, meshing and timestep. The model domain is divided into the three coordinate axes, each with slightly different methodology. The width perpendicular to the track across the surface can easily be obtained through measuring the same point in the model. The depth can only go to a certain point before solid rock is struck. The seismic testing of the studied area found no clear transition between the soil and rock so the iteration continued to the lowest point of the test which is 15 meters. The analysis in the direction of the track

is complicated by the cart always being placed in the center of the model. This means that the node number is different each time the model is run and with the cart moving, the same nodal placement was difficult to find. Therefore, the comparison is not done through one specific node, but the node with peak displacement at each timestep. This occurred at different points on the rail.

Figure 5.2 shows signs of converging through an exponential decay function, although it occurs slowly. The choice of depth is not entirely determined by convergence as the seismic data shows that the modulus increases with depth but the test is finite. Because of these factors, the depth is chosen as 10 meters. The convergence analysis for the distance perpendicular to the track in the horizontal direction is shown in figure 5.3. Since there is no convergence in the outfield, a value of 8 meters is chosen. This is done since no value seemed to be better than any other and this choice saves on computation time. The convergence in the direction of the track is seen in figure 5.4. Here, the value of 60 meters is chosen as there seems to be a periodic change after this length. This analysis does not give the exact value to use in all analyses, since the required length depends on other factors such as speed and train dimensions. Instead, the value is converted to a distance from the edges of the cart to the boundary, which is given a value of 20 meters.

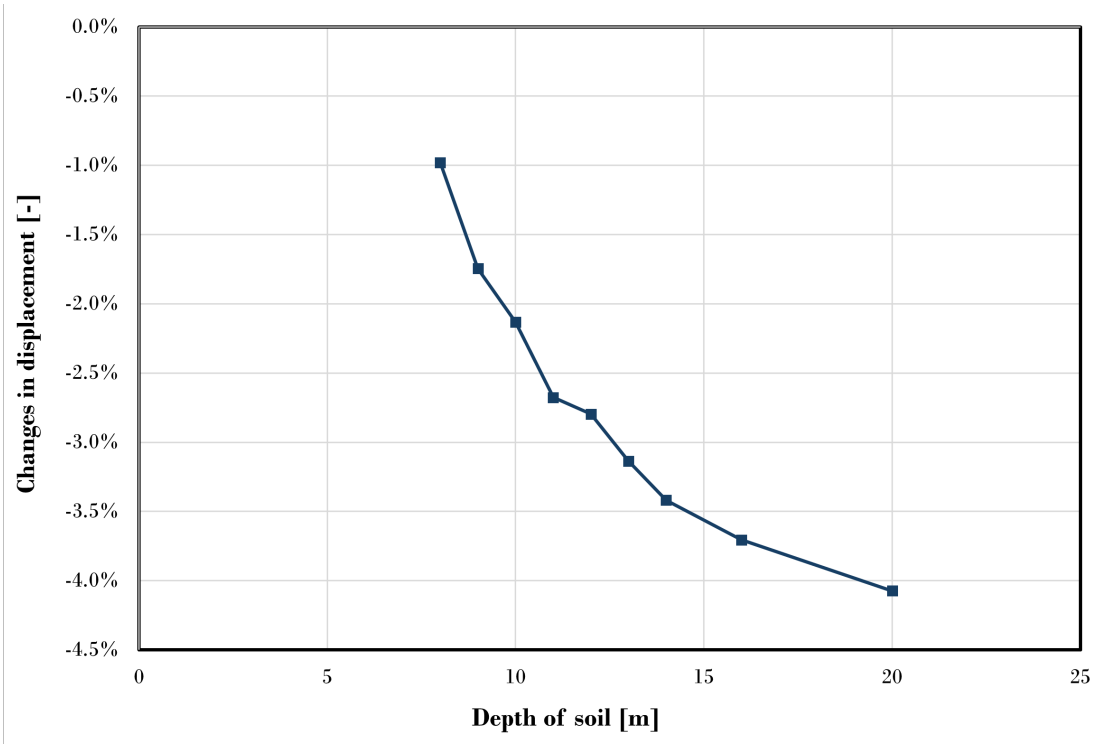

Figure 5.2: Depth convergence conducted with the iron ore train in STEM

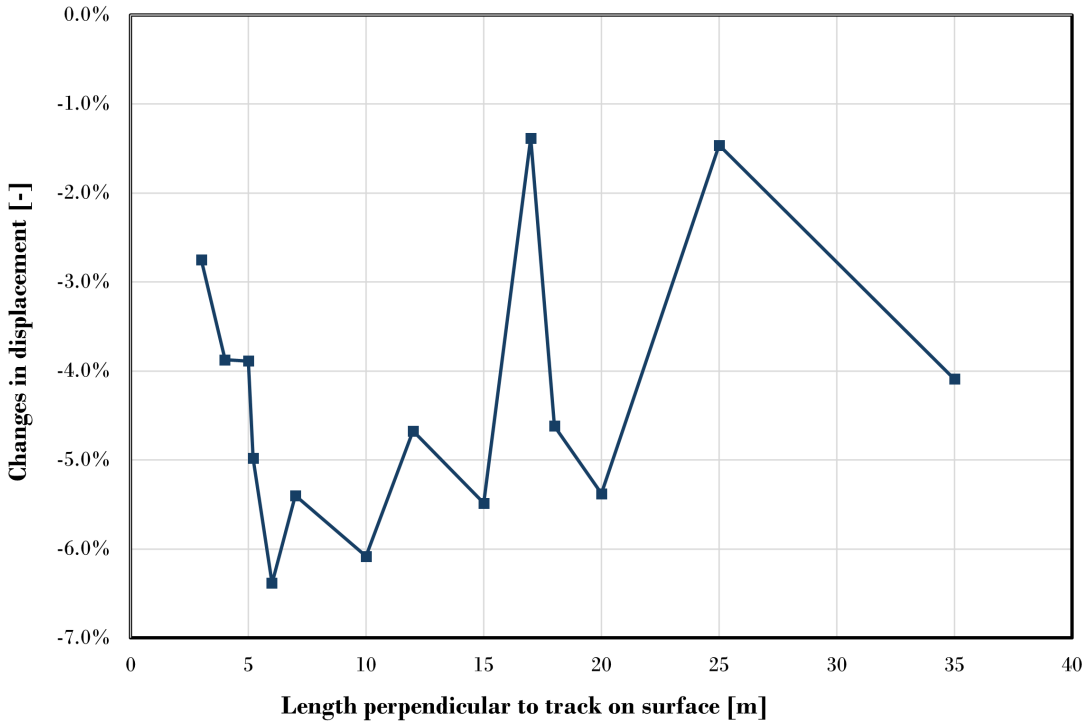

Figure 5.3: Width convergence conducted with the iron ore train in STEM

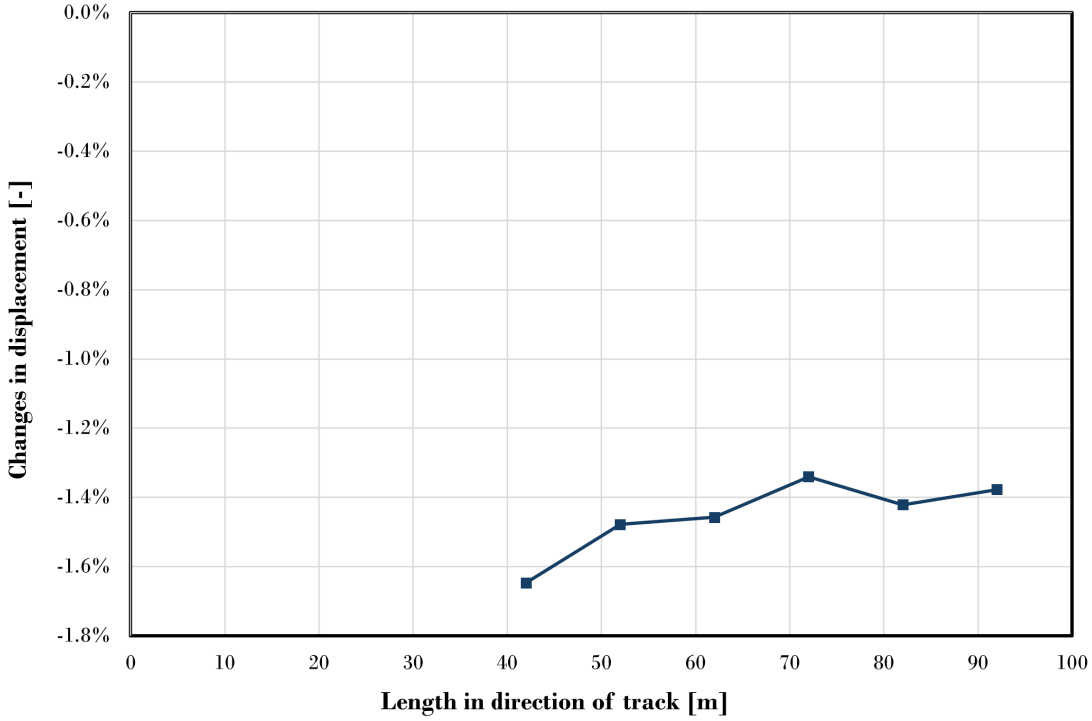

Figure 5.4: Length convergence conducted with the iron ore train in STEM.

Timestep convergence increases the number of steps studied for each iteration, which means that a direct comparison of values is impossible. Because of this, each iteration is a multiple of the first, to ensure that the same timesteps can be compared for all tests.

To determine the number of carts that are modeled it is not a convergence study, but an iterative analysis, which is done in a similar way. It is impractical to model the full train since each added cart requires a larger model to be able to fit within the boundaries. For each added cart the soil model in the track direction is increased in length by one cart. This removes the problem of fewer carts using a relatively larger area and removes the need for part of the train being on Winkler springs.

The timestep convergence is shown in figure 5.5 where the convergence seems to have already occurred due to the small changes between different timesteps. The analysis is done for a 0.5 second time-span which results in the timestep of 0.001 seconds to be used. A larger timestep in the analysis cannot be chosen due to the tolerance of the system. The iteration analysis of the number of carts shows that three or four carts are a reasonable simplification to use for the model. Figure 5.6 shows the analysis compared with the starting number of 2 carts. The analysis indicates a periodic trend and the results are not fully correspondent with what is tested as only the maximum displacement in each moment is tested.

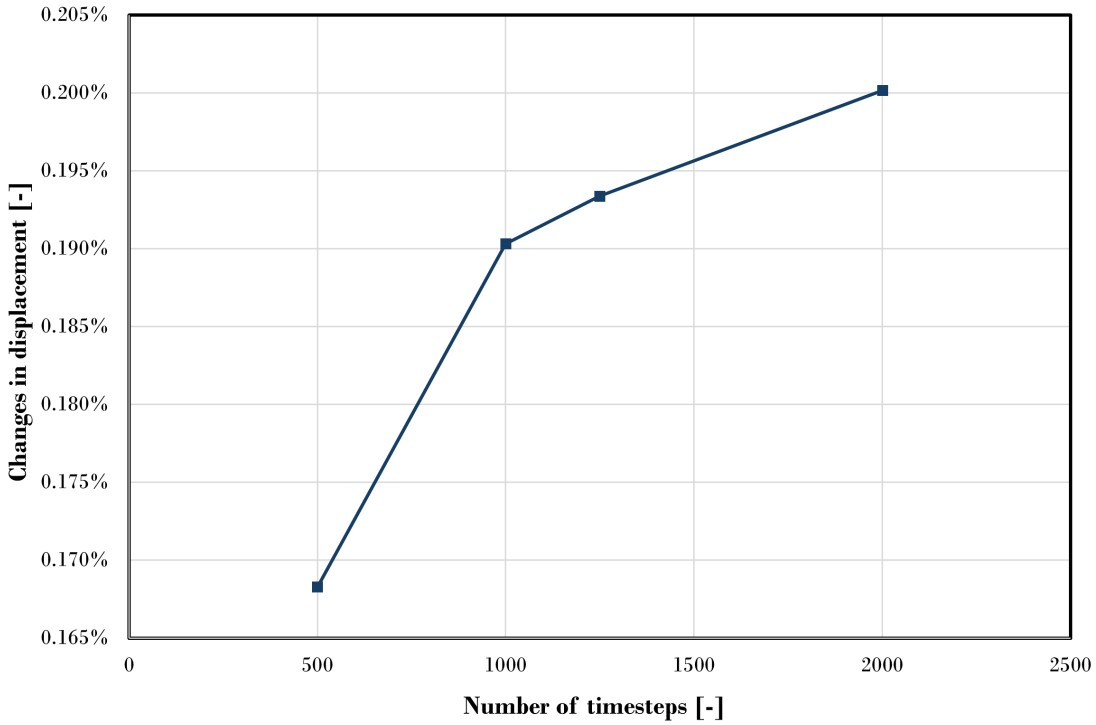

Figure 5.5: Timestep convergence conducted with the iron ore train in STEM.

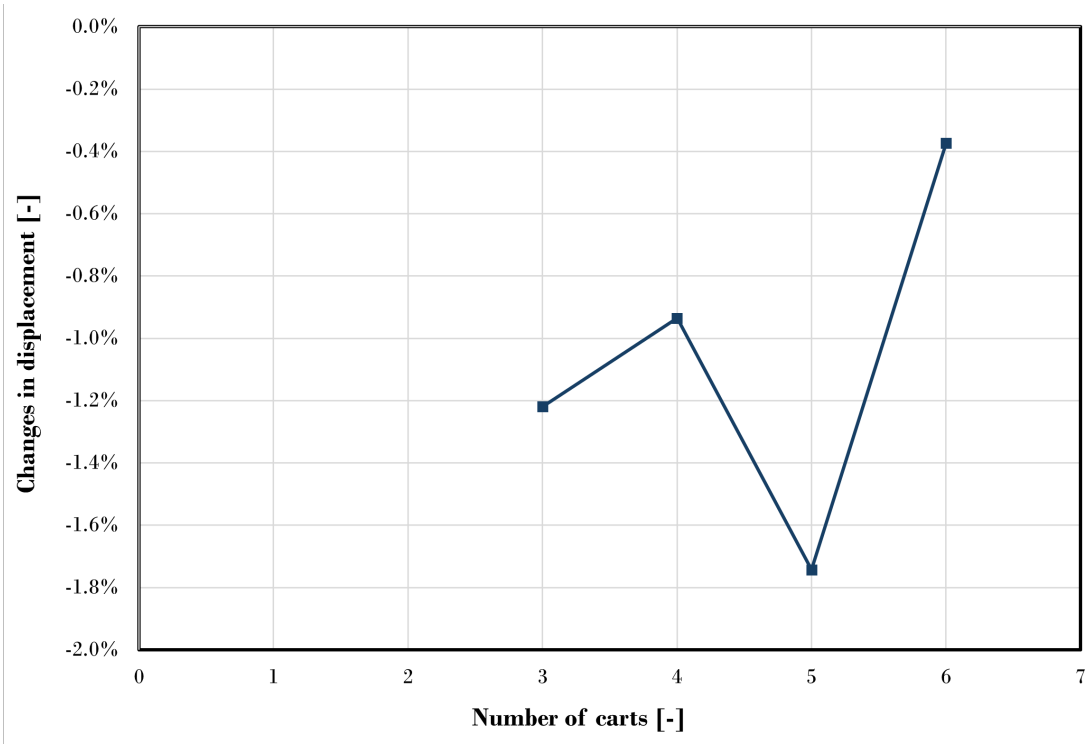

Figure 5.6: Iterative cart analysis conducted with the iron ore train in STEM.

The analysis and convergence of the mesh is impacted by many factors other than the mesh size. The two main factors are the soil layering and sleeper spacing. This interaction makes a mesh convergence difficult since it is dependent on several parameters. The layering thickness is important due to the relation with the aspect ratio to create uniform elements. If the mesh size exceeds the element height, the triangles in the mesh are not the optimal equilateral shape. The second and more critical aspect is the sleeper spacing. These interact with the meshing since STEM models sleepers as nodes. Each sleeper must correspond to a node in the soil and there needs to be a line of nodes through the rail without any elements crossing it. Therefore, the size of the elements connected to the sleeper node is very influential in how the load is distributed. Further, the element size determines the area where the load of the sleeper is distributed. The determination of the mesh size from the interaction of different systems is described in further detail in appendix B. With the analysis from appendix B it is determined that having a mesh size slightly below the sleeper distance creates the best compromise with all considerations, see figure 5.7 for the final meshing of the model. The results from the iterative and convergence analysis are described in table 5.3.

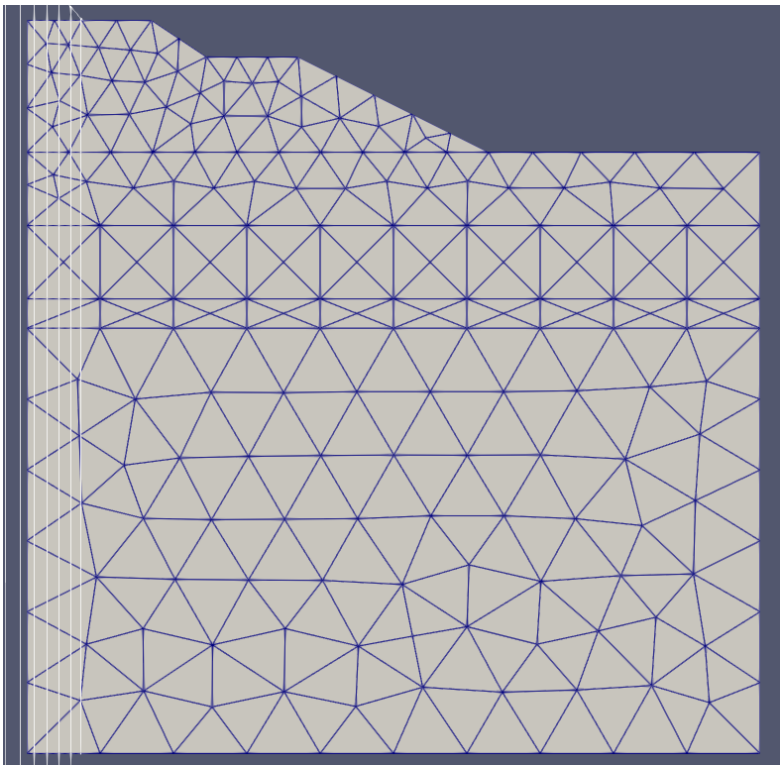

Figure 5.7: The final mesh in STEM for cross section in Area 2

Table 5.3: Varying parameters in STEM

Model length away from cart	20 m
Model depth	13 m
Model width	8 m
Mesh size on top layer	0.6
Timestep	0.001 s
Number of carts	4
Sleeper distance	0.63 m

Since the geometry is finite, boundary conditions are required to model the edges. The bottom boundary is fixed and represents bedrock, the symmetry line uses the symmetrical boundary condition and the boundaries demarcating non-modeled soil are absorbing. The absorption factor of these boundaries is a parameter outside the scope of this study and is therefore set to the default values in STEM. Rayleigh stiffness and soil damping are also left as default values.

Determination of soil layers

The soil parameters of Malmbanan are derived from seismic testing of the site (Mattsson, 2020). These seismic tests are done in a section along the railway. The location of the measured experimental data is within the area of the seismic tests. However, the exact location is an approximation. The tests are done directly on the soil resulting in the ballast not being tested. The ballast is placed on the surface of the soil in the models. Different layers of soil from the tests are used and compared to find the data which

correspond to the measured data. From the shear wave velocity, the elastic modulus is calculated from equation 5.1. The remaining soil parameters required are retrieved from the Nasrollahi 2023 report, where the same layers are measured at a different point Nasrollahi et al., 2023).

$$E = 2\rho V_s^2(1 + v) \tag{5.1}$$

When it is determined which soil layering corresponds to the experimental data in STEM for both the iron ore train and X2000, the same layering is used to determine the spring soil stiffness to use in ROSE. Since soil parameters cannot directly be input in ROSE the determination of dynamic soil stiffness and dashpot damping from the seismic tests is done through a code named Wolf stiffness (P. J. Wolf and Deeks, 2004). The Wolf stiffness code uses a semi-analytical cone model to estimate the soil spring stiffness and damping of a multi layered soil profile. The stiffness and damping are dependent on the dimensions of the sleeper and sleeper frequency, and thus the train speed dependent. The results from ROSE and STEM are then compared.

This method is complicated by the fact that the top layer of the soil along with the ballast layer is 0.3 meters thick. The low thickness makes this layering difficult to model in STEM since the mesh size cannot be larger than the layer thickness. The two top layers are therefore combined, and a new soil parameter is derived for this layer. To retrieve the modulus for the combined layer, the Wolf stiffness code is used. The shear modulus of this layer is iterated until the combined layering gave the same spring stiffness as the original. This layering is used in STEM and the stiffness is used in ROSE to perform the main analyses for Malmbanan. The chosen layering is shown in table 5.4 and parameters for ROSE are shown in table 5.5.

Table 5.4: Soil parameters of Malmbanan

Soil layer	Thickness $[m]$	Density $[kg/m^3]$	Youngs modulus $[MPa]$	Porosity [-]	Poissons ratio [-]
Ballast	0.6	1800	67.5	0.3	0.2
Sub ballast	1	2200	175	0.3	0.3
First subgrade	2.7	1750	337	0.3	0.25
Second subgrade	4.3	1750	800	0.3	0.25

Table 5.5: Soil equivilant spring parameters of Malmbanan

Equivalent soil stiffness $[MN/m]$	Equivalent soil damping $[kNs/m]$
Ballast	0.6

With the soil profile determined the iterative analysis on the sleeper distance is performed. The determination of sleeper distance affected the shape and amplitude of the displacement. A combination of both factors led to a determination of the final sleeper distance as 0.63 meters.

5.2 Högsjö

To study the dynamic effect of low stiffness soil, soil improvements and natural transitions, the Högsjö case is studied. The Högsjö bypass is studied as if it were a track capable of high-speed traffic. Project planning documents (Kruse and Emanuelsson, 2021) are used to retrieve the soil and track parameters. The cart is of an X2000 train with parameters presented table 3.2. Track parameters are shown in table 5.6.

Table 5.6: Track parameters of Högsjö

Rail area $[m^2]$	Rail inertia I_{33} $[mgm^2]$	Rail inertia I_{22} $[mgm^2]$	Torsional inertia $[mgm^2]$
0.00767	30.4	5.1	35.5

Rail pad thickness $[m]$	Rail pad stiffness $[MN/m]$	Rail pad damping $[kNs/m]$	Sleeper mass $[kg]$	Sleeper distance [m]
0.01	150	750	140	0.65

The soil parameters are derived from the geological surveying presented in the project planning documents (Kruse and Emanuelsson, 2021). The density of the layers are given for fill, peat and moraine. The modulus is given for the fill layers and estimated from the testing for the granular subgrade layers. The other parameters are unknown and chosen based on the soil type. The bedrock in the area is granite that is given a characteristic value from a piling manual (Bredenberg, 2000). The governing unknown parameter is the modulus of the peat. To estimate a value for this parameter, reports on the deformation parameters of peat are investigated (Meyer and Olszewska, 2021, Stetens geotekniska institut, 2020). The peat is described as consolidated in the planning documents (Kruse and Emanuelsson, 2021) which results in a higher end estimate for the modulus for the soil. Although the ballast and fill layers are constant in both the geometry and the soil parameters for all areas, the subgrade changes over the length of the track. Therefore, several different subgrade layering are tested and compared.

There are five distinct subgrade layering in the Högsjö bypass described in the project planning documents (Bredenberg, 2000). Four of the areas have measurements of soil parameters for the granular soil. From the measurements, the thickness and modulus of each layer are determined. The cohesive soil layering is described as varying within a span for each area. Therefore, the upper estimate of the thickness of these layers is chosen as it is most critical for this report. One area has a soil layering depicted in the report, while the rest are estimated based on text description of the document. The geographic distribution of the soil layers can be seen in figure 5.8.

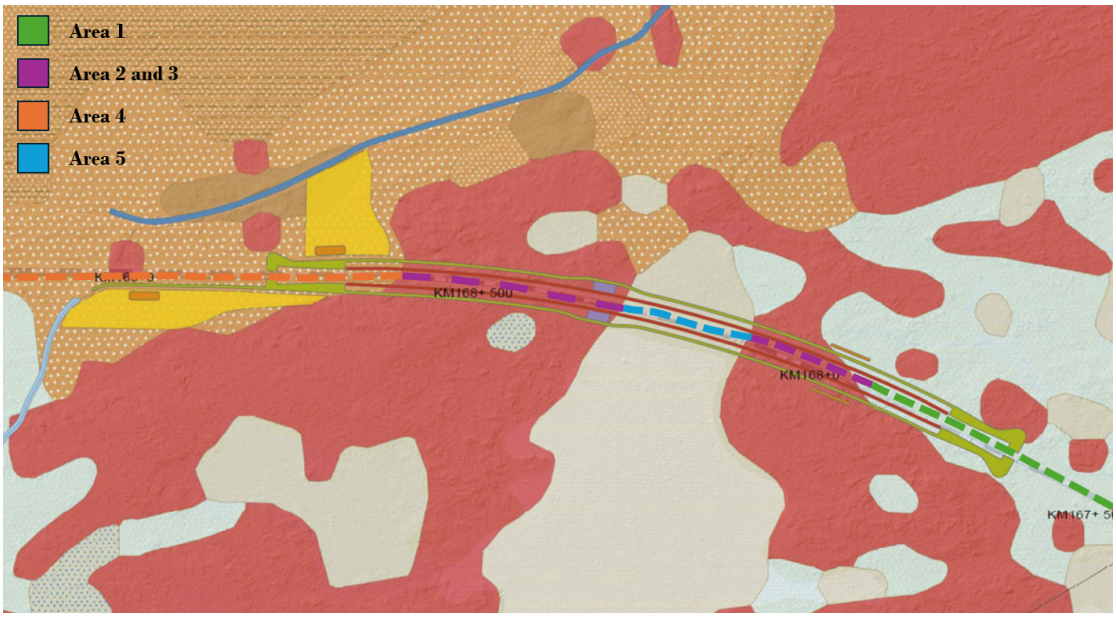

Figure 5.8: Geographic distribution of soil areas. (from Kruse and Emanuelsson, 2021).

The first of the five areas studied is mostly moraine and is named Area 1. Area 1 also has a filling above the measured granular soil with a composition similar to the area below. Therefore, the fill is chosen to have the same proprieties the silty moraine below, see figure 5.9 for the soil profile of Area 1. The soil layers in the figure correspond to the parameters in table 5.7. Area 2 has a shallow soil area with a mix of peat and moraine. The depth of the peat layer is estimated based on the total thickness of the soil and the granular soil layers. Area 3 has a surface rock. Area 4 has granular soil, but only some parts of the depth have measured parameters. Since the depth is known, the soil parameters of the gravely moraine layer is extended to the bedrock. Area 5 has a thick layer of mossy peat.

All areas have a granite bedrock. The granite is input in the Wolf stiffness code as a half-space or infinite, see tables 5.7 - 5.11. In STEM, the total depth of the model is always modeled as 10 meters. This means that the thickness of the granite layer varies in each area depending on the modeled layers above. See figures 5.9-5.13 for the respective soil profile.

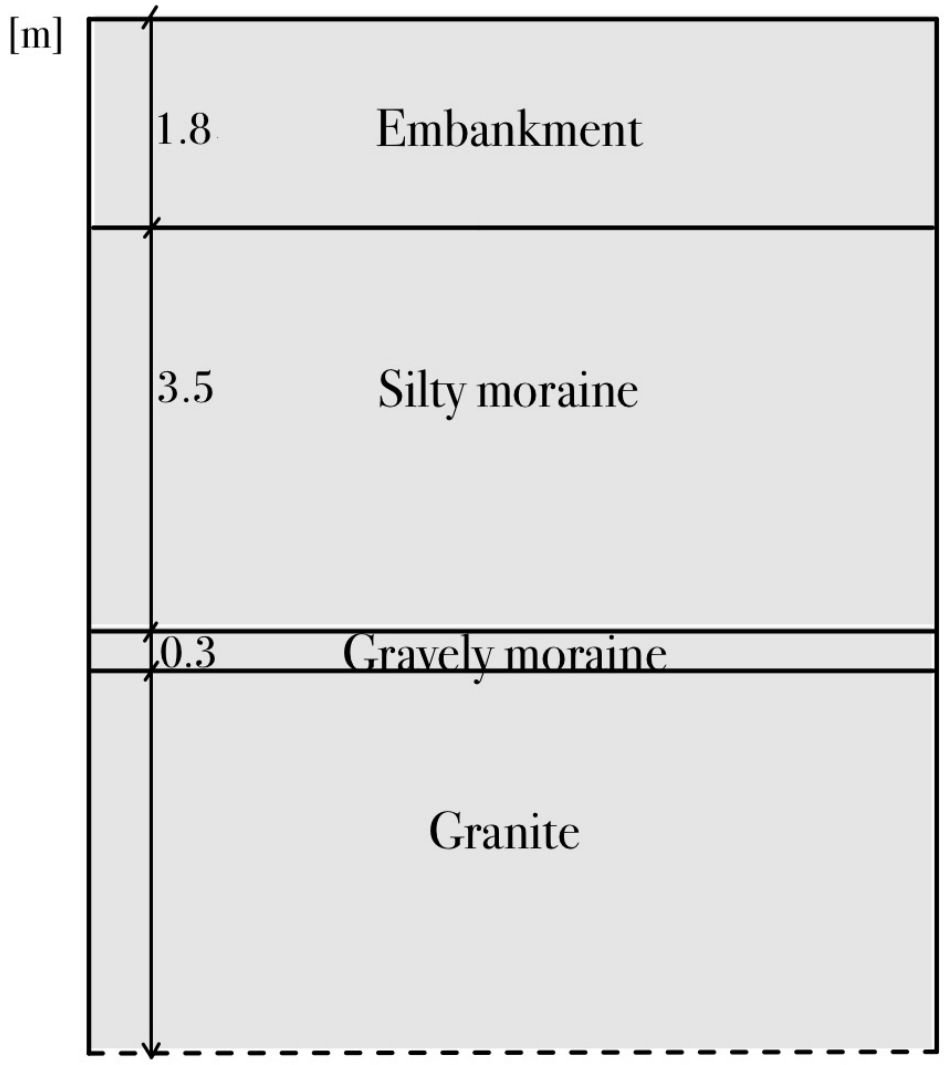

Figure 5.9: Soil profile in Area 1

Table 5.7: Soil parameters of Area 1 in Högsjö

Soil layer	Thickness $[m]$	Density $[kg/m^3]$	Youngs modulus $[MPa]$	Porosity [-]	Poissons ratio [-]
Embankment	1.8	1800	50	0.3	0.25
Silty moraine	3.5	2000	12	0.3	0.25
Gravely moraine	0.3	2000	40	0.3	0.25
Granite	inf & 4.4	3000	70 000	0.3	0.25

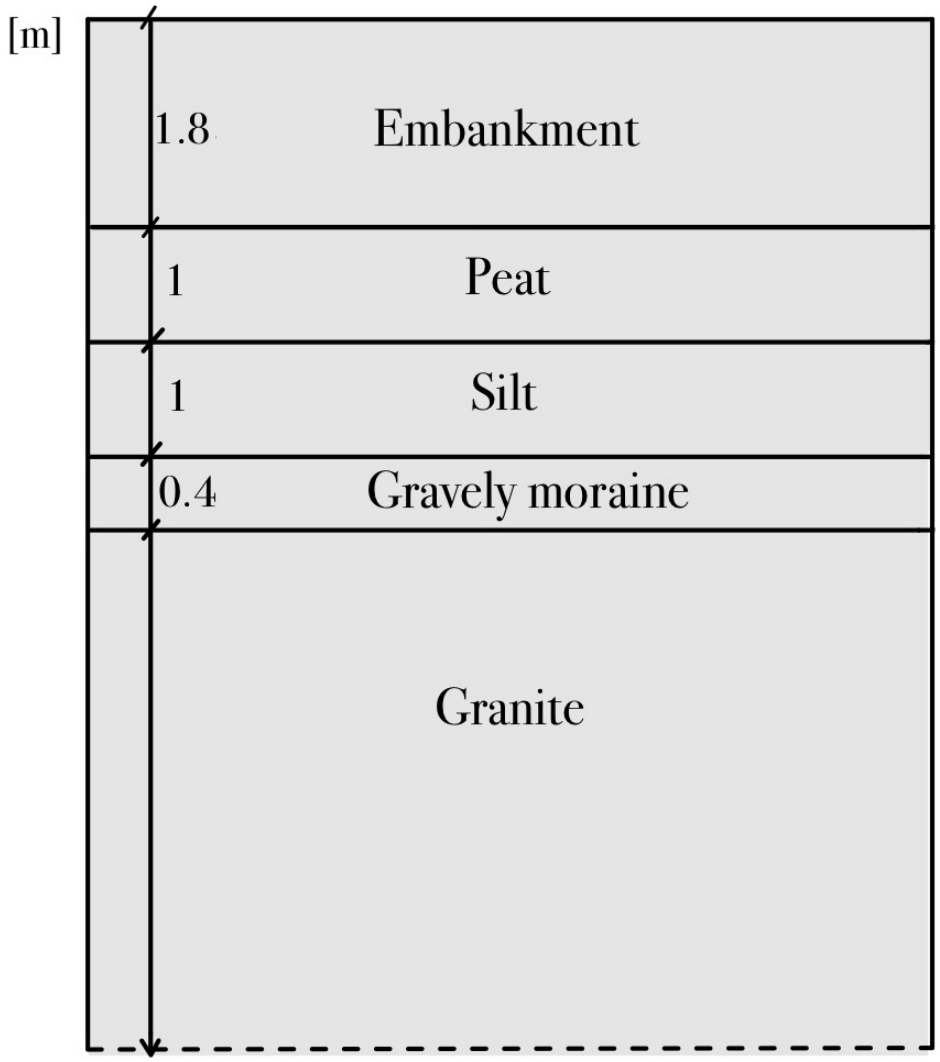

Figure 5.10: Soil profile in Area 2.

Table 5.8: Soil parameters of Area 2 in Högsjö

Soil layer	Thickness $[m]$	Density $[kg/m^3]$	Youngs modulus $[MPa]$	Porosity [-]	Poissons ratio [-]
Embankment	1.8	1800	50	0.3	0.25
Peat	1	1000	1	0.3	0.25
Silt	1	2000	12	0.3	0.25
Gravely moraine	0.4	2000	40	0.3	0.25
Granite	inf & 5.8	3000	70 000	0.3	0.25

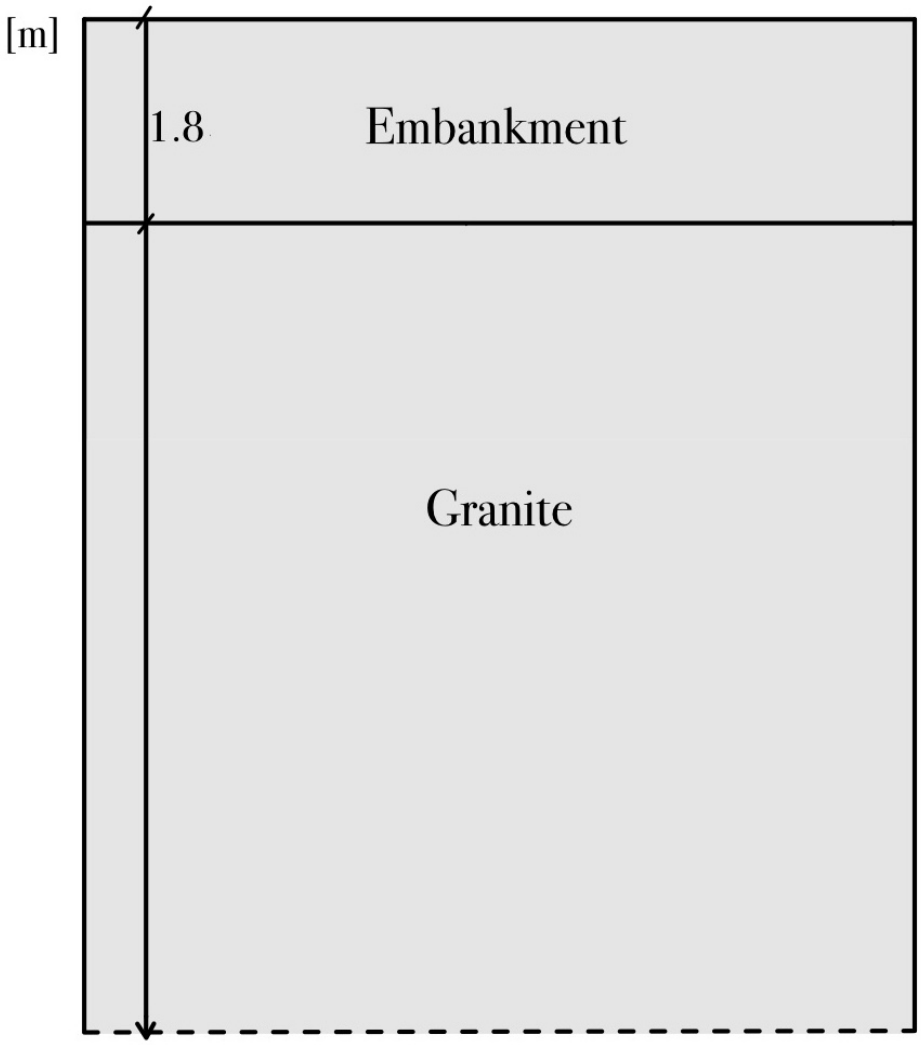

Figure 5.11: Soil profile in Area 3.

Table 5.9: Soil parameters of Area 3 in Högsjö

Soil layer	Thickness $[m]$	Density $[kg/m^3]$	Youngs modulus $[MPa]$	Porosity [-]	Poissons ratio [-]
Embankment	1.8	1800	50	0.3	0.25
Granite	inf & 8.2	3000	70 000	0.3	0.25

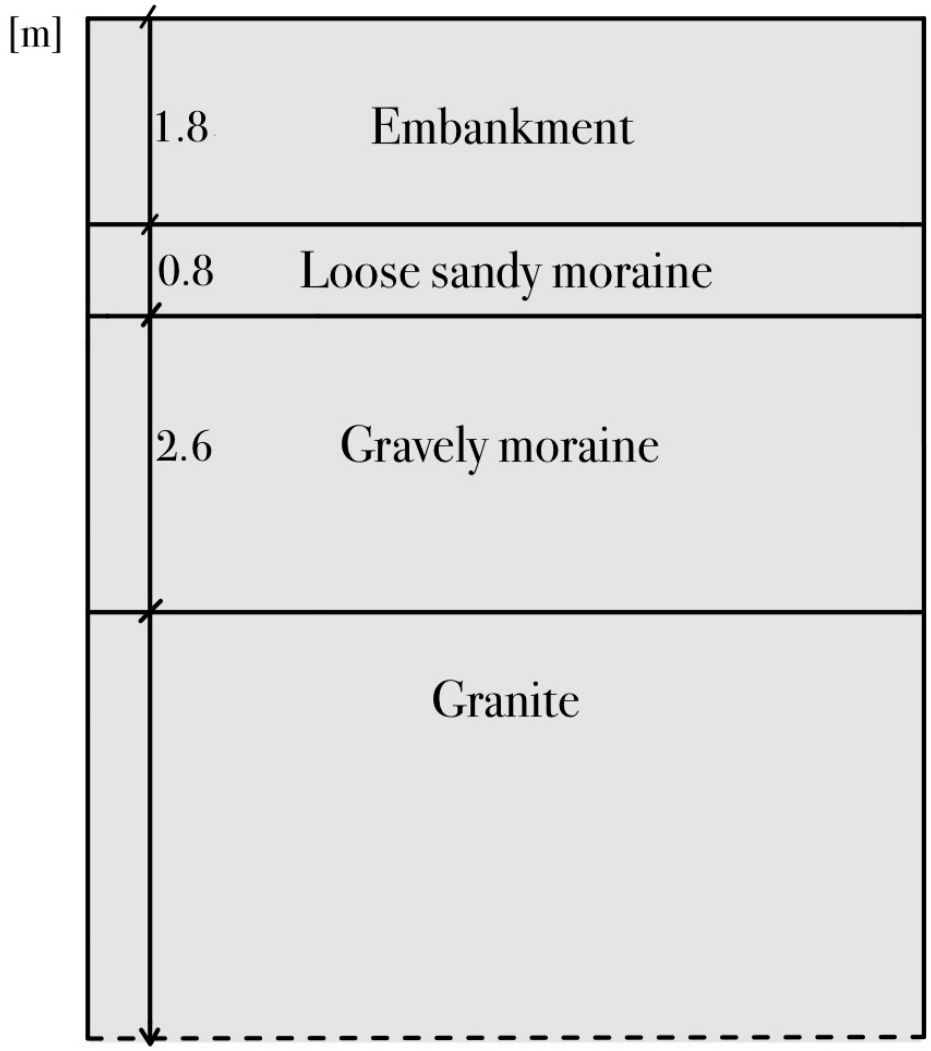

Figure 5.12: Soil profile in Area 4.

Table 5.10: Soil parameters of Area 4 in Högsjö

Soil layer	Thickness $[m]$	Density $[kg/m^3]$	Youngs modulus $[MPa]$	Porosity [-]	Poissons ratio [-]
Embankment	1.8	1800	50	0.3	0.25
Loose sandy moraine	0.8	2000	6	0.3	0.25
Gravely moraine	2.6	2000	40	0.3	0.25
Granite	inf & 4.8	3000	70 000	0.3	0.25

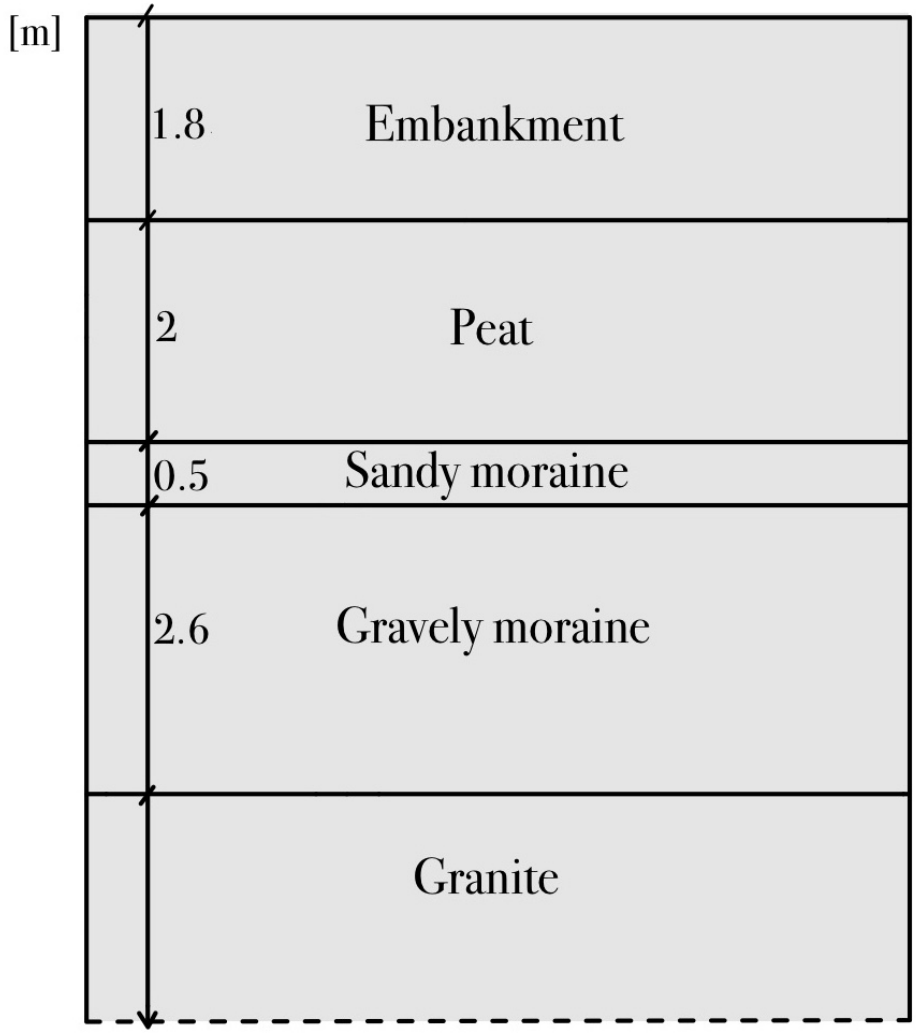

Figure 5.13: Soil profile in Area 5

Table 5.11: Soil parameters of Area 5 in Högsjö

Soil layer	Thickness $[m]$	Density $[kg/m^3]$	Youngs modulus $[MPa]$	Porosity [-]	Poissons ratio [-]
Embankment	1.8	1800	50	0.3	0.25
Peat	2	1000	1	0.3	0.25
Sandy moraine	0.5	2000	20	0.3	0.25
Gravely moraine	2.6	2000	40	0.3	0.25
Granite	inf & 3.1	3000	70 000	0.3	0.25

The soil spring stiffness for ROSE is retrieved by running the parameters in tables 5.7-5.11 through the Wolf stiffness code. The ROSE model is run for the different soil layering and is used as a point of comparison with STEM. STEM uses the soil parameters from table 5.7-5.11 directly as input.

Soil improvement

The dynamic effects of Högsjö are measured through the displacement of the rail to use as a comparison with dynamic rail guidelines in Sweden (Arm et al., 2021). There are requirements of velocity and acceleration in soil, but these refer to maximum vibrations in nearby construction (Moritz and Karlsson, 2022). The guidelines express that the dynamic rail displacement for a railway with an axle load over 13 tonnes should be between 2-4 millimeters. Therefore, a maximum rail displacement of 4 millimeters is chosen as the limit. If this value is exceeded, soil mitigations are implemented. Mitigations are not implemented on the vehicle or track because their parameters have been previously determined for the specific cases of this study.

Lime cement columns

One method of soil improvement related to soil vibrations is the usage of lime cement columns (LCC). The improved soil is modeled using the equal strain theory where the load is distributed in accordance to the modulus of the soil and column respectively. This method gives an equivalent modulus for the improved soil using equation 5.2.

$$E_{tot} = aE_{col} + (1 - a)E_{soil} \tag{5.2}$$

The modulus of the soil is determined in tables 5.8 and 5.11. The column modulus is derived from the lower end of measurements of LCC, which is 200 MPa (Wong et al., 2024). The area ratio of the columns in the soil is therefore the only variable parameter and is iterated until the guideline is fulfilled. The new values for the modulus are then input in ROSE through the Wolf stiffness code and in STEM for the rail displacement calculations. Table 5.12 shows the changes in the soil from the implementation of lime cement columns.

Table 5.12: Changes from added Lime cement columns to modulus from table 5.11 and table 5.8

Soil area	Changed soil layer	Area ratio [-]	New modulus [MPa]
Area 2	Peat	0.05	11
Area 2	Silt	0.05	19
Area 5	Peat	0.05	11

Soil replacement

Soil replacement is another improvement method tested. Here, the peat layer is replaced by the granular soil layer below the peat. This soil is used with the assumption of it being available in the construction site. The new displacement with soil replacement is calculated in STEM and ROSE by imputing the new layering. Table 5.13 shows the parameters that are changed due to soil replacement. Figures for the change in the soil profile due to soil replacement are shown in 5.14 and 5.15.

Table 5.13: Changes of soil replacement from table 5.11 and table 5.8

Soil area	Removed soil layer	Replaced by layer of	Size of replaced layer [m]	New modulus $[MPa]$
Area 2	Peat	Silt	1	10
Area 5	Peat	Sandy moraine	2	20

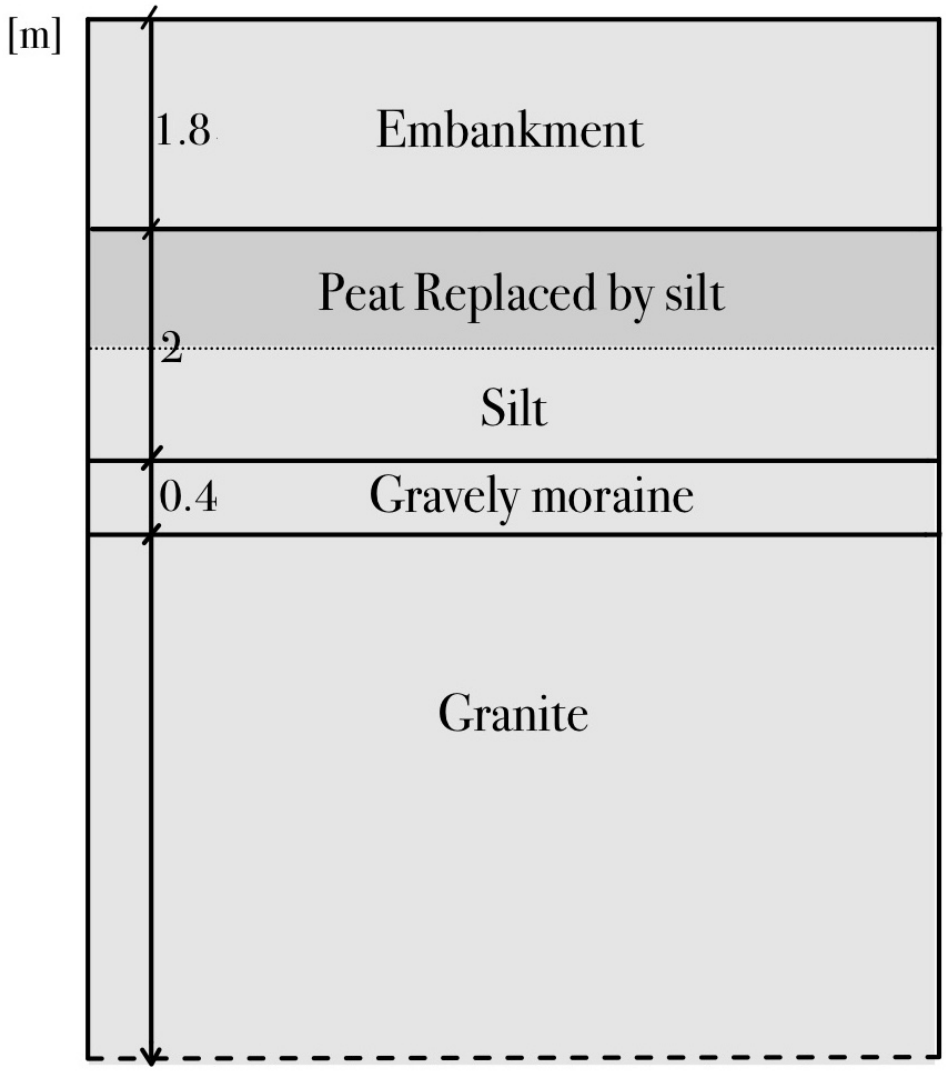

Figure 5.14: Soil replacement profile in Area 2.

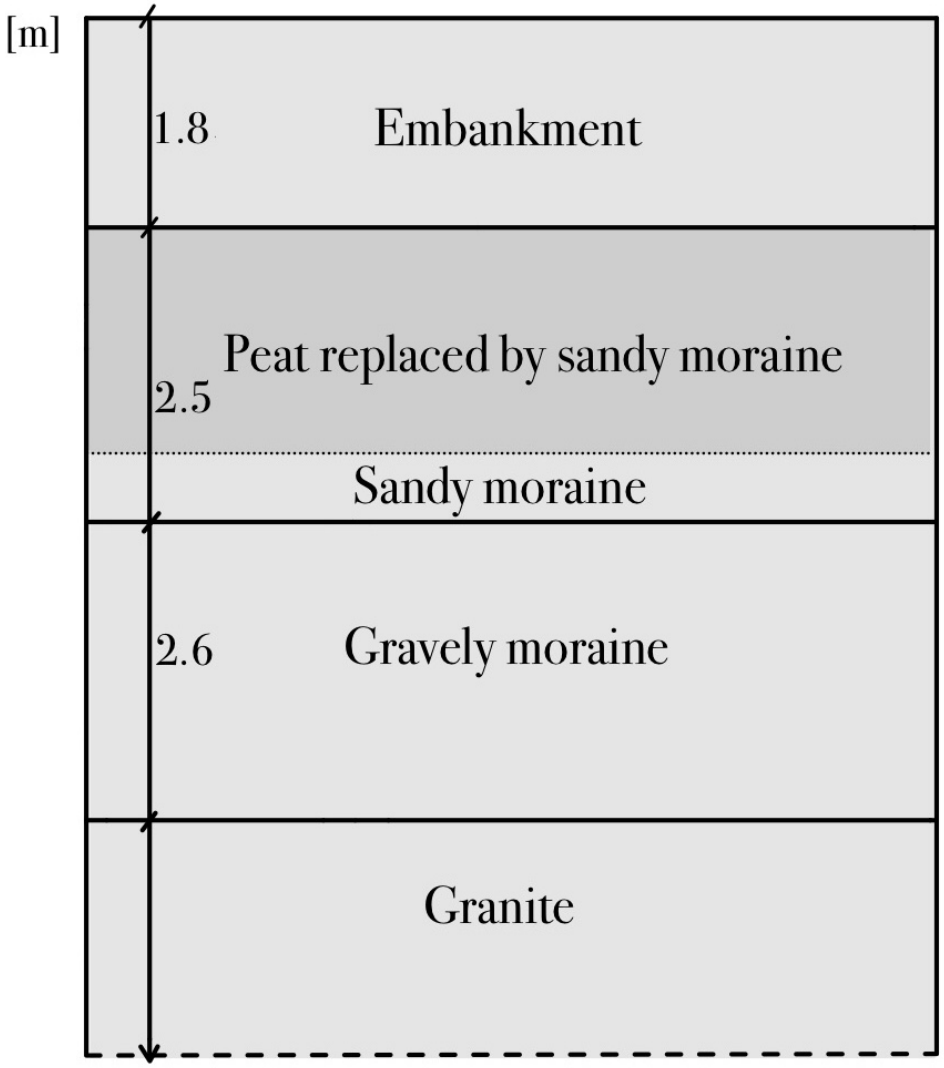

Figure 5.15: Soil replacement profile in Area 5.

Transition zones

The transition zone from Area 2 to Area 3 is modeled in both ROSE and STEM. These are part of a 200-meter area where a transition between the zones occurs. The modeling of the transition occurs over 40 meters. Both STEM and ROSE model transitions through non-sloped elements. The transition therefore consists of a finite number of zones with a sudden transition between parts. The transition is divided into five cases, where the first case, Transition 1 has one transition from Area 2 to Area 3 directly. The number of transitions increases gradually, up to the fifth case, Transition 5, which has five transitions in the area. The soil layers in the transition zones have the same soil parameters as in Area 2 but with different thicknesses. A figure of the layer distribution of Transition 5 is shown in figure 5.16. The layer distribution for the other cases are in Appendix D, both as figures for each case and also a table describing the soil thicknesses in the transition zones.

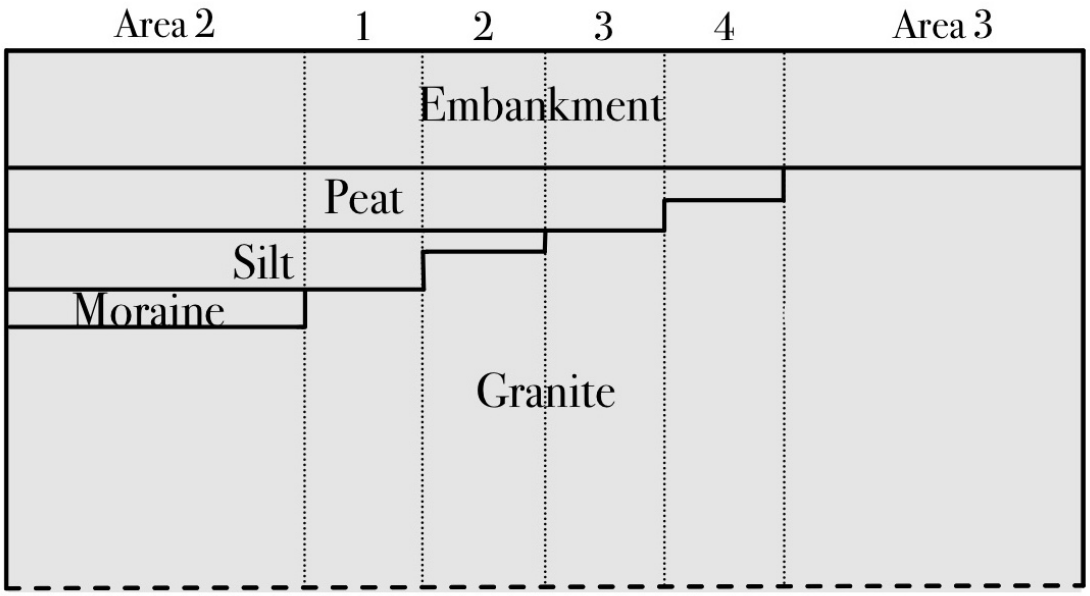

Figure 5.16: Soil profile of Transition 5.

Speed analysis

In order to analyze the dynamic effects of changing velocities, four speed analyses are conducted in STEM. These cases are studied as they represent different conditions that are expected to respond to speed changes differently. Two of the cases represent different types of soil conditions, with Area 2 used to test soft soil and Area 1 that represents stiffer soil. Area 2 is further tested through the transition zone with Area 3. The speed analysis was conducted on a specific node on the rail. For the transition zone this was directly on the node in Area 2 closest to the transition.

6 Results and discussion

The results presented focus on the displacement of the rail or the soil directly under the rail. Acceleration and velocity are tested for the same locations for some of the calculations but the relative differences were the same as that of displacement. The results all have a similar shape with parts of the cart corresponding to changes in displacement as seen in figure 6.1.

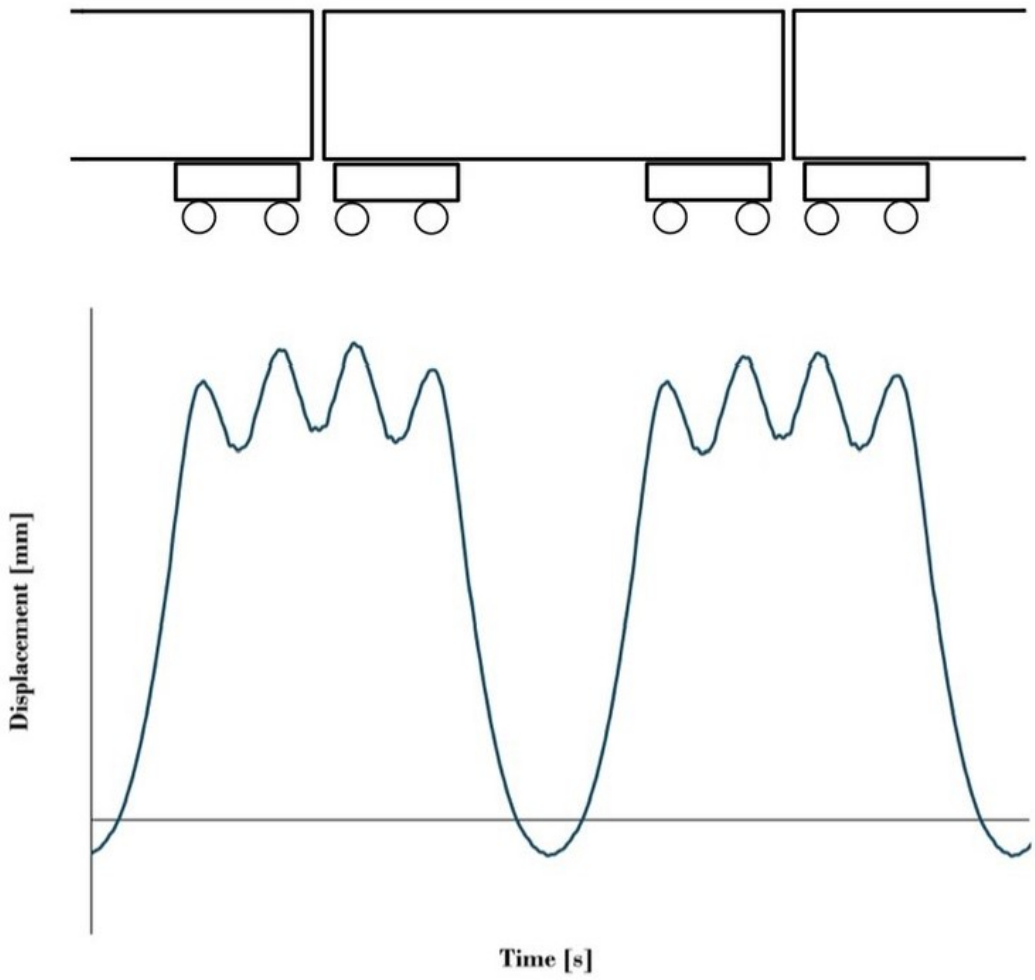

Figure 6.1: Visualization the interpretation of results.

The models have several simplifications that limit their possible applications. In both models the superstructure mostly consists of mass-spring systems which cannot fully account for the full mechanism of a train-track interaction. The soil spring stiffness in ROSE is an even greater simplification, where several soil layers and the embankment are considered as a single row of springs. STEM uses a linear elastic soil model which does not account for shear strain dependency, anisotropy or any other nonlinear effects.

6.1 Malmbanan

The Malmbanan case is used as a validation study to test how closely the results from STEM and ROSE correspond to the experimental data. The goal is not to match the

data, as both the experimental data and the model do not fully reflect reality. The monitoring of the experimental data is set up to measure the long-term settlement of sleepers, and while the displacement is measured continuously, it is not intended for short-term effects (Nasrollahi et al., 2024). The measured data also drifts over time, where each peak is higher than the previous due to drift in the measuring instrument. This requires a normalization of the values for an adequate comparison. Field tests are not fully reliable and are dependent on the quality of equipment, the on site setup, the studied sleeper and the load of the train. These factors can introduce sources of errors. The train and track parameters vary due to their condition, which is a further source of error. The sources of error, together with the simplifications, make it impossible to match the data. Instead, a rough similarity is sought in shape and amplitude of the displacement.

The result of the analysis in both methods and their comparison to experimental data is shown for the iron ore train in figure 6.2 and the X2000 train in figure 6.3. The figures show that the displacement values obtained from STEM more closely resemble the experimental data in both shape and amplitude. In both cases, ROSE has a lower amplitude than both experimental data and STEM with a difference of eleven percent for the iron ore train and twenty-two percent for the X2000 train. Both models, but especially ROSE overestimates the dips between each wheel of the train compared to the measured data. The dips between bogies on the same cart are also larger in ROSE, where the displacement becomes negative.

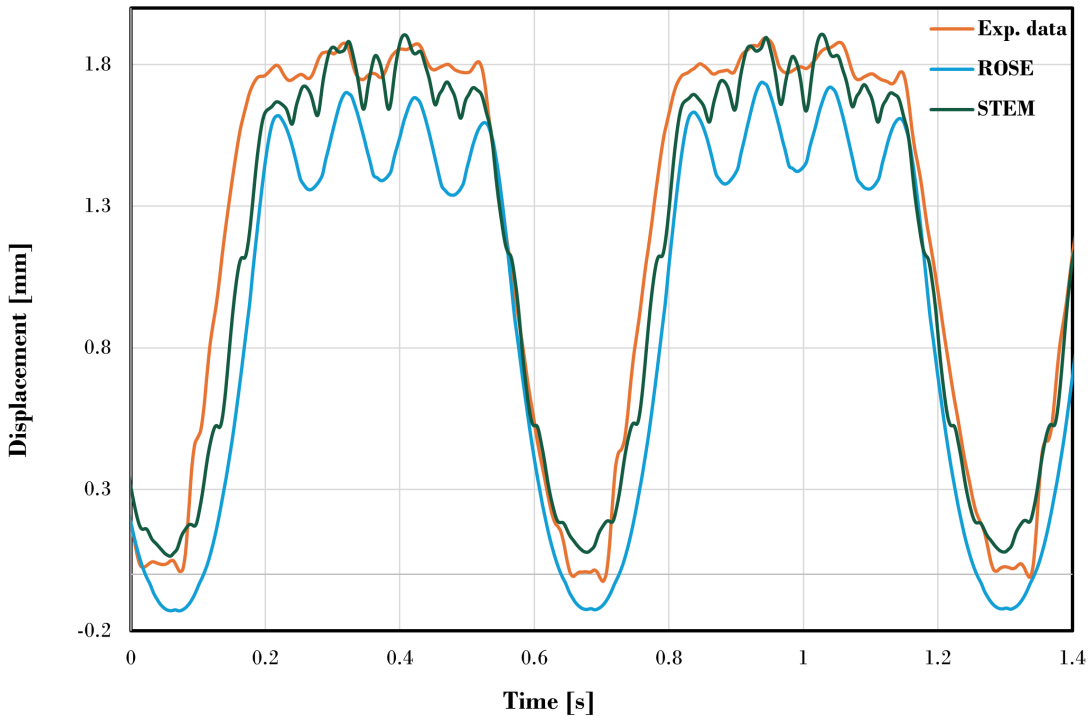

Figure 6.2: Sleeper displacement over time for iron ore train on Malmbanan.

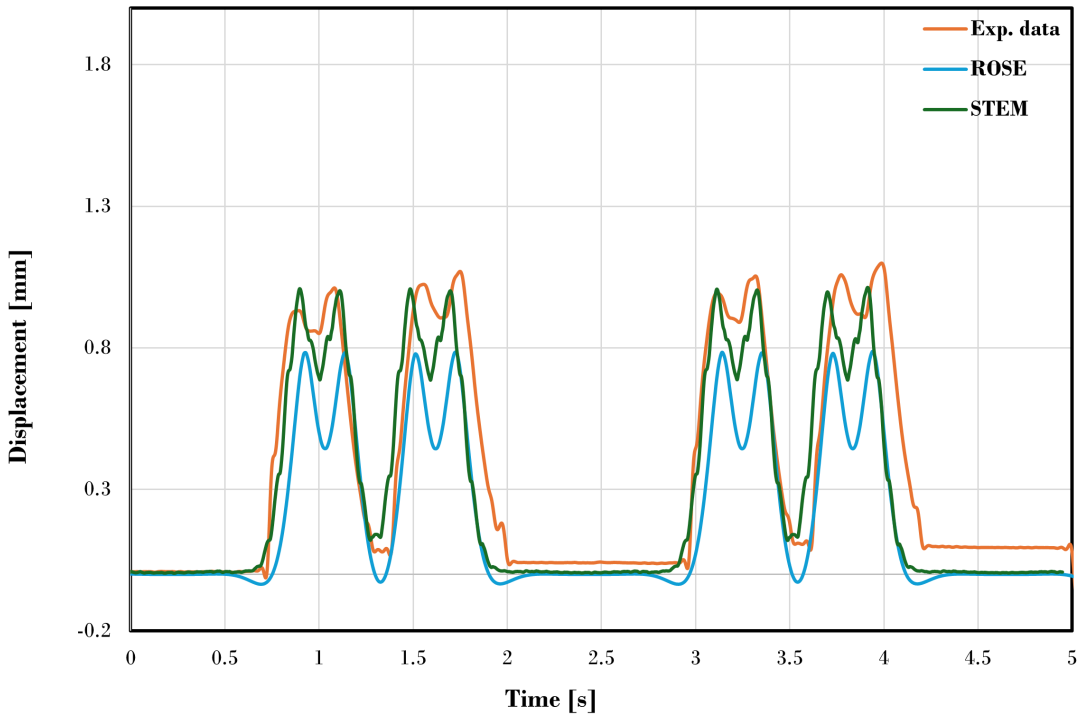

Figure 6.3: Sleeper displacement over time for X2000 train on Malmbanan.

Irregularities

The implementation of irregularities in the models resulted in unexpected values. In both ROSE and STEM the rail irregularities are expected to increase the dynamic displacement with an increasing velocity. However, in ROSE, the displacement decreases with increased velocity when irregularities are implemented, see figure 6.4. This result contradicts the affect irregularities are expected to have on dynamic response (M. Chen et al., 2023). An increased speed without irregularity shows little to no fluctuation in displacement at different velocities. This can be due to the speed being lower than the critical speed and therefore the increase in velocity does not have a significant impact. Irregularities are also implemented in STEM, but due to computational time it is not as extensive. The results show that the irregularities have no significant effect and neither had the increased speed on the displacement. The analysis of the irregularities are further presented in Appendix C.

The results for a specific speed with and without irregularities show great differences in ROSE and STEM in both shape and amplitude. See figure C.1 and figure C.2 in Appendix C. The same irregularity parameter does not reflect similar amplitudes in the models. An increase of the irregularity parameter shows that STEM is capable of implementing irregularities. However, the increased value for Av is one hundred and fifty times higher than the highest line grade value to get a result similar to that of ROSE (Podworna, 2015).

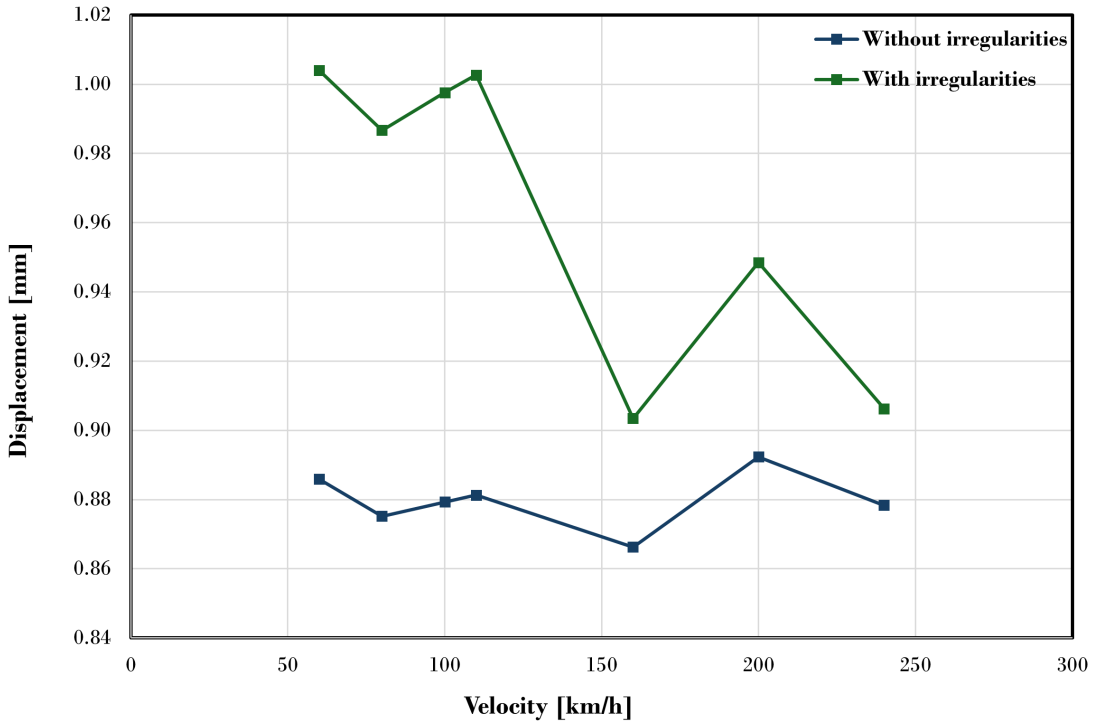

Figure 6.4: Speed analysis in ROSE for iron ore train on Malmbanan with and without irregularities.

6.2 Högsjö

The testing of the different soil areas resulted in significant differences in results between ROSE and STEM. The rail displacement from ROSE is presented in figure 6.5 and the rail displacement from STEM in figure 6.6. The differences between the soft and stiff layers is significantly larger in STEM. The minor differences in ROSE indicate that the method used is inadequate for the modeling of dynamic displacement. The inadequacy stems from the large differences in soil profile not resulting in any major differences. The very soft Area 5 only results in a twenty-five percent increase in displacement compared to the firm outcrop rock of Area 3.

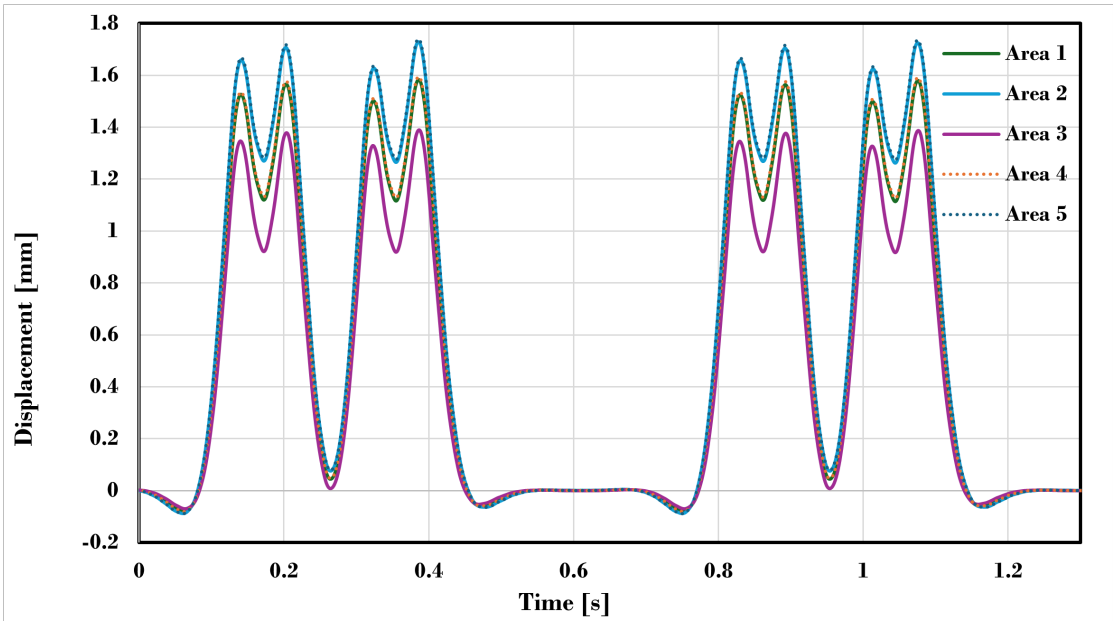

Figure 6.5: Rail displacement over time in ROSE for Högsjö.

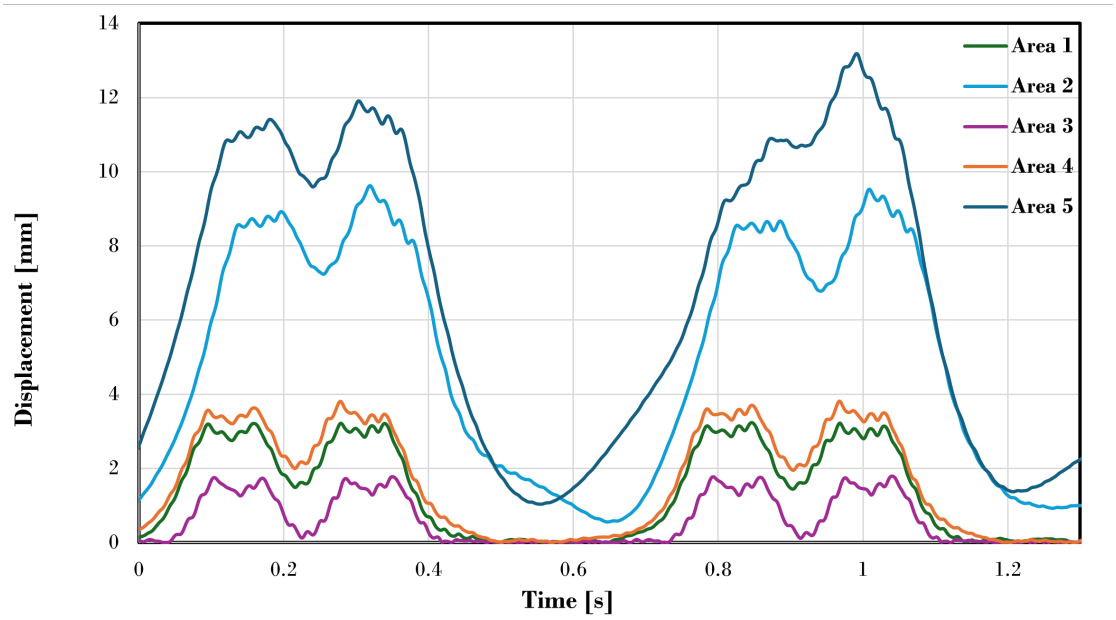

Figure 6.6: Rail displacement over time in STEM for Högsjö.

The soil displacement is also tested for the soil areas with the result for ROSE presented in figure 6.7 and for STEM in figure 6.8. The rail displacement is very similar to the soil displacement with only minor shape differences. The differences in rail and soil displacement do not appear to be significantly affected by total displacement. The difference is between 0.1 mm and 0.4 mm. This variance is very small for the larger displacement seen for the areas 2 and 5 while it is more substantial for the low displacement areas such as Area 3 and in ROSE.

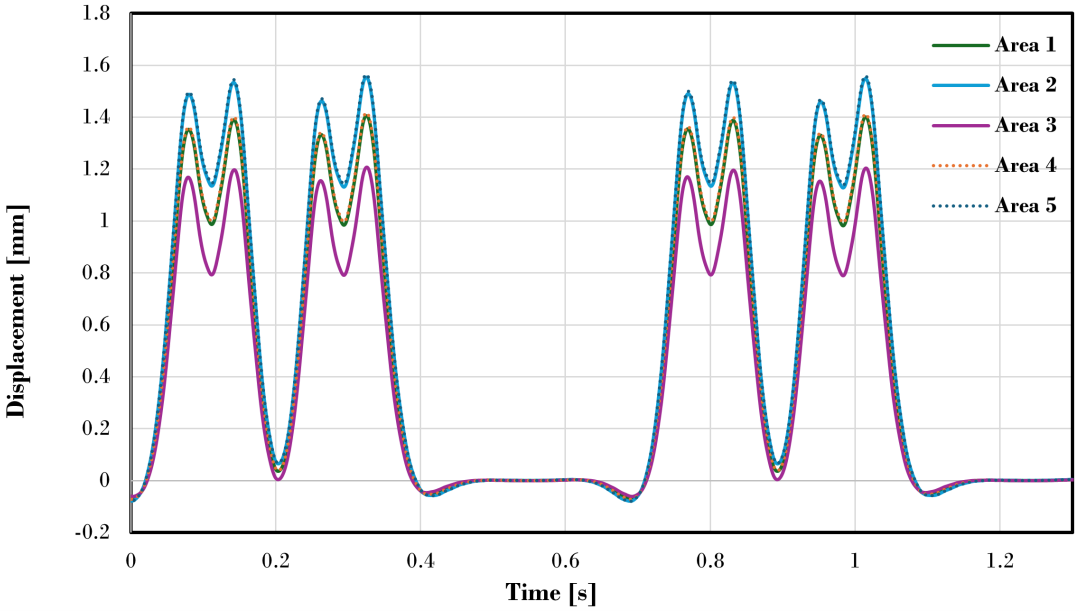

Figure 6.7: Soil displacement over time in ROSE for Högsjö.

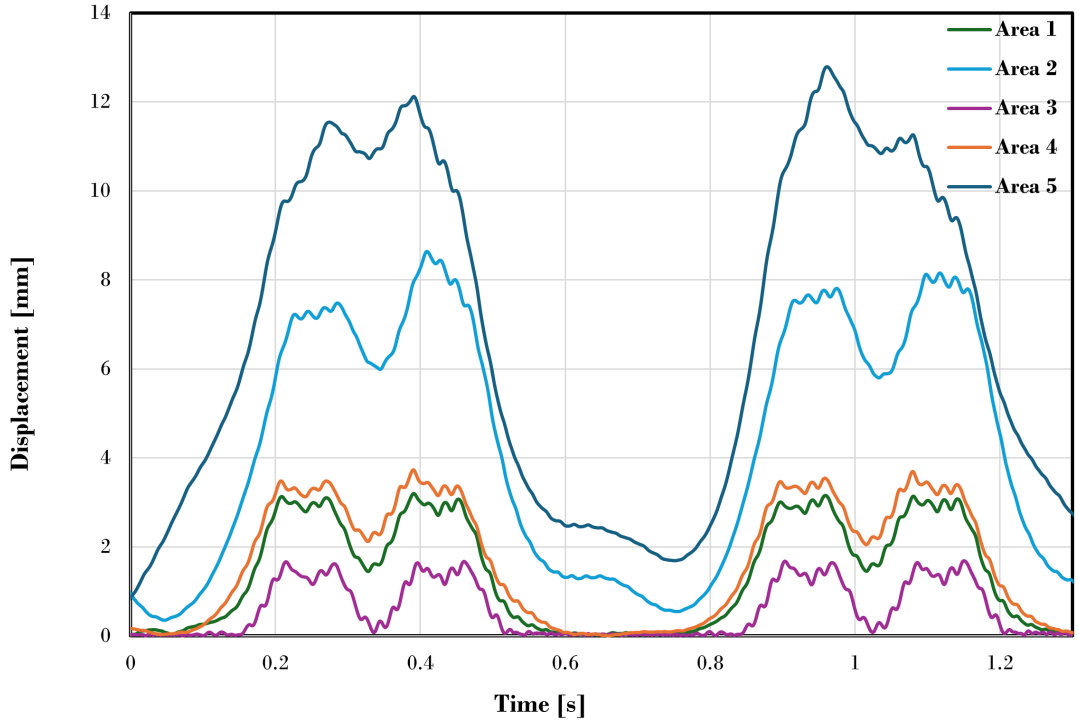

Figure 6.8: Soil displacement over time in STEM for Högsjö.

The results retrieved from ROSE are expected given the soil spring stiffness retrieved from the Wolf stiffness code, since these had a similar relative difference. A possible explanation for the discrepancy is that the cone method used in the Wolf stiffness code overestimates the impact of the top soil layer. The top layer is often governing, but for these cases the top layer is the stiffest, which should result in the lower layers having a larger impact. Other uses of the Winkler method, model the embankment separately for this reason (Nielsen and Igeland, 1995). To test this hypothesis, a test is conducted

for modeling the soil in ROSE through the Wolf stiffness code without an embankment. The results of this are shown in figure 6.9. These results instead over-exaggerate the impact while clearly showing that the original results with an embankment are inadequate. Because of these results in ROSE, the results in STEM are concluded to be more reliable and are focused on for the rest of the analysis.

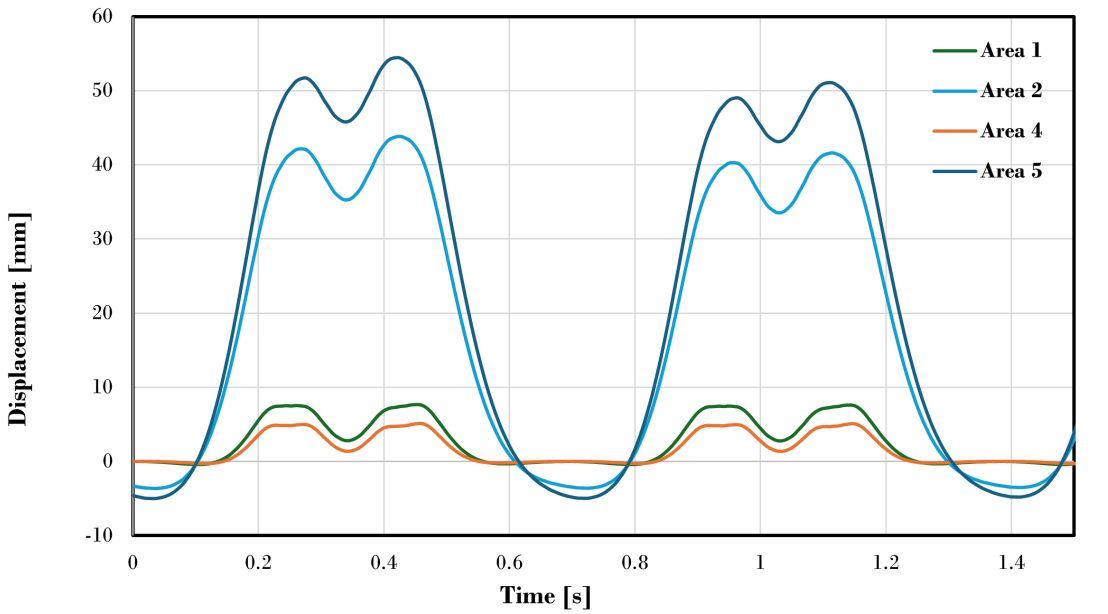

Figure 6.9: Rail displacement over time in ROSE for Högsjö without embankment.

The results from STEM for the rail displacement show substantial differences between the outcrop rock in Area 3, granular soil in areas 1 and 4 and the peaty areas 2 and 5. Area 3 primarily contains the displacement from the embankment. This is the only area which somewhat resembles the results from ROSE which is to be expected as it is the embankment that has the largest impact in the method used in the ROSE model. Area 1 has a stiffer first soil layer but with a substantially larger depth compared to Area 4 with a smaller layer of lower stiffness. Area 4 having a lower displacement shows that it is not always the layer of lowest stiffness that creates the largest difference and that the depth is a substantial factor. The importance of the layer depth is further shown in the difference between areas 2 and 5. Both areas have a similar layer distribution below the peat but the larger peat depth in Area 5 results in a larger difference in displacement.

The guideline for maximum rail displacement is 4 mm which is surpassed for areas 2 and 5. These areas are therefore subjected to soil improvement. Lime cement columns and soil replacement are tested for both areas. Both methods gave results for the displacement that is within the guidelines which is shown in figure 6.12 for Area 5 and figure 6.13 for Area 2. The lime cement columns required an area ratio of 0.05 to surpass the guideline. This area ratio corresponds to a center to center distance of 2.8 meters,which is the maximum distance to keep two columns within the top part of the embankment. The resulting distribution of columns is displayed in figures 6.10 and 6.11. The area ratio for the lime cement columns is low. The distribution resembles individual columns rather than soil mixing. The results indicated that dynamics are unlikely to cause a problem when soil improvement is implemented. Short-term effects are unlikely to be governing when implementing lime cement columns. More inves-

tigations on the area ratio for dynamic displacement would be required to corroborate these findings.

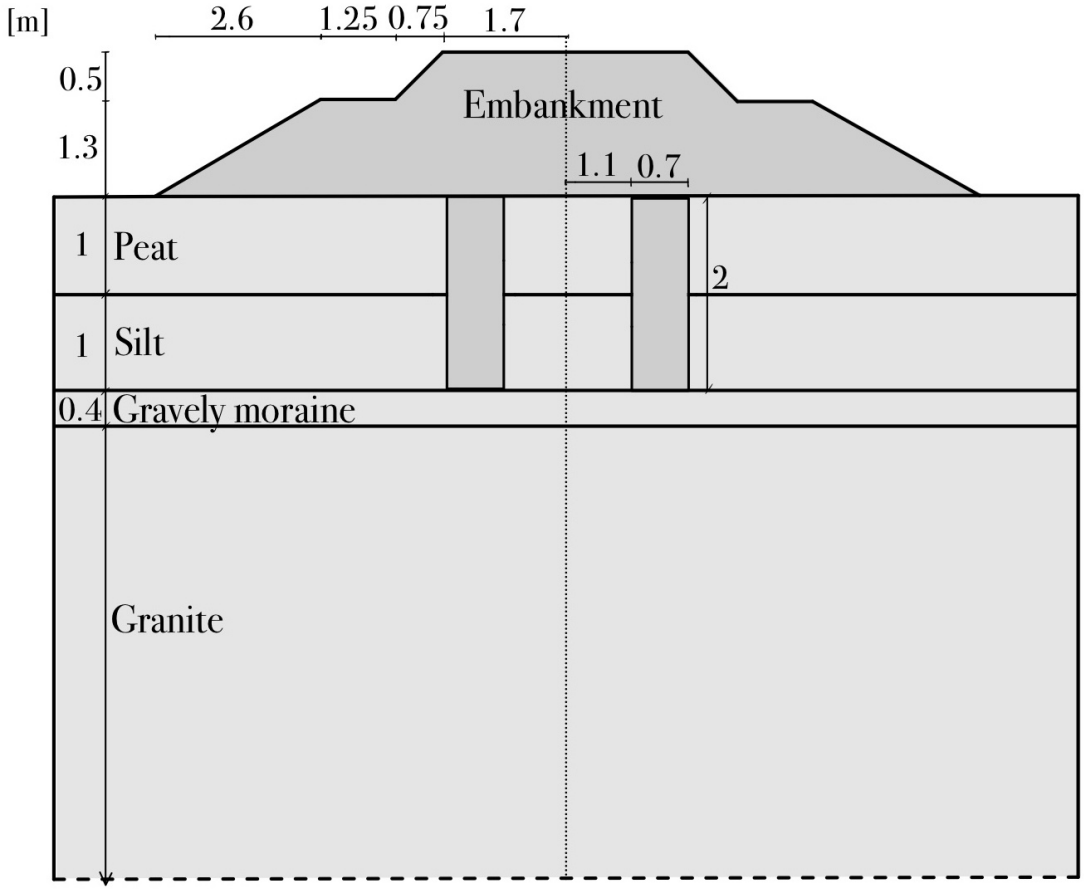

Figure 6.10: Soil profile with lime cement columns in Area 2.

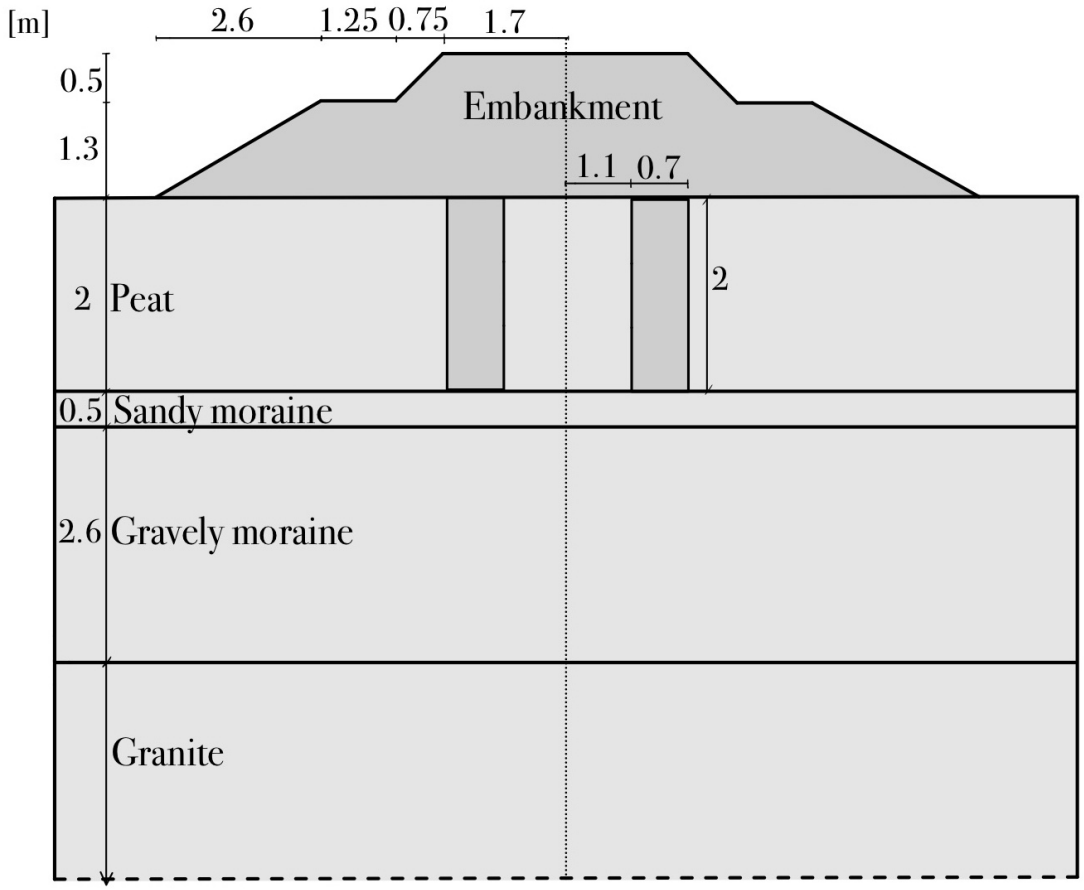

Figure 6.11: Soil profile with lime cement columns in Area 5.

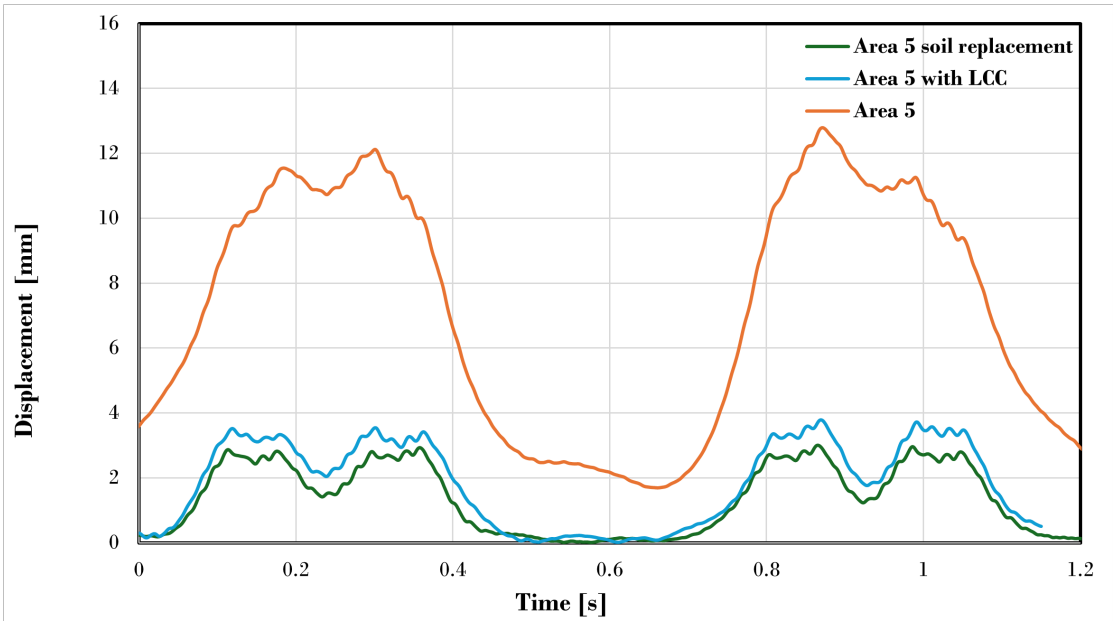

Figure 6.12: Soil displacement for Area 5 with soil improvement.

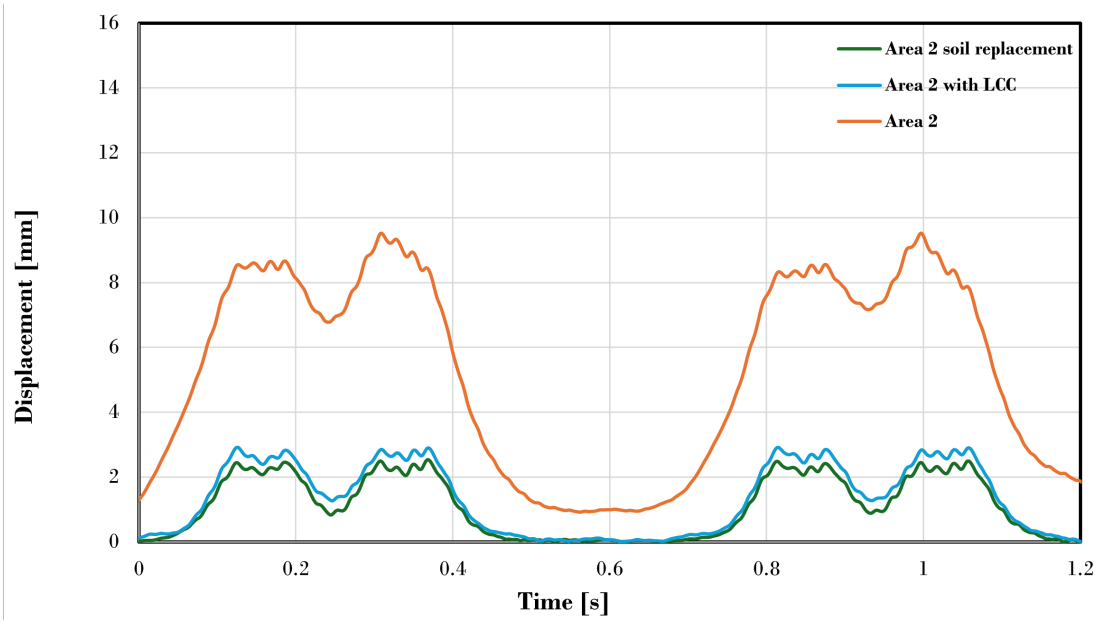

Figure 6.13: Soil displacement for the Area 5 with soil improvement.

Transition zones

Transition zones are modeled in both STEM and ROSE and both observe little to no impact as seen in figures 6.15 and 6.16. The tests are conducted at a speed of 135 km/h. The results from the ROSE transitions with more than one zone seem to have some increased displacement, but this is likely from some of the zones having a lower stiffness with less soil. Both methods save the impact of the transition zones as a gradual shift at each transition without any extra dynamic effect. This gradual shift is likely the effect of the rail being modeled as a beam which spreads the load over an area. The full impact of the transition zones is not considered as the long-term effects such as the differential settlements are not being modeled. These would contribute to further dynamic forces and increased displacement in the transition zone.

Figure 6.14: ROSE transition with two zones

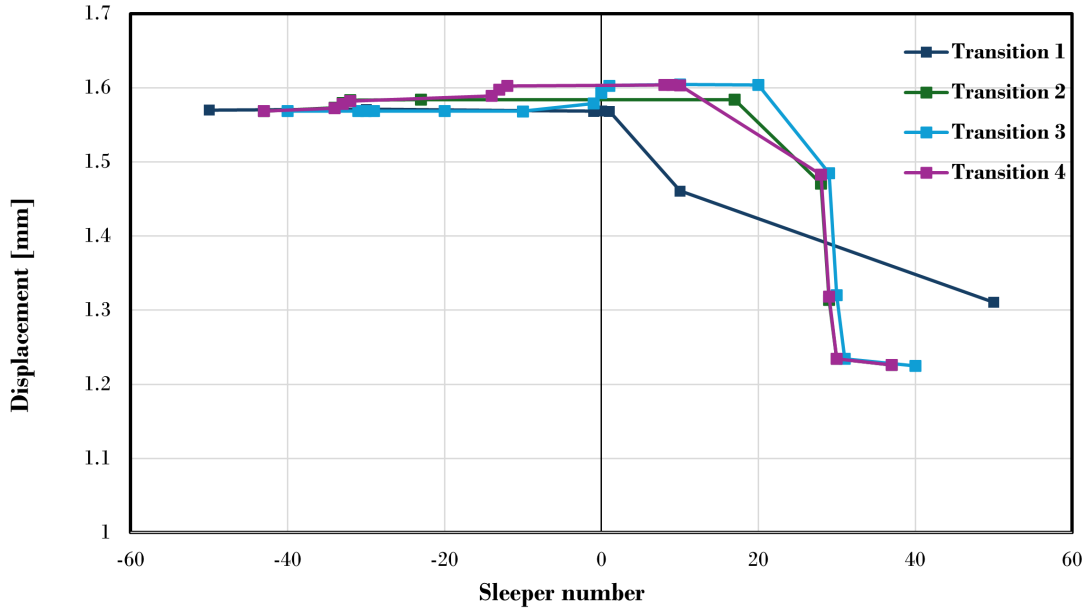

Figure 6.15: Change in displacement over the different transition zones in ROSE.

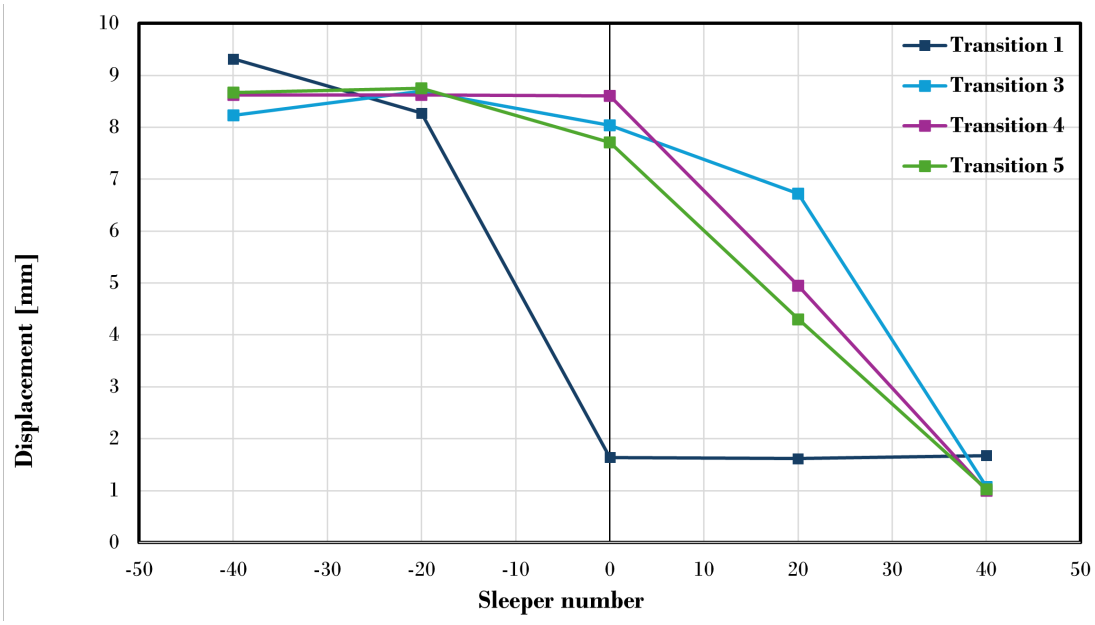

Figure 6.16: Change in displacement over the different transition zones in STEM.

Speed dependency in STEM

The speed analysis on the soft soil of Area 2 and the stiff soil of Area 1 is shown in figure 6.17. The curves are very similar until the velocity exceeds 270 km/h. Here, the area with softer soil experiences a larger dynamic increase of displacement compared to the stiff soil. After the increase, the soft soil dips below the stiff one. The close adherence of the curves at velocities below 270 km/h is likely due to the soil not having a major impact on dynamic loading. The soil should only start to play a governing role when

approaching the critical speed. The curve of Area 2 in figure 6.17 resembles the critical speed curve with a peak formed by a transition. The smaller decrease compared to an ideal curve for critical speed Costa et al., 2015 is likely due to the effects of dynamic loading. The larger amplification of Area 1 at a speed of 400 km/h indicates that the critical speed of this area is close to this value. The analysis is done at velocities higher than what would be reasonable for Swedish rail to test if the simulation corresponds to the theory of critical velocity.

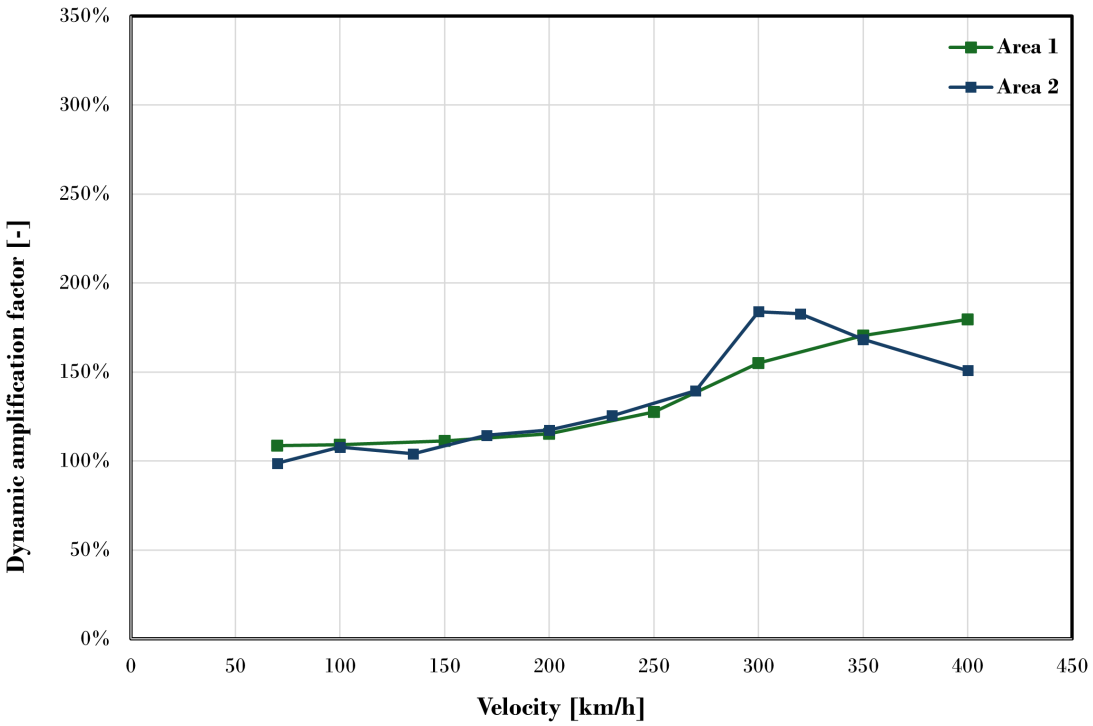

Figure 6.17: Speed analysis for stiff soil in area 1 and soft soil in area 2.

The speed analysis is also conducted for transition zones. Transition 4, 2 and 1 are tested at different velocities and the results are presented in figures 6.18 and 6.19. The first sleeper away from the transition zone in soft soil is studied in figure 6.18. The result shows that the sleeper directly connected to a stiff area takes on a lot of properties of that area. The peat elements are in direct contact with rock, which contributes to the peat elements resisting deformation. Because of this, the second analysis is run eight sleepers away from the transition to lower the impact of the stiff area while still keeping the effects from the transition. The displacement results from this sleeper are shown in figure 6.19 where the effects of the transition zone create a larger dynamic amplification. The results are very similar for all cases below 200 km/h, with only slightly larger amplification from the transition zones. The differences become substantial above this speed with the more gradual transitions experiencing fewer differences. The gradual transitions also have a peak indicating a critical speed, but it occurs before the peak of the non-transitioned area. The sudden transition has no such peak, at least at velocities below 400 km/h.

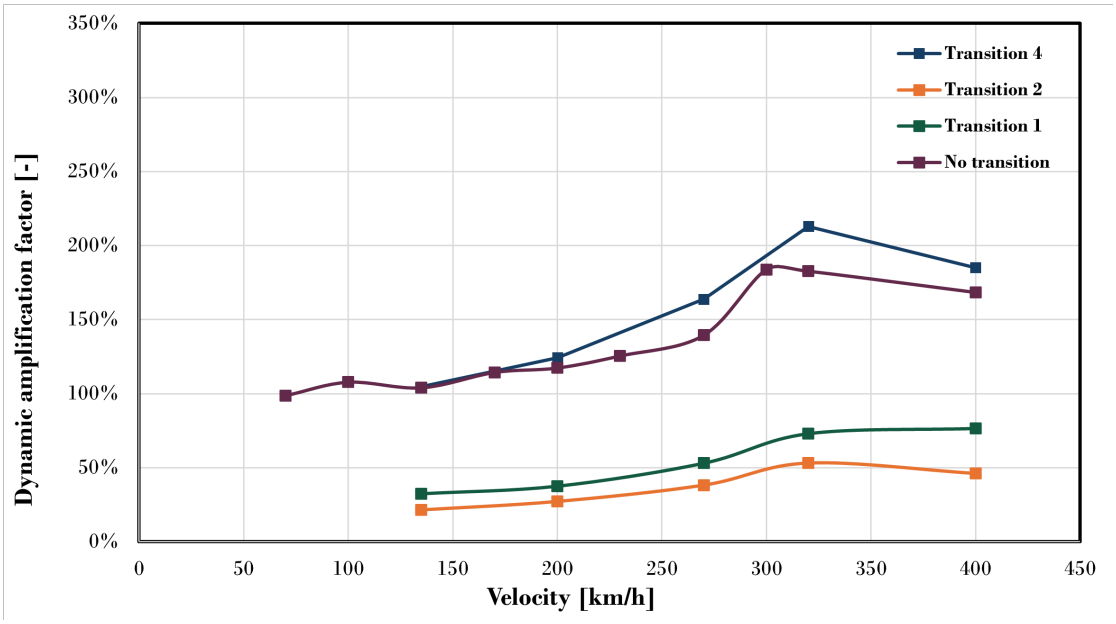

Figure 6.18: Speed analysis for transition zones, one sleepers into the softest area.

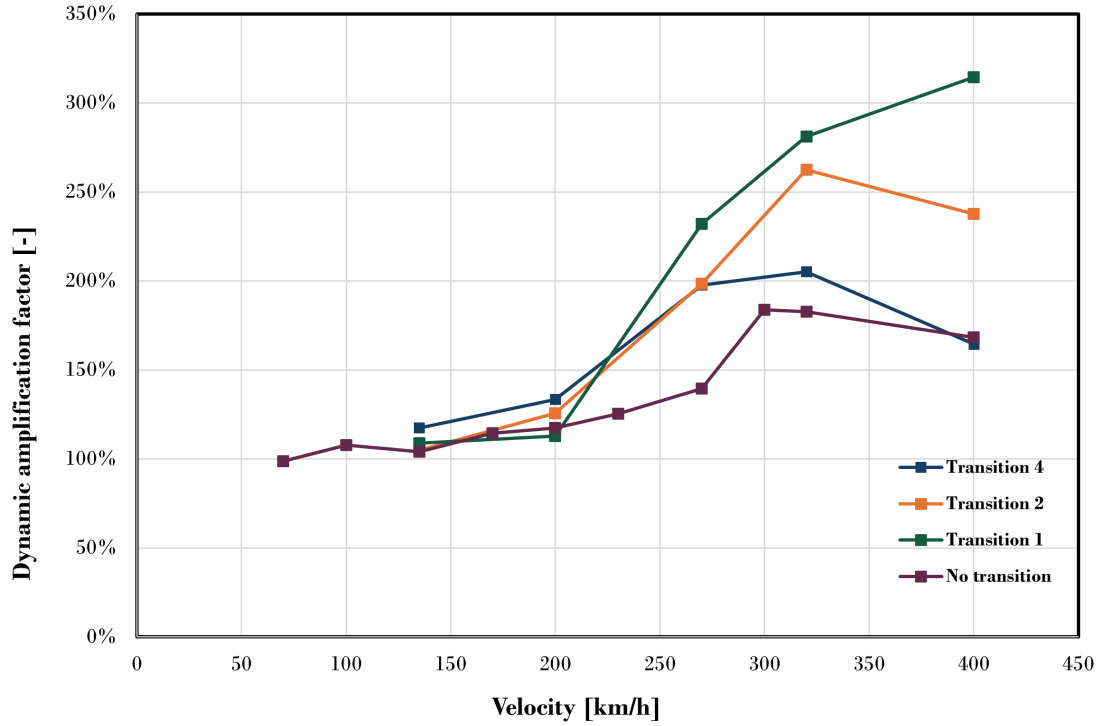

Figure 6.19: Speed analysis for transition zones, eights sleepers into the softest area.

How gradual the transition is has a large impact. Sloping layers or further granularity in the transitions could be further studied. The transition studied is also between two natural areas and a similar analysis on a bridge or built up structure would also be of interest for further study. The transition shown is also not fully representative of reality as the softer Area 2 would be subject to soil improvement.

6.3 Model evaluation

ROSE is a simplified model, that could be improved while still keeping the computationally efficient Winkler springs. In ROSE the ballast and all soil layers are modeled as one soil spring stiffness and damper. An improvement of this model would be to model the different layers as separate rows of springs and dampers. Having multiple layers of soil spring stiffnesses will complicate the model and the method for determining spring stiffness. The Wolf stiffness code indicates that the top layers have a larger influence on the total stiffness and this somewhat reflects reality. However, the influence is believed to be overestimated by the code. Therefore, obtaining the stiffness for each layer separately through the Wolf stiffness code is not possible without further tests.

The Wolf stiffness code is used as a connection between ROSE and STEM but the results are significantly different between the the two locations. In the Malmbanan case, ROSE and STEM are close in displacement, and in Högsjö they differ greatly. This is another indication that the Wolf stiffness code may not be a good approximation for this case. For the different areas in Högsjö the stiffness and damping determined by the Wolf stiffness code do not vary significantly. In Malmbanan the young's modulus for the soil layers used in the Wolf stiffness code increase gradually, while the modules for the soil layers in Högsjö fluctuate. This can be one of the reasons behind the great differences in the displacements between the methods. ROSE is a model that could work well if the soil stiffness can be adequately approximated. A good estimation is difficult without specific soil tests for stiffness. This is required since there is no good analytical or numerical model to determine soil stiffness from regularly tested parameters.

STEM is a less simplified model than ROSE which the results reflect. This mainly stems from the more accurate representation of soil layers through the linear elastic method and increased complexity from three dimensions. The main problem identified with STEM is the meshing. Meshing in STEM works well for all layers except in the top layer. This is because the elements connected to sleeper nodes take the full force from the sleeper. The displacement of the rail and soil beneath it is therefore very reliant on the mesh size as it determines the area that resists the load from the wheels. There is also a discrepancy close to the sleeper spacing, from the code requiring a specific number of nodes along the rail depending on the ratio between spacing and mesh size.

The severe discrepancy of results between mesh sizes requires that the choice of mesh size depends on the sleeper spacing. This results in the other aspects of mesh size, such as convergence and aspect ratio being unable to be accounted for. The estimation made is that the mesh size should be determined such that the surface area of the elements around the sleeper node should correspond to the sleeper area. If this judgment is wrong, the results from all analyses would be inaccurate. The many uncertainties and large differences brought by the meshing in STEM makes the program somewhat unreliable before this problem is accounted for.

The results from Högsjö mainly focus on testing the impact of different dynamic effects in STEM. The result indicate that STEM can model these systems but does not say anything about the reliability of the results. This is because there is no experimental data that can be compared. The experimental data comparison for Malmbanan provided similar results for STEM but further testing is required to determine the reliability of the model. Experimental data could be explored for more locations, but also in the same location with different types of trains and loads to compared with results from STEM.

7 Conclusions

Accurate results can be obtained from ROSE and STEM when benchmarked against data for Malmbanan, based on available input data and the method used in the two different numerical models. The difference was at a maximum 22 percent between the measured displacements and the models. Both models are accessible and easy to use. However, it is important to acknowledge the influence of parameters, such as mesh size and timestep, which if input incorrectly give inaccurate results. Other input parameters that have varying values along the track or through the lifespan such as sleeper spacing, irregularities and soil distribution creates large differences in soil dynamics depending on properties. For these parameters, either the worst case possible should be studied or a safety factor could be added.

From this study, a model with ground vibrations from wave propagation such as the one used in STEM works a lot better for dynamic problems. In certain conditions where there is a chance that dynamic effects could cause problems for railways, it would be of great use in initial stages. Currently, there does not seem to exist a standardized procedure for these cases. Therefore, it would be preferable to use a model such as STEM which can account for these effects. The **results** we have retrieved suggest that this only needs to occur when the soil is soft and the velocity is high, otherwise dynamic effects seem inconsequential. To determine the exact speed and stiffness where such analyses start to be necessary requires further study.

ROSE meanwhile does not have the same benefits but could be possible to use in certain circumstances, which would be beneficial due to its computational speed. For this to be possible, a better spring stiffness determination method should be used such as direct determination from field testing. To use the ROSE model there should be no risk of ground vibrations having an impact on the system and the train speed should be low. The simplifications of the model and that it is uncoupled may not be applicable to all conditions, such as transition zones and speed analyses. The model is open source and if a suitable way of getting soil stiffness is used adequate results could be obtained.

The analysis conducted concluded that dynamic effects impact the ground vibrations and, therefore, a model that simulates wave vibrations is required to account for these effects. While the STEM method consists of several parts with low complexity, its combined nature simulates many dynamic effects which would not be modeled in a method with separated parts with transferring loads.

8 References

Aggestam, E., & Nielsen, J. C. (2019). Multi-objective optimisation of transition zones between slab track and ballasted track using a genetic algorithm. *Journal of Sound and Vibration*, *446*, 91–112. https://doi.org/10.1016/J.JSV.2019.01.027

Arm, M., Karlsson, M., & Olsson, E. L. (2021). *VÄGLEDNING Projektering och utförande av bärighetsförbättring av järnväg* (tech. rep.). Trafikverket. Borlänge.

Bredenberg, H. (2000). *Stålkärnepålar Anvisningar för projektering, dimensionering utförande och kontroll* (tech. rep.). Linköping.

Chen, J., & Zhou, X. (2024). Advanced absorbing boundaries for elastodynamic finite element analysis: The added degree of freedom method. *Computer Methods in Applied Mechanics and Engineering*, *420*, 116752. https://doi.org/10.1016/J.CMA.2024.116752

Chen, M., Zhu, S., Zhai, W., Sun, Y., & Zhang, Q. (2023). Inversion and identification of vertical track irregularities considering the differential subgrade settlement based on fully convolutional encoder-decoder network. *Construction and Building Materials*, *367*, 130057. https://doi.org/10.1016/J.CONBUILDMAT.2022.130057

Coelho, B. Z., Fathian, M., Noordam, A., Nuttall, J., Moretti, D., Pennings, J., Van den Eijnden, B., & Smyrniou, E. (2023). STEM Vibrations.

Connolly, D., Giannopoulos, A., & Forde, M. C. (2013). Numerical modelling of ground borne vibrations from high speed rail lines on embankments. *Soil Dynamics and Earthquake Engineering*, *46*, 13–19. https://doi.org/10.1016/J.SOILDYN.2012.12.003

Costa, P. A., Colaço, A., Calçada, R., & Cardoso, A. S. (2015). Critical speed of railway tracks. Detailed and simplified approaches. *Transportation Geotechnics*, *2*, 30–46. https://doi.org/10.1016/J.TRGEO.2014.09.003

Dadvand, P., Rossi, R., & Oñate, E. (2010). An Object-oriented Environment for Developing Finite Element Codes for Multi-disciplinary Applications. *Archives of Computational Methods in Engineering*, *17*(3), 253–297. https://doi.org/10.1007/s11831-010-9045-2

Dahlberg, T. (2010). Railway Track Stiffness Variations – Consequences and Countermeasures. *International Journal of Civil Engineering*, *8*.

Esveld, C. (2001). *Modern railway track* (D. Zwarthoed-van Nieuwenhuizen, Ed.; 2nd ed.).

Fernández-Ruiz, J., Medina Rodríguez, L. E., Alves Costa, P., & Martínez-Díaz, M. (2021). Benchmarking of two three-dimensional numerical models in time/space domain to predict railway-induced ground vibrations. *Earthquake Engineering and Engineering Vibration*, *20*(1), 245–256. https://doi.org/10.1007/s11803-021-2017-8

Fernández-Ruiz, J., & Pereira, C. (2024). Non-linear critical speed in high-speed ballasted railways with ground reinforcement. *Transportation Geotechnics*, *48*, 101325. https://doi.org/10.1016/J.TRGEO.2024.101325

Galvín, P., François, S., Schevenels, M., Bongini, E., Degrande, G., & Lombaert, G. (2010). A 2.5D coupled FE-BE model for the prediction of railway induced vibrations. *Soil Dynamics and Earthquake Engineering*, *30*(12), 1500–1512. https://doi.org/10.1016/J.SOILDYN.2010.07.001

Galvín, P., Romero, A., & Domínguez, J. (2010). Fully three-dimensional analysis of high-speed train–track–soil-structure dynamic interaction. *Journal of Sound and Vibration*, *329*(24), 5147–5163. https://doi.org/10.1016/J.JSV.2010.06.016

Google Maps. (2025).

Hall, L. (2003). Simulations and analyses of train-induced ground vibrations in finite element models. *Soil Dynamics and Earthquake Engineering*, *23*(5), 403–413. https://doi.org/10.1016/S0267-7261(02)00209-9

Hall, L., Shih, J. Y., Zangeneh, A., & Pacoste, C. (2023). A methodology for control and design of required ground reinforcement measures regarding train-induced ground vibrations. *Transportation Geotechnics*, *42*, 101038. https://doi.org/10.1016/J.TRGEO.2023.101038

Hov, S., & Larsson, S. (2023). Strength and Stiffness Properties of Laboratory-Improved Soft Swedish Clays. *International Journal of Geosynthetics and Ground Engineering*, *9*(1), 11. https://doi.org/10.1007/s40891-023-00432-3

Karlsson, M., & Moritz, L. (2016, February). *Trafikverkets tekniska krav för geokonstruktioner-TK Geo 13* (tech. rep.). Trafikverket.

Khakpour, M., & Hajialilue Bonab, M. (2018). Soil-Structure-Interaction using Cone Model in Time Domain for Horizontal and Vertical Motions in Layered Half Space. *Journal of Earthquake Engineering*, *24*, 1–26. https://doi.org/10.1080/13632469.2018.1441766

Kok, S., Ti, Huat, B., Noorzaei, J., & Jaafar, S. (2009). A Review of Basic Soil Constitutive Models for Geotechnical Application. *Electronic Journal of Geotechnical Engineering*, *14*.

Kouroussis, G., Connolly, D. P., & Verlinden, O. (2014). Railway-induced ground vibrations – a review of vehicle effects. *International Journal of Rail Transportation*, *2*(2), 69–110. https://doi.org/10.1080/23248378.2014.897791

Kouroussis, G., & Verlinden, O. (2013). Prediction of railway induced ground vibration through multibody and finite element modelling. *Mechanical Sciences*, *4*(1), 167–183.

Kruse, E., & Emanuelsson, P. (2021, December). *HÖGSJÖ VÄSTRA FÖRBIGÅNGSSPÅR KM 167+655 - 168+810 GEOTEKNIK SYSTEMHANDLING* (tech. rep.). Tyréns. Högsjö.

Krylov, V. (2000). Track-soil critical velocities and their effects on railway-generated ground vibrations.

Lamprea-Pineda, A. C., Connolly, D. P., & Hussein, M. F. (2022). Beams on elastic foundations – A review of railway applications and solutions. *Transportation Geotechnics*, *33*, 100696. https://doi.org/10.1016/J.TRGEO.2021.100696

Lei, X., & Noda, N. A. (2002). ANALYSES OF DYNAMIC RESPONSE OF VEHICLE AND TRACK COUPLING SYSTEM WITH RANDOM IRREGULARITY OF TRACK VERTICAL PROFILE. *Journal of Sound and Vibration*, *258*(1), 147–165. https://doi.org/10.1006/JSVI.2002.5107

Loukidis, D., & Tamiolakis, G. P. (2017). Spatial distribution of Winkler spring stiffness for rectangular mat foundation analysis. *Engineering Structures*, *153*, 443–459. https://doi.org/10.1016/J.ENGSTRUCT.2017.10.001

Lu, F., Gao, Q., Lin, J. H., & Williams, F. W. (2006). Non-stationary random ground vibration due to loads moving along a railway track. *Journal of Sound and Vibration*, *298*(1-2), 30–42. https://doi.org/10.1016/J.JSV.2006.04.041

Mattsson, H. (2020, December). *Ytvågsseismik (MASW) Gransjö, Boden* (tech. rep.). Geovista.

Meyer, Z., & Olszewska, M. (2021). Methods Development for the Constrained Elastic Modulus Investigation of Organic Material in Natural Soil Conditions. *Materials*, *14*(22). https://doi.org/10.3390/ma14226842

Moritz, L., & Karlsson, M. (2014, May). *Trafikverkets tekniska råd för geokonstruktioner-TK Geo 13* (tech. rep.). Trafikverket.

Moritz, L., & Karlsson, M. (2022). *KRAV TRVINFRA-00230 Geokonstruktion, Dimensionering och utformning Trafikverkets infrastrukturregelverk* (tech. rep.). Trafikverket. Borlänge.

Mossaiby, F., Shojaei, A., Boroomand, B., Zaccariotto, M., & Galvanetto, U. (2020). Local Dirichlet-type absorbing boundary conditions for transient elastic wave propagation problems. *Computer Methods in Applied Mechanics and Engineering*, *362*, 112856. https://doi.org/10.1016/J.CMA.2020.112856

Naeini, S., Ziaie moayed, R., & Allahyari, F. (2014). Subgrade Reaction Modulus (K s) of Clayey Soils Based on Field Tests. *Journal of Engineering Geology*.

Nasrollahi, K., Dijkstra, J., & Nielsen, J. C. (2024). Towards real-time condition monitoring of a transition zone in a railway structure using fibre Bragg grating sensors. *Transportation Geotechnics*, *44*, 101166. https://doi.org/10.1016/J.TRGEO.2023.101166

Nasrollahi, K., Nielsen, J. C., Aggestam, E., Dijkstra, J., & Ekh, M. (2023). Prediction of long-term differential track settlement in a transition zone using an iterative approach. *Engineering Structures*, *283*, 115830. https://doi.org/10.1016/J.ENGSTRUCT.2023.115830

Nielsen, J. C., & Igeland, A. (1995). VERTICAL DYNAMIC INTERACTION BETWEEN TRAIN AND TRACK INFLUENCE OF WHEEL AND TRACK IMPERFECTIONS. *Journal of Sound and Vibration*, *187*(5), 825–839. https://doi.org/10.1006/JSVI.1995.0566

Noordam, A., & Zuada Coelho, B. (2024). ROSE.

Norén-Cosgriff, K., Berggren, E. G., Kaynia, A. M., Dam, N. N., & Mortensen, N. (2018). A new method for estimation of critical speed for railway tracks on soft ground. *International Journal of Rail Transportation*, *6*(4), 203–217. https://doi.org/10.1080/23248378.2018.1474811

O'Brien, J., & Rizos, D. C. (2005). A 3D BEM-FEM methodology for simulation of high speed train induced vibrations. *Soil Dynamics and Earthquake Engineering*, *25*(4), 289–301. https://doi.org/10.1016/J.SOILDYN.2005.02.005

Ouakka, S., Kouroussis, G., & Verlinden, O. (2021). *Mitigation Measures Dedicated to Railway Induced Ground Vibration: an Analysis of Recent Advances Université de Mons MITIGATION MEASURES DEDICATED TO RAILWAY-INDUCED GROUND VIBRATION: AN ANALYSIS OF RECENT ADVANCES* (tech. rep.). Annual Congress of the International Institute of Acoustics and Vibration. https://www.researchgate.net/publication/353193251

Ouakka, S., Verlinden, O., & Kouroussis, G. (2022, March). Railway ground vibration and mitigation measures: benchmarking of best practices. https://doi.org/10.1007/s40534-021-00264-9

Podworna, M. (2015). MODELLING OF RANDOM VERTICAL IRREGULARITIES OF RAILWAY TRACKS. *Applied Mechanics and Engineering*, *20*, 647–655.

Powrie, W., Yang, L. A., & Clayton, C. R. I. (2007). Stress changes in the ground below ballasted railway track during train passage. *Proceedings of the Institution of Mechanical Engineers, Part F*, *221*(2), 247–262. https://doi.org/10.1243/0954409JRRT95

Puzavac, L., Popović, Z., & Lazarević, L. (2012). Influence of Track Stiffness on Track Behaviour Under Vertical Load. *PROMET - Traffic&Transportation*, *24*. https://doi.org/10.7307/ptt.v24i5.1176

Sañudo, R., Dell'Olio, L., Casado, J. A., Carrascal, I. A., & Diego, S. (2016). Track transitions in railways: A review. *Construction and Building Materials*, *112*, 140–157. https://doi.org/10.1016/J.CONBUILDMAT.2016.02.084

Sheng, X., Jones, C. J., & Thompson, D. J. (2003). A comparison of a theoretical model for quasi-statically and dynamically induced environmental vibration from trains with measurements. *Journal of Sound and Vibration*, *267*(3), 621–635. https://doi.org/10.1016/S0022-460X(03)00728-4

Sheng, X., Jones, C. J., & Thompson, D. J. (2006). Prediction of ground vibration from trains using the wavenumber finite and boundary element methods. *Journal of Sound and Vibration*, *293*(3-5), 575–586. https://doi.org/10.1016/J.JSV.2005.08.040

Stetens geotekniska institut. (2020). Torv – deformationer och brottmekanismer i modellförsök. *SGI Publikation*, (49).

Thompson, D. J., Kouroussis, G., & Ntotsios, E. (2019). Modelling, simulation and evaluation of ground vibration caused by rail vehicles*. *Vehicle System Dynamics*, *57*(7), 936–983. https://doi.org/10.1080/00423114.2019.1602274

Trafikverket. (2024, December). *SAMRÅDSUNDERLAG Plan-och miljöbeskrivning Högsjö västra, förbigångsspår* (tech. rep.). Trafikverket. Borlänge.

Trafikverket. (2025, March). Malmbanan, Boden-Riksgränsen.

Wang, H., & Markine, V. L. (2018). Methodology for the comprehensive analysis of railway transition zones. *Computers and Geotechnics*, *99*, 64–79. https://doi.org/10.1016/J.COMPGEO.2018.03.001

Wang, J., & Zeng, X. (2004). Numerical Simulations of Vibration Attenuation of High-Speed Train Foundations With Varied Trackbed Underlayment Materials. *Journal of Vibration and Control*, *10*(8), 1123–1136. https://doi.org/10.1177/1077546304043268

Wolf, J. P. (1985). *Dynamic soil structure interaction* (T. A. Soler, Ed.). Prentice-Hall, Inc.

Wolf, P. J., & Deeks, J. A. (2004). *Foundation Vibration Analysis: A Strength of Materials Approach* (1st ed.). Elsevier.

Wong, D. Y. C., Sadasivan, V., Isaksson, J., Karlsson, A., & Dijkstra, J. (2024). Trans-scale spatial variability of lime-cement mixed columns. *Construction and Building Materials*, *417*, 135394. https://doi.org/10.1016/J.CONBUILDMAT.2024.135394

Yang, L. A., Powrie, W., & Priest, J. A. (2009). Dynamic Stress Analysis of a Ballasted Railway Track Bed during Train Passage. *Journal of Geotechnical and Geoenvironmental Engineering*, *135*(5), 680–689. https://doi.org/10.1061/(ASCE)GT.1943-5606.0000032

Yang, Y. B., Hung, H. H., & Chang, D. W. (2003). Train-induced wave propagation in layered soils using finite/infinite element simulation. *Soil Dynamics and Earthquake Engineering*, *23*(4), 263–278. https://doi.org/10.1016/S0267-7261(03)00003-4

Ziaie-Moayed, R., & Janbaz, M. (2009). Effective Parameters on Modulus of Subgrade Reaction in Clayey Soils. *Journal of Applied Sciences*, *9*(22), 4006–4012.

Zuada Coelho, B., & Hicks, M. A. (2016). Numerical analysis of railway transition zones in soft soil. *Proceedings of the Institution of Mechanical Engineers, Part F: Journal of Rail and Rapid Transit*, *230*(6). https://doi.org/10.1177/0954409715605864

A Appendix A: Soil models

To depict the impact of dynamic forces on the soil, a model is required. There is no universal model for soils and their interaction with railway structures. However, there are several different models with varying complexity (Kouroussis et al., 2014). For numerical models, increased complexity and correspondence to reality is a tradeoff with computational power.

A.1 Winkler method

The Winkler spring method is a computationally efficient soil model for dynamic analysis (Lamprea-Pineda et al., 2022). The Winkler method in its simplest form models a mass placed on an elastic spring (Loukidis and Tamiolakis, 2017), see figure A.1. For a railway system, this consists of a beam that is placed on springs that correspond to the stiffness of the soil. The stiffness parameter k for each spring (also called subgrade modulus) is derived by dividing force by displacement.

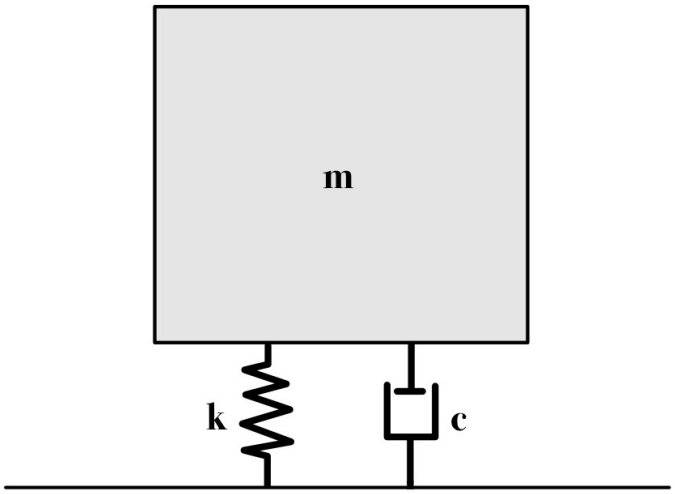

Figure A.1: Mass-spring model with a damper.

Vibration isolation is a simple method for modeling the reduction of vibration through a material. The vibration isolator is based on the idea of a rigid body connected to a foundation by an isolator (Ouakka et al., 2022). The isolator model consists of two parts, one is resilience and is modeled as a spring, and the second on is dissipation, modeled as a damper. Multiple springs and dampers are modeled as separated single-degree-of-freedom systems. The isolator is evaluated by three characteristics, absolute transmissibility, relative transmissibility and motion response. Absolute transmissibility measures the reduction of transmitted motion or force by the isolator while relative

transmissibility is a ratio between the isolator and foundation. Motion response is obtained by dividing excitation force with isolator stiffness.

The main benefit of the Winkler method is the low computational time for a numerical model (Ziaie-Moayed and Janbaz, 2009). The simplicity and ease of implementing the Winkler method is useful as basis for further design or when a large uncertainty already exists from other factors. To adhere the Winkler model closer to reality, several additions can be made. One such modification is the addition of damping to the springs, which models the energy dissipating characteristics of the soil (Lamprea-Pineda et al., 2022). Damping can be modeled in several different ways but for the time domain and Winkler springs, viscus damping is a suitable fit. This method models damping as a linearly dissipating parameter through the damping coefficient c, which can be seen in figure A.1.

The Winkler model can be improved by increasing the number of mass-spring elements modeled (Lamprea-Pineda et al., 2022). A railway has a vibration isolating system between cart and bogie, bogie and wheel, wheel and track and within the track pad. All of these could be modeled using the spring series approach, in which the stiffness of each part is combined. Each spring is then affected by the respective masses separately.

In the classic Winkler method, each spring is modeled as an independent and uncoupled system (Loukidis and Tamiolakis, 2017, Naeini et al., 2014). Modeling of several independent structures conflicts with the rail as a continuous structure where changes in one node affect those connected to the first. To reduce this simplification, the Euler-Bernoulli beam model of the rail can be exchanged for an elastic membrane with a Filonenko-Borodich foundation (Loukidis and Tamiolakis, 2017). For this system,the previously rigid body bends in accordance to the deformation of the springs which couples the system and gives a continuous response. The main drawback of using this method is that several other input parameters are required, increasing the complexity and requiring expanded field tests. Further ground coupling is required for a system to be able to model wave propagation. For a spring-based system such as Winkler this is an impossibility. This is due to the linear and one-directional nature of springs which cannot model waves adequately.

The Winkler model can be coupled with a vehicle model through the use of a Hertzian spring (Lamprea-Pineda et al., 2022). These are placed between the wheel of the cart and the rail to simulate the contact between these two elements. The most accurate Winkler model is non-linear where the spring parameter depends on the degree of contact. From this ideal model, a linearization can be made where the assumption of constant full contact between the rail and wheel is made. The system therefore becomes linear elastic, increasing computational speed, lowering required parameters but reducing accuracy of the model.

A.2 Linear elastic model

The linear elastic constitutive model is a deformation based model with no strength or failure parameters(Kok et al., 2009). For the purposes of wave propagation in soil this is the simplest possible constitutive model. The model simplify the many non-linear behaviors of soil and approximate the conditions to linearity. For most soil behaviors, other soil modeling methods exist that portray the soil conditions more accurately. Even with this being the case, linear elastic models are still in use today due to their simplicity

and easily obtained parameters.

A.3 Absorbing boundary

Finite element modeling, as the name implies, requires a finite space. Soil is a nearly infinite domain where wave propagation can occur without significant wave reflection (Mossaiby et al., 2020). The finite nature of the domain is more limited if the problem is static. The problems with regular boundaries in soil problems occur dynamically, where waves need to be modeled. The difficulty arises when waves propagate to reach a boundary. At this point, the wave energy will reflect. This phenomenon occurs only due to the confines of the finite element model (J. Chen and Zhou, 2024). To counteract this effect, absorbing boundary conditions built to absorb the waves can be added to the model boundaries. There are several different versions of the absorbing boundary which work well for different cases and types of waves.

B Appendix B: Mesh convergence

Convergence analysis for meshing is more difficult compared to the geometrical convergence analysis since each soil layer can have a different mesh size. Optimally, this would mean a convergence analysis for each layer and thus change with every case study. The process was simplified when finding that the top layer had a substantially larger effect on displacement compared to the layers below. Therefore, only the top layer is used for the convergence study. The meshing could also make it difficult to find a node in the same spot each time but STEM meshes around the sleeper spacing resulting in a node below a specific sleeper being chosen due to its consistency. The 3D geometry results in a halving of the element size increase the amount nodes by eight.

The convergence analysis is conducted for two different cases. The main convergence analysis of the iron ore train on Malmbanan is shown in figure B.1. The second case is from a reference built into STEM, which is used to test the veracity of the results, which are displayed in figure B.1. As the figures show, there is no hint of convergence. The meshing starts to converge in some areas before experiencing a large and rapid increase. Figure B.2 pictures a 40 percent increase between a mesh size of 0.4955 and 0.496. The change is therefore very rapid and the mesh convergence analysis is not adequate to determine what mesh size to use.

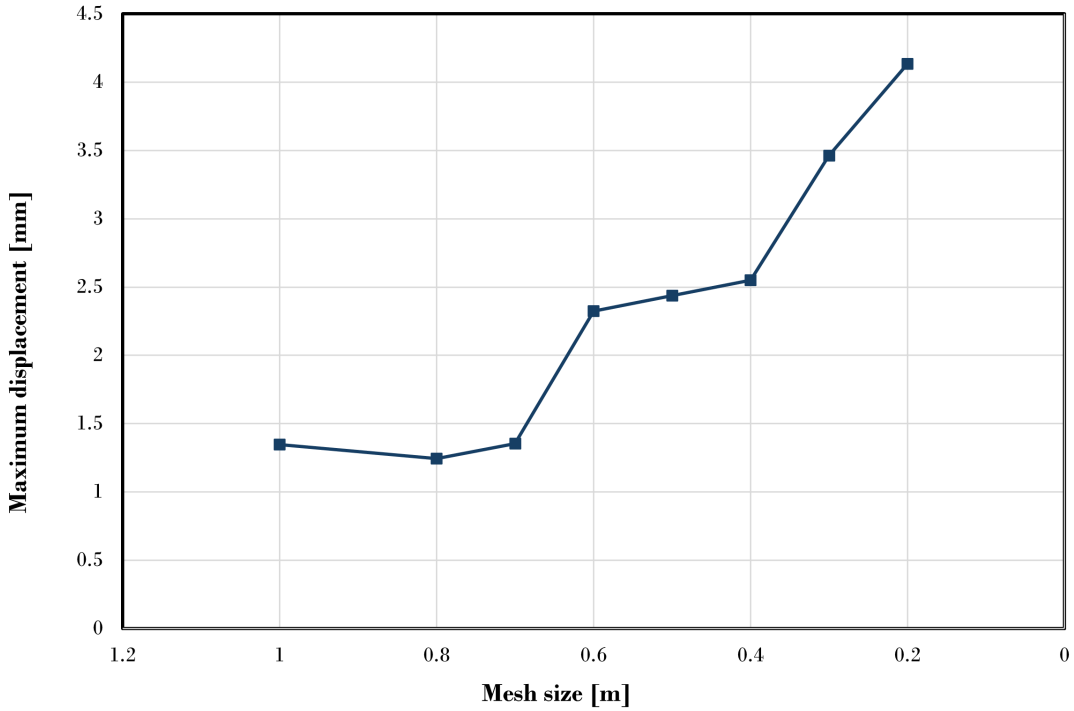

Figure B.1: Mesh convergence for Malmbanan with ore train

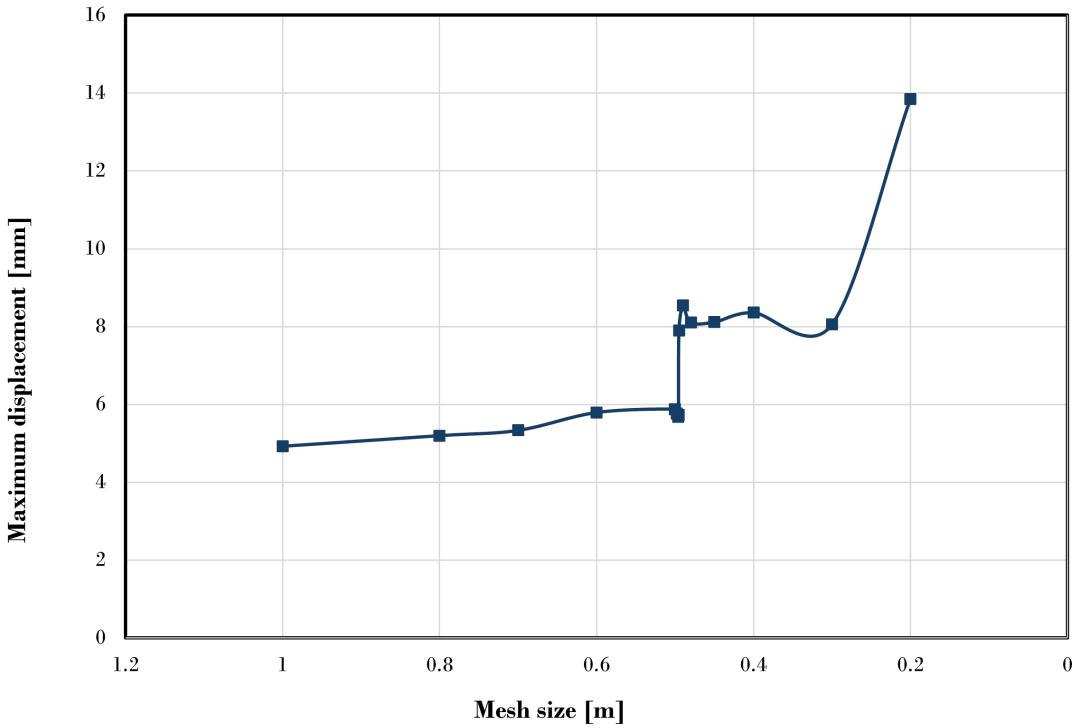

Figure B.2: Mesh convergence for tutorial.

The rapid increases in displacement correlates with fractions of the sleeper distance. To test if this correlation, a visual analysis of the mesh is done. For this test a sleeper distance of 1 meter is employed with a mesh size of 1.1 in figure B.3 and 0.9 in figure B.4. The figures show that a decreasing mesh size below the sleeper distance creates an extra node in the soil between the two sleepers. This is true for every fraction of the sleeper distance. Since the sleepers are modeled as nodes instead of areas, the displacement is difficult to adequately model.

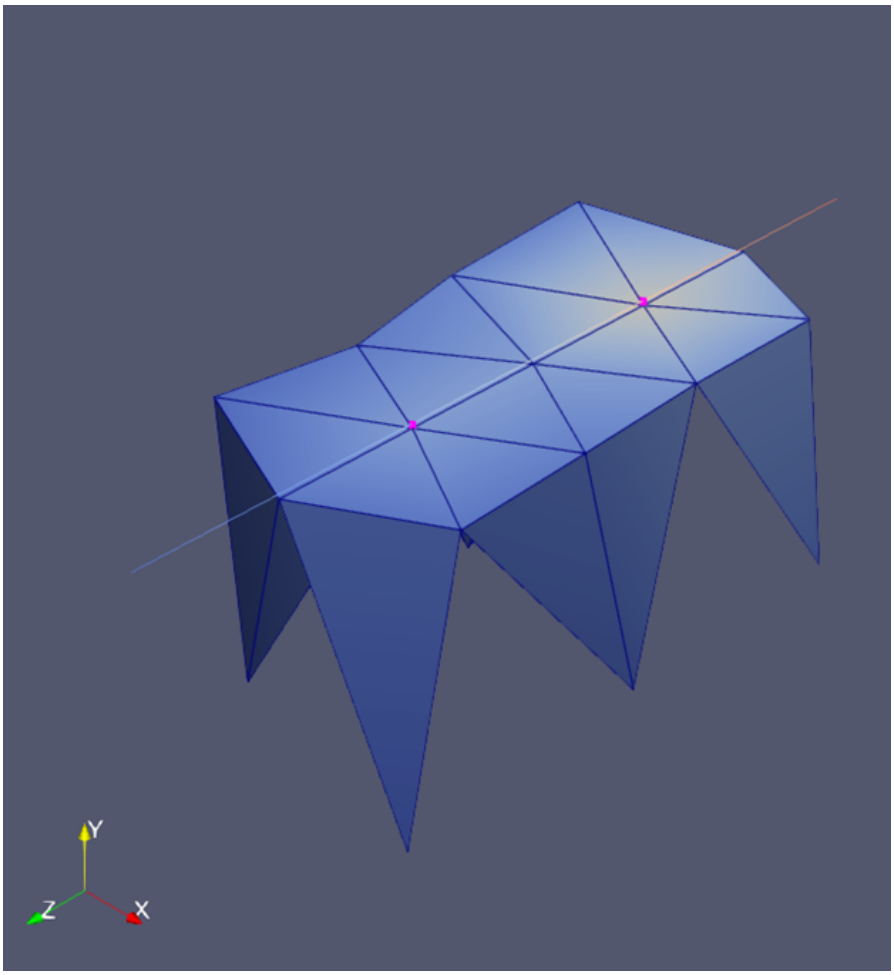

Figure B.3: Mesh with sleeper distance 1 and mesh size 0.9.

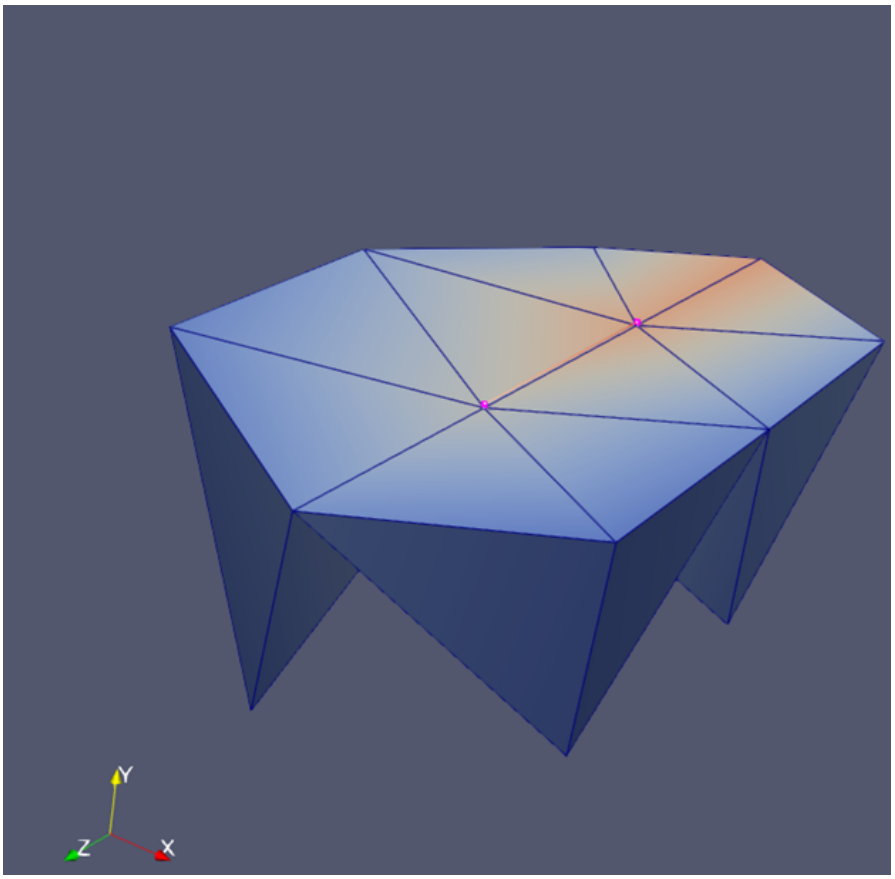

Figure B.4: Mesh with sleeper distance 1 and mesh size 1.1.

For the top layers where vibrations are critical and directly impacted by the vehicle, the interaction between sleeper spacings and mesh size is critical. It impacts how much of the soil that resists the point load. For the model in STEM, this corresponds to the area of the elements in contact with the sleeper node. In reality the area which resists the force from the sleeper in the top layer of soil is the area below the sleeper.

A way to approximate the sleeper area and thus the loaded area in STEM is to have the element area connected to sleeper nodes equivocate to the area of the sleeper. This solution is not optimal since the shape is very different to the one of a sleeper due to the meshing structure of the program. The meshing in STEM requires that nodes are placed under each sleeper and that each fractal of the sleeper distance adds an extra node between each sleeper. The top surface area of the elements close to the rail is therefore fairly constant within a fraction of the sleeper spacing. The element volume instead changes through depth which is not as influential to the displacement. Calculating the areas connected to the sleeper node it is found that a mesh size slightly below the sleeper spacing gives the most similar area to that of a sleeper.

C Appendix C: Irregularities

The irregularities on the rail are one of the main sources of dynamic loading on the rails (M. Chen et al., 2023). This is since the wheel contact disruption from irregularities creates vertical acceleration which leads to a dynamic effect in the rail and soil. Without the presence of irregularities or other sources of vertical discontinuities, the vertical dynamic effects of the numerical simulation are nonexistent as no acceleration occurs in the model (Lei and Noda, 2002). Rail irregularities are caused by wear of the track, which in turn facilitates further degradation from the dynamic effect caused by the irregularities. The irregularities also cause the dominant source of rolling noise, decrease comfort and creates safety concerns.

One method used to calculate the effect of irregularities in a model is through a power spectral density function(Podworna, 2015). This function creates a random variance distribution that correlates to railway irregularities based on wavelengths. The amplitude of this function and thus the maximum irregularity is described by the vertical track irregularity parameter (Av). In the America railway standard this parameter is based on line grade. This is the method used for ROSE and STEM.

Irregularity analysis is conducted for Malmbanan for the iron ore train at a speed of 60 km/h. Further analyses on the implementation of irregularities in the programs and their impact on different velocities need to be conducted for a better understanding.

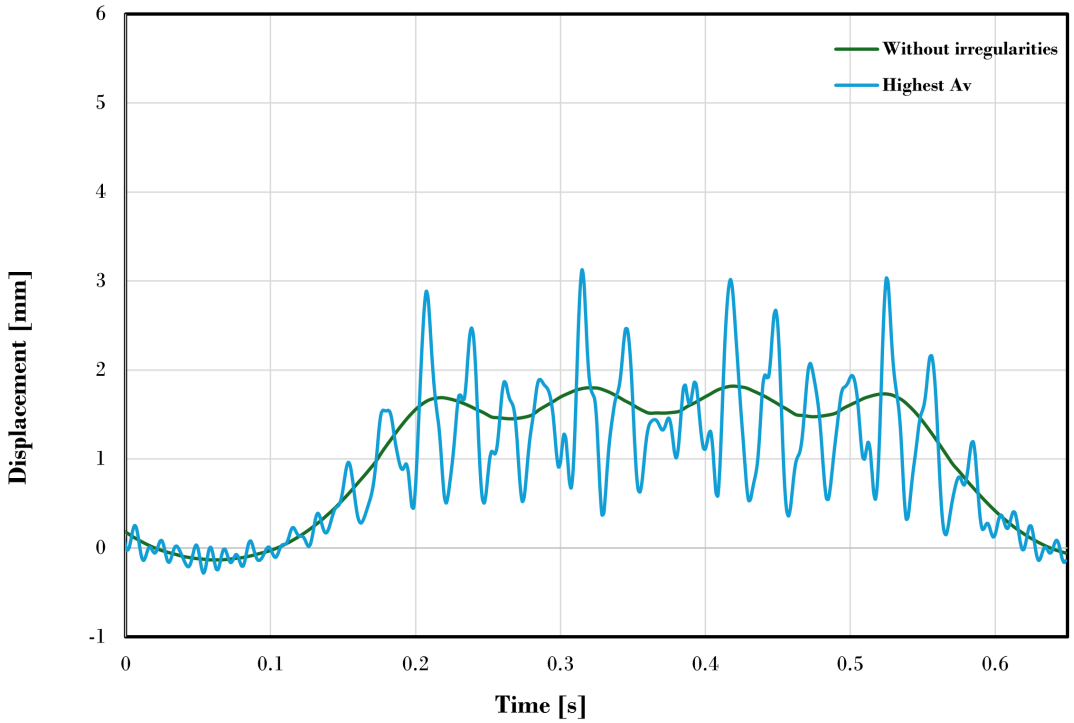

Figure C.1: One passage with the iron ore train in ROSE with differing irregularities.

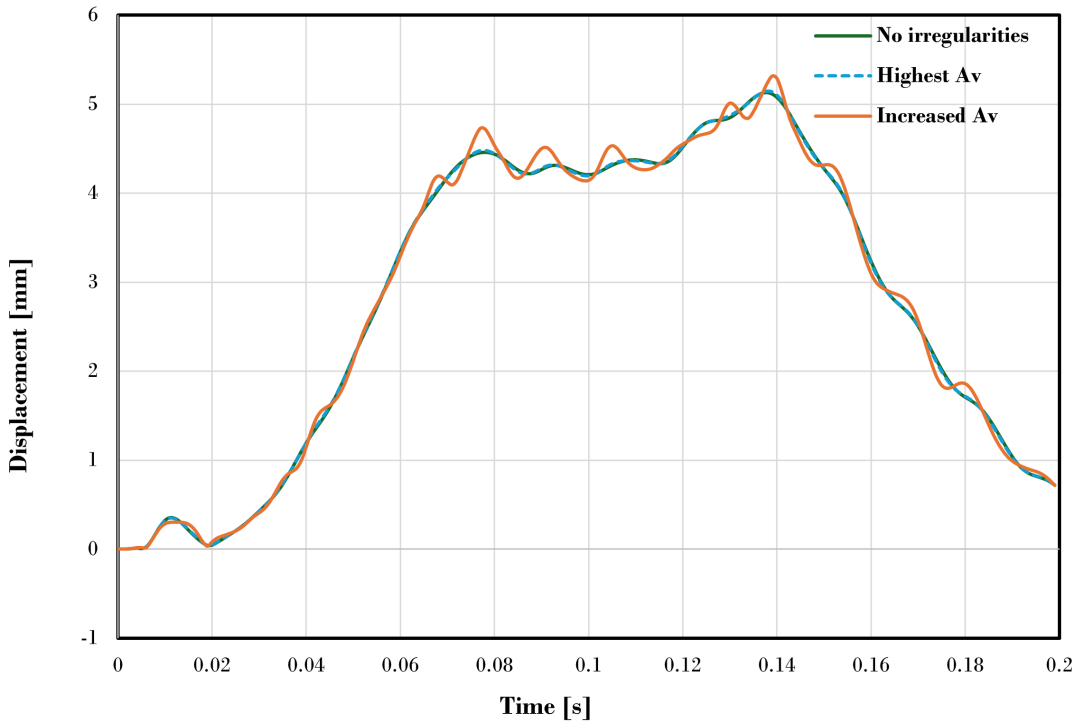

Figure C.2: One passage with the iron ore train in STEM with differing irregularities.

D Appendix D: Transition zones

Transition zones are investigated in both ROSE and STEM at the transition between areas 2 and 3. The 40-meter transition zone is modeled with five different layering depending on how many zones the transition consisted of. The distribution of transition is shown in table D.1. In ROSE the length is instead input as the number of sleepers which is obtained by dividing length by the sleeper distance of 0.65 m. The soil profiles of the transition based on table D.1 are displayed in the figures D.1 to D.5.

Table D.1: Soil layer distribution for transition zones

Layer depth	Area 2	Transition 1	Transition 2	Transition 3	Transition 4	Area 3
Two zones						
Length	90					90
Embankment	1.8					1.8
Peat	1					0
Silt	1					0
Moraine	0.4					0
Three zones						
Length	70	40				70
Embankment	1.8	1.8				1.8
Peat	1	1				0
Silt	1	0				0
Moraine	0.4	0				0
Four zones						
Length	70	20	20			70
Embankment	1.8	1.8	1.8			1.8
Peat	1	1	0.8			0
Silt	1	0.5	0			0
Moraine	0.4	0	0			0
Five zones						
Length	70	13	14	13		70
Embankment	1.8	1.8	1.8	1.8		1.8
Peat	1	1	1	0.7		0
Silt	1	1	0.3	0		0
Moraine	0.4	0	0	0		0
six zones						
Length	70	10	10	10	10	70
Embankment	1.8	1.8	1.8	1.8	1.8	1.8
Peat	1	1	1	1	0.5	0
Silt	1	1	0.3	0		0
Moraine	0.4	0	0	0		0

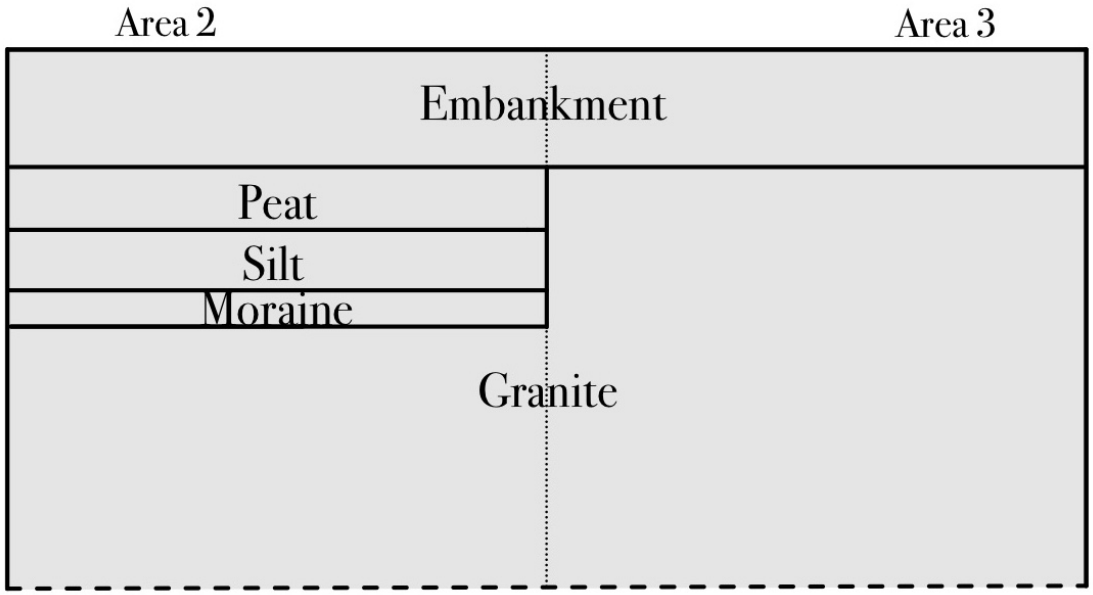

Figure D.1: Soil profile of Transition 1.

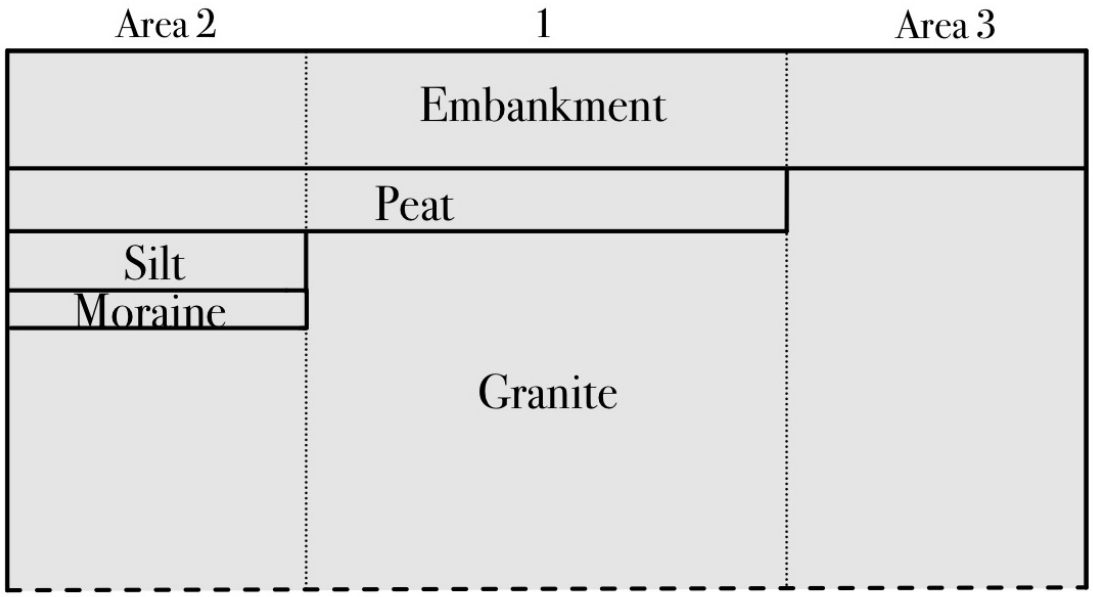

Figure D.2: Soil profile of Transition 2.

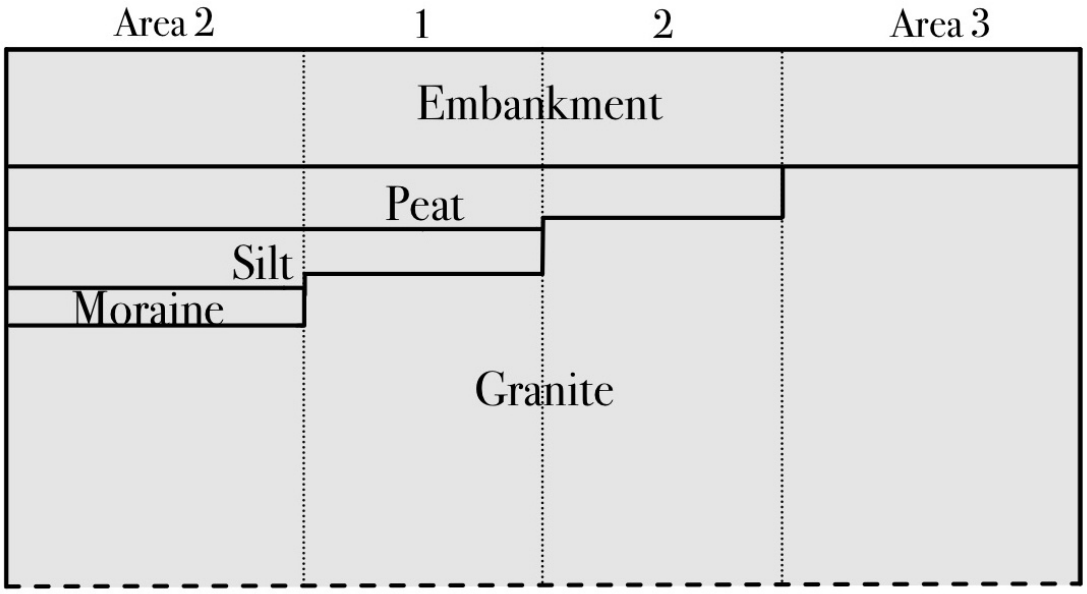

Figure D.3: Soil profile of Transition 3.

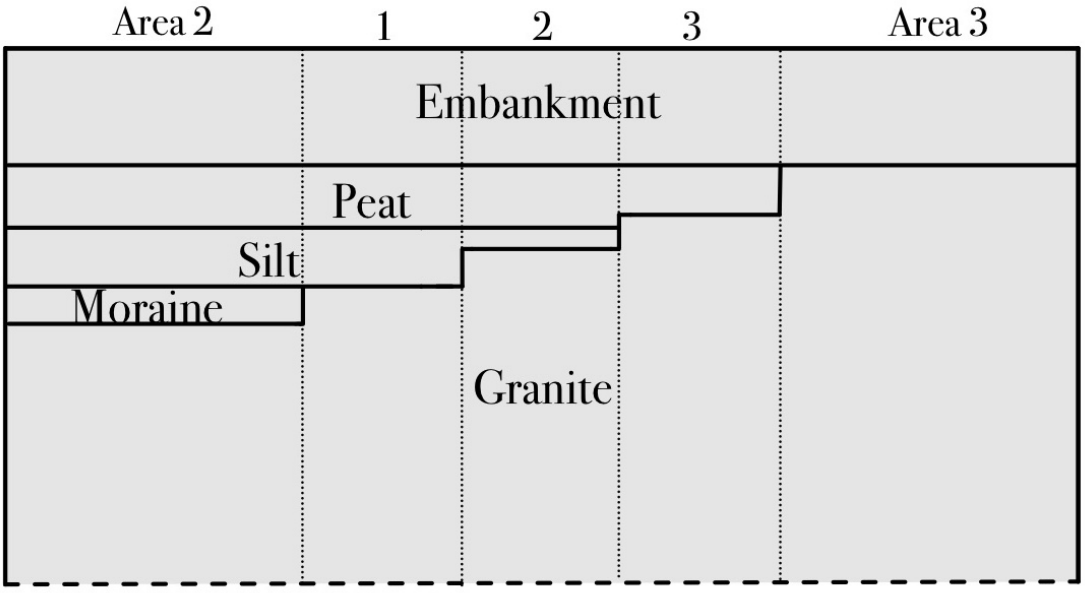

Figure D.4: Soil profile of Transition 4.

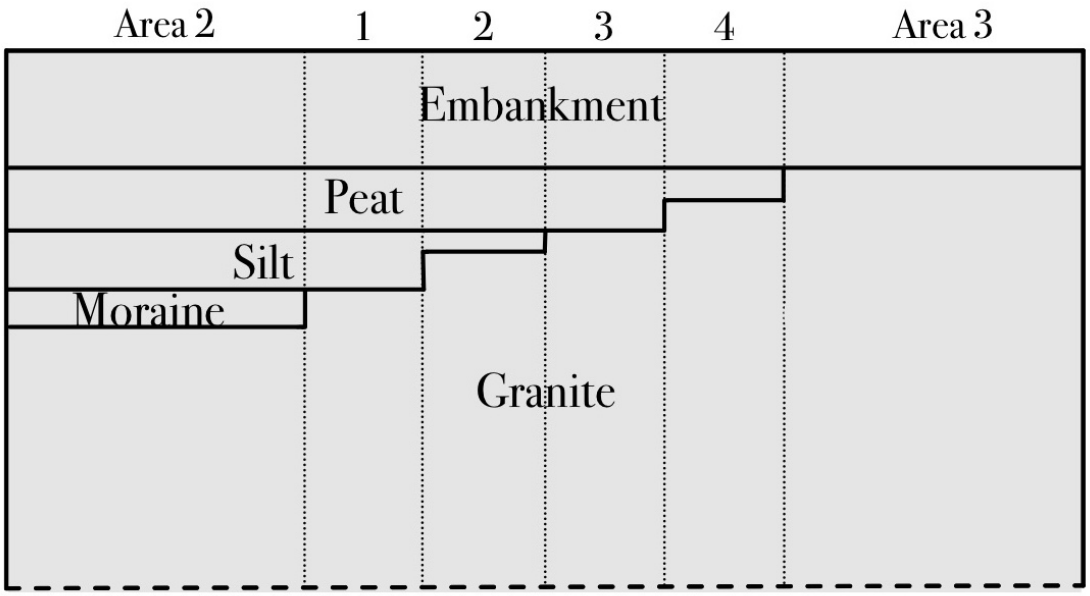

Figure D.5: Soil profile of Transition 5.

DEPARTMENT OF ARCHITECTURE AND
CIVIL ENGINEERING
CHALMERS UNIVERSITY OF TECHNOLOGY
Gothenburg, Sweden 2025
www.chalmers.se

CHALMERS
UNIVERSITY OF TECHNOLOGY